CARDIFF UNIVERSITY
PRIFYSGOL CAERDYDD

BINDING SERVICES
Tel +44 (0)29 2087 4949
Fax +44 (0)29 20371921
e-mail bindery@cardiff.ac.uk

Polyaromatic Molecules:

Structure and Reactivity on Copper Single Crystals

Thesis submitted for the degree of Doctor of Philosophy of the University of St. Andrews

By
Alexander Joseph McDowall

2003
School of Chemistry
University of St. Andrews,
St. Andrews, Fife

I, Alexander McDowall, hereby certify that this thesis, which is approximately 33 000 words in length, has been written by me, that it is the record of work carried out by me and that it has not been submitted in any previous application for a higher degree.

Date. 6th JAN 2004 .....Signature of candidate. .....

I was admitted as a research student in Oct 1999 and as a candidate for the degree of PhD Oct 1999; the higher study for which this is a record was carried out in the University of St. Andrews between 1999 and 2002.

Date. 6th JAN 2004 .....Signature of candidate .....

I hereby certify that the candidate has fulfilled the conditions of the Resolution and Regulations appropriate for the degree of PhD in the University of St. Andrews and that the candidate has qualified to submit this thesis in application for that degree.

Date. 13th January 2004 .....Signature of supervisor....

In submitting this thesis to the University of St. Andrews I understand that I am giving permission for it to be made available for use in accordance with the regulations of the University Library for the time being in force, subject to any copyright vested in the work not being affected thereby. I also understand that the title and abstract will be published, and that a copy of the work may be made and supplied to any *bona fide* library or any research worker.

Date. 6th JAN 2004 .....Signature of candidate .....

ACKNOWLEDGEMENTS 1

ABSTRACT 2

INTRODUCTION 4

A Possible Application *6*

AIMS 8

SUBSTRATES 11

MOLECULES AND PROPERTIES OF MOLECULES 13

3,4,9,10-Perylene Tetracarboxylic Dianhydride (PTCDA) *13*

Perylene *18*

Tetracene *21*

EXPERIMENTAL METHODS 24

Ultra-High Vacuum (UHV) *24*

X-Ray Photoelectron Spectroscopy (XPS) *26*

XPS Transmission Function *29*

Low Energy Electron Diffraction (LEED) *31*

Vibrational Spectroscopies: Reflection/Absorption Infra-Red Spectroscopy(RAIRS)

Transmission Infra-Red and Electron Energy Loss Spectroscopy (EELS) *34*

Scanning Tunnelling Microscopy (STM) *40*

Auto-Correlation of STM Images *44*

Mass Spectrometry *45*

Temperature Programmed Desorption (TPD) – by fragment, pressure and vibrational mode *47*

Luminescence *50*

Photo-Luminescence *51*

Sample Preparation - Chemicals 56

Sample Preparation - Substrates 58

Characterisation of Clean Surfaces 58

Oxygenated Cu(110) Surfaces 60

Dosing Apparatus 63

Organic Molecular Beam Deposition 66

Gaussian 98® and Hyperchem™ 68

EXPERIMENTAL RESULTS **69**

3,4,9,10-PERYLENETETRACARBOXYLICDIANHYDRIDE (PTCDA) 69

X-Ray Photoelectron Spectroscopy (XPS) 70

STM of PTCDA on Cu(211) 82

PTCDA on Cu(110) 89

Infra-red Spectroscopy of PTCDA on Cu(110) 89

STM of PTCDA on Cu(110) 93

PERYLENE 98

Infra-Red Spectroscopy - Perylene 98

RAIRS - Perylene on Cu(110) 101

Desorption of Perylene from Cu(110) 105

Low Energy Electron Diffraction (LEED) 107

STM 111

Photoluminescence of Perylene on Cu(110) 128

TETRACENE 135

Infra-Red Spectroscopy 135

RAIRS 137

STM 140

LEED *144*

High Temperature Deposition *152*

PERYLENE AND TETRACENE ON OXYGEN COVERED COPPER 154

Perylene on Oxygen Covered Cu(110) *154*

Tetracene on Oxygen Covered Cu(110) *158*

CONCLUSIONS AND COMPARISONS 159

REFERENCES 161

Acknowledgements

I would like to thank Neville for giving me the opportunity to do the PhD and all the support and help he has given me over the last four years. Special mentions to Steve for technical support, help with doing experiments, explaining how things work and for letting me squat in his office. Thanks to Chen for the regular interesting and heated discussions on results and experimental methods (and Scottish independence!).

Thanks to all the technical staff who promptly tackled any problems I threw at them or manufactured bits and bobs to make life easier in the lab. Thanks also to all members of the surface science groups in St. Andrews and Imperial College London who at points have provided not only valuable help with the project but also friendship and generally made life a lot easier.

I would also like to thank my parents for their support and gentle encouragement to get my thesis finished. Thanks also to anyone else who has contributed in any small way but has not been covered in the above list.

Finally, I would like to thank Lisa who has had to put up with the stresses of my PhD as much as I have. The support she has given is truly appreciated.

Abstract

In recent years there has been a significant interest in the use of polyaromatic molecules in (opto-) electronic devices. This family of molecules tends to be vibrantly coloured and have interesting optical and semiconductor properties hence a specific interest in display devices. In this thesis, thin films of organic polyaromatic molecules 3,4,9,10-perylenetetracarboxylic dianhydride (PTCDA), perylene and tetracene on copper single crystals were investigated. The molecules were deposited in Ultra High Vacuum (UHV) onto clean copper crystals under a number of different substrate conditions where they formed ordered thin films. The films were characterised using scanning tunnelling microscopy (STM), low energy electron diffraction (LEED), thermal desorption, X-ray photoelectron spectroscopy (XPS) and vibrational spectroscopies, electron energy loss spectroscopy (EELS) and reflection/absorption infra-red spectroscopy (RAIRS).

PTCDA, the most widely investigated of the molecules, was analysed on Cu(211) and (110) surfaces and was shown to have strong interactions with the copper rows of the substrates strongly influencing the structures formed. XPS results indicate a strong bond to the surface through loss of the anhydride oxygen atoms with subsequent layers physisorbed. On Cu(211) PTCDA formed a unit cell of a = 16.1Å, b = 24.1Å, $\beta = 85°$. On Cu(110), PTCDA forms a unit cell of a = 18.9Å, b = 18.9Å, $\beta = 75°$.

Perylene proved to be the most complex molecule with annealing of the initial monolayer vital in determining the structure of the subsequent layers. A highly ordered structure with molecular rows far larger than the terraces of the underlying copper could be formed after heating as opposed to a less ordered structure. The three thin film structures of perylene recorded were: α-phase: a = 11.0Å, b = 11.0Å, $\beta = 77°$, β-phase: a = 10.84Å, b = 10.84Å, $\beta = 65°$ and γ-phase: a = 20.7Å, b = 19.3Å, $\beta = 90°$ all of which are significantly different

from the bulk crystal structures. Photoluminescence experiments show that the different multilayer structures lead to different wavelengths of emission due to different intermolecular interactions within the films. The recorded photon emission results from a excimer due to overlapping of π-orbitals in the novel crystal structure. Below two monolayers, no emission is recorded due to quenching by the substrate.

Tetracene forms only monolayers at room temperature. If cooled, multilayers can be formed. Two tetracene monolayer structures were observed, the first driven by interactions with the copper rows produced a centred 12 x 2 structure, and the second, formed by annealing the first, involved molecules which were close packed and interdigitated, giving a compressed primitive 6 x 1.83 structure.

Introduction

In recent years, the production of cheap, high technology electronic and opto-electronic devices has increased greatly. Different materials have been investigated to try to improve both performance and economy of these devices[1,2,3,4,5].

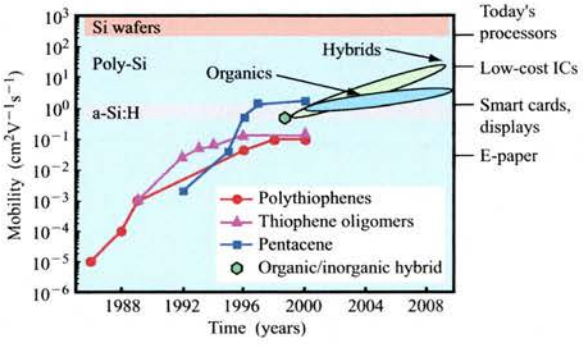

Fig. 1 Performance of organic and hybrid semiconductors, taken from ref[6]. Organic devices are predicted to be increasingly competitive with inorganic devices.

From Fig. 1, it can be seen that over the last decade and a half, performance of some organic semiconductors has increased sufficiently that they are equivalent to some silicon-based systems. It is projected that over the next few years their electron mobility will increase such that they become fast enough to compete with inorganic devices on a level footing[4,6]. Organic films have a number of advantages over the old inorganic systems. Relatively low pressures and temperatures are used to produce devices and they can be deposited easily onto a large number of substrates while retaining their "activity". Initial successes in electronic paper have been due to the flexibility of the organic (pentacene) transistors[7]. One of the major factors driving the research in this field is the huge increase in the use of small portable electronic devices like mobile phones, personal data assistants (PDAs) and laptop computers. These constantly need to be made lighter, more powerful and more efficient to cater to the increasing product demand and market forces. The organic film devices tend to use much less power than equivalent inorganic systems so can

last longer on the same battery power. They are also lighter, increasing portability and cheaper to produce therefore cheaper to sell[6]. There is also evidence that they can be used to produce extremely efficient solar cells[8,9,10].

Within the umbrella of organic chemistry, there are many families of molecules that are under investigation for such electronic applications - nano-tubes, polymers, polyaromatic molecules and more. Some molecules of these families have the same common property that allows them to conduct electricity, which is a large de-localised π-electron system. Investigations of 3,4,9,10-perylenetetracarboxylic dianhydride (PTCDA), one of the molecules to be investigated in this thesis, show that when the molecule is deposited onto a flat semiconductor surface -Si(111)[11], the thin film structure is the same as the bulk crystal structure with the molecules aligned parallel to the substrate. This structure provides stacks of molecules through which the π-electron orbitals overlap providing an easy path for the current to flow. Experimentally, conductivity perpendicular to the surface is 100 to 1000 times that parallel to the surface, which supports the theory that the current is carried through the overlapping π-electron system[11]. It is expected that other planar molecules with similar de-localised aromatic electron systems will have similar useful electronic properties.

At the interface of inorganic/organic chemistry are macrocyclic molecules such as the phthalocyanines and triquinolines. Like the organic molecules under investigation, these families also have delocalised π-electron systems that stack during crystallisation allowing conduction. These molecules are well known as industrial dyes and have well documented opto-electronic properties[12]. Through molecular orbital calculations, it is believed that light emission is produced via a charge transfer from the benzene rings to the inner macrocyclic ring[5]. The colour of these molecules can therefore be controlled by choice of metal ion in the centre of the molecule, affecting the charge around the inner ring[5].

A Possible Application

One application of macrocyclic and polyaromatic molecules is an organic light emitting diode (OLED).

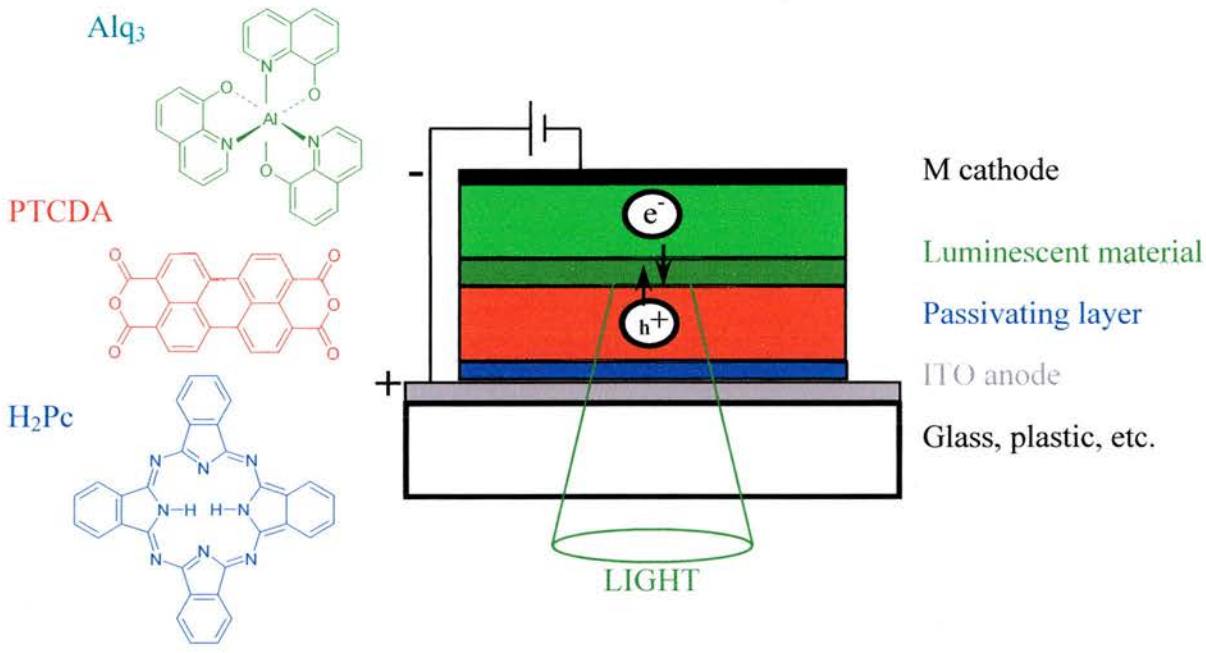

Fig. 2 Organic light emitting diode (OLED) taken from ref[13]

The OLED (Fig.2) was produced at Imperial College London and shows how these materials might be combined to form a working device. The three molecules chosen for this device have been extensively studied with a view to being incorporated in devices[14,15,16]. They also represent the three colours used in current cathode ray tube (CRT) displays and are therefore of particular interest in the opto-electronic area.

When a voltage is passed across the device, the positive anode produces holes by drawing electrons off the PTCDA, and electrons are added to the Alq_3 from the negative cathode. Recombination of holes and electrons at the transition between materials can occur to produce light[17,18]. The differences in energy between the hole state and electron state lead

to different colours of light, achieved by constructing the devices from different materials. The metal cathode also acts as a mirror to reflect all the light outwards. H_2Pc acts as a passivating layer and as a colour filter for the light. In the case of this device, the blue H_2Pc layer absorbs a significant quantity of the light produced at the PTCDA/Alq_3 interface severely reducing the efficiency of this device in this application. If light of the correct wavelength is shone onto such a device, a current will flow. This shows how these molecules are also suitable for photovoltaic devices.

Aims

PTCDA was the first molecule to be investigated as an organic/inorganic heterojunction[19], taking the first step towards organic devices. Because of this, PTCDA has probably been the most investigated material for organic device applications. However, the problem of how to harness its properties is yet to be fully addressed. Deposition onto amorphous surfaces such as glass is commercially viable, as the substrate needs little preparation. When PTCDA is deposited by molecular beam epitaxy, the molecules are seen to grow in crystallites with size and shape dependent on exact growth conditions but sharing the same structure as the bulk crystal[20,21]. When deposited onto metal single crystals, the interactions of the molecules with the surface structure can have an effect on the thin film structure. When deposited onto Cu(100), PTCDA forms a structure that is almost identical to the (102) plane of the bulk crystal structure[22]. On Cu(110), the slightly larger spacing of the copper rows leads to a slightly different structure where the molecules are perfectly quadrupole coupled without being offset[23]. Varying the substrate structure can affect the thin film structure, which may allow finer tuning of the film properties. The drawback is that it is a far more time consuming and therefore less commercially viable production method.

This project aims to investigate thin films of PTCDA on Cu(110) and Cu(211) single crystals and investigate their structures from sub-monolayer to multilayer. The effects of substrate temperature both during and subsequent to deposition will be investigated as heat increases the mobility of molecules on the surface and may allow increased ordering or the formation of different structures. Previous studies have implied that the initial monolayer of PTCDA bonds to copper through loss of the anhydride oxygen atoms[24]. To investigate this further, as well as studying PTCDA deposition on copper single crystals, perylene (the

core of PTCDA with no functional groups) will also be investigated under the same conditions. It has been suggested that the interactions between aromatic molecules and substrates increase with the increase in the number of aromatic rings[25]. As perylene and PTCDA have the same aromatic system, differences should be attributable to the different functional constituents.

The shape of these molecules is important as the precise two-dimensional structure depends on the interactions of the molecules with the substrates but also requires that there is little or no strain from the intermolecular interactions. Tetracene is chemically similar to perylene as it is constructed of benzene rings but is linear instead of rectangular. This shape difference should highlight any structural differences that molecular packing provides over substrate interactions. Tetracene also relates to anthracene and pentacene, which have three and five benzene units respectively. Anthracene was used as the photo-conductor in the first ever photocopier[5] and pentacene has been investigated for use in a number of applications[6,26,27,28]. Tetracene has been relatively little studied but, as it sits between anthracene and pentacene and is closest to perylene in molecular weight, it seems an obvious choice.

With all three molecules, sub-monolayer investigations should provide a description of the molecule-substrate interaction. At a thickness of several monolayers, the film surface should no longer be experiencing any direct substrate interactions. It can be assumed that the film is exhibiting the characteristics of the bulk although structural influences from the substrate may persist. Of particular interest are the methods through which the molecules actually attach to the surface. They may undergo decomposition or dislocation to form a new covalent chemical bond to the surface. Alternatively, they could remain fully intact and bond to the surface through hydrogen, Van der Waals, or π-bonds. This distinction is

important in terms of stability of the films as they may be subjected to high temperatures in their various applications or device processing.

Substrates

For this project, two substrates were used, the Cu(110) and the Cu(211) (Fig. 3). Copper is less likely than other metal surfaces to suffer contamination from H_2O, H_2 and CO - typical gases in UHV systems – so the creation and maintenance of clean surfaces is relatively easy. The two surfaces are both "flat" low index surfaces with C_{2v} and C_s symmetry respectively. The low rotational index of these surfaces opposed to the (111) and (100) faces (6-fold and 4-fold rotational symmetry respectively) means there are a maximum of two rotational and reflectional domains. If there are no specific interactions between the substrate and the molecules, then there are an infinite number of possible orientations molecules may take on the surface.

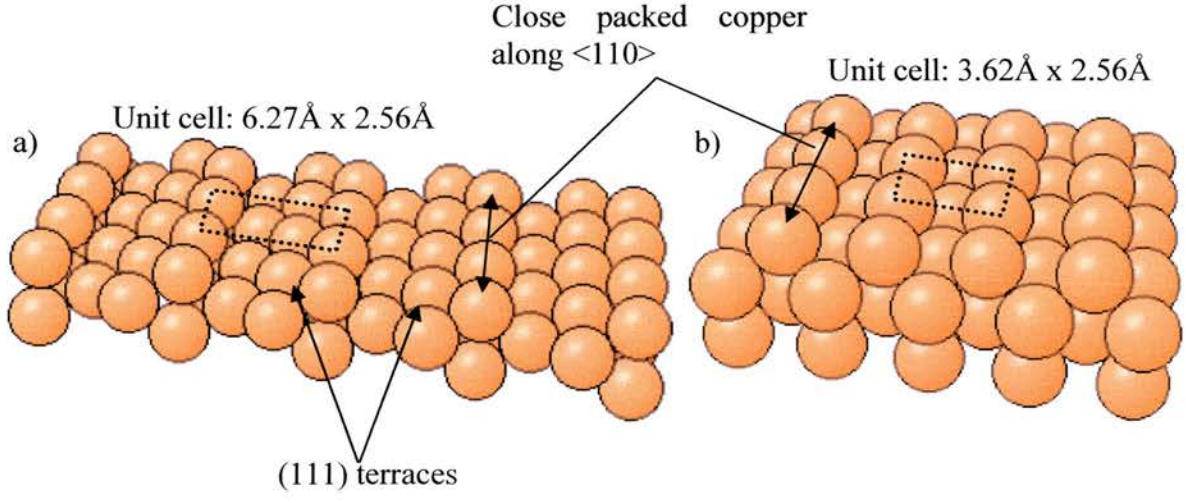

Fig. 3 a) Cu(211) and b) Cu(110) surfaces: Generated using ref[29]

The unit cells of the two surfaces are both rectangular with dimensions 6.27Å x 2.56Å and 3.62Å x 2.56Å for Cu(211) and Cu(110) respectively. As they are both the same along the <110> direction, the close packed copper rows, the reasons behind any differences in

structures of the absorbed molecules should relate to the different spacing of the copper rows parallel to <110>. It has been shown that on low index metal surfaces e.g. copper and silver, the PTCDA molecules lie flat on the substrates[30,22]. The Cu(211) has a "flat" surface as defined by that of the unit cell but there are narrow terraces which have significant character of the (111) plane. As PTCDA is known to lie flat on other metal (111) faces e.g. silver[31] and gold[32], the (111) character of the surface may encourage the molecules to be flat with respect to the terrace and therefore tilted with respect to the surface normal. This in turn may lead to novel structures.

Molecules and Properties of Molecules

3,4,9,10-Perylene Tetracarboxylic Dianhydride (PTCDA)

PTCDA is an organic semiconductor and industrial dye. Its deep red colour and associated optical properties make it an obvious molecule to investigate. The molecule consists of a rectangular five ring aromatic system with a dicarboxylic anhydride group on each end. Molecular orbital calculations suggest that the electron density of the delocalised π-electron system is evenly distributed across the whole perylene core of the molecule[33,34] and not two joined naphthalene units as was thought previously. The two dicarboxylic anhydride groups provide the molecule with significant functionality and lead to the possibility of some novel interactions with the surface.

The geometry and dimensions of PTCDA and all other molecules were optimised in Hyperchem™ using a single point optimisation (determines the total energy of the molecule in Kcal/mole, and the electron charge distribution in the molecule) followed by a Polak-Ribiere algorithm geometry optimisation. This allows the lowest energy conformation of the molecule to be calculated by optimising the geometry. In the case of PTCDA, this shows the molecule to be planar with molecular dimensions of 10.86Å x 6.64Å not including Van der Waals radii. These were obtained from the literature[35], which leads to molecular dimensions of 13.86Å x 8.64Å (Fig. 4).

N.B. Molecules are measured from atomic centre to atomic centre. Adding the literature Van der Waals radii values to this gives the total dimension of the molecule.

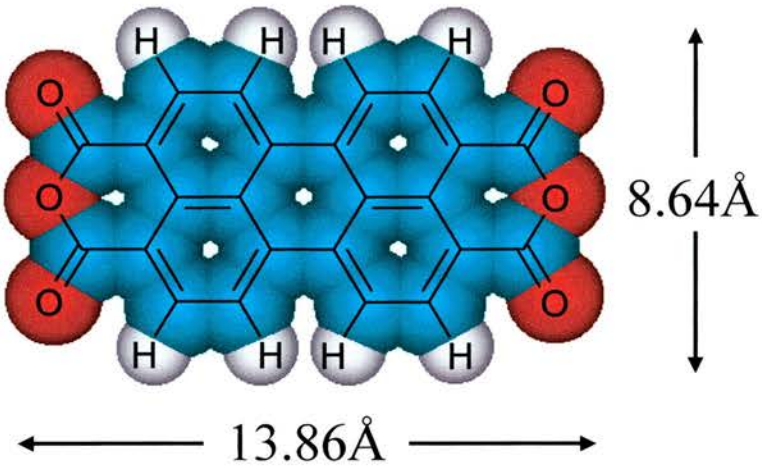

Fig. 4 3,4,9,10-Perylenetetracarboxylic dianhydride (PTCDA): Molecular dimensions include Van der Waals radii. M_r = 392.3g

The molecule, like all those being investigated in this project has (D_{2h}) symmetry[36], which combined with the rectangular shape of the molecule, should allow it to undergo molecular close packing.

PTCDA was one of the first organic molecules to be extensively studied for devices. This has lead to a large number of papers, relative to those discussing similar polyaromatic organic molecules, discussing structure and properties on many semiconductor surfaces including Si(111)[11,37], InAs(111), InSb(111) [38], GaAs(111)/(100)[39,40,41], graphite[42,43,44,45,46] and various low index metal surfaces - Au(111)[47,48,49,50], Ag(111)[51,52]/(110)[53,54,55,56]/(100)[57] and Cu(110)[58,59]/(100)[60,61,62]. Studies of PTCDA have shown that structural templating can be maintained through layers in excess of 300nm thick[63]. On the Cu(100) surface, the initial monolayer of molecules form a commensurate rectangular lattice ((4√2 x 5√2) R45°) with a unit cell dimension of 18.1Å x 14.5Å[64]. The molecules grow in islands and form domains of up to 200nm wide. This unit cell is approximately the same on all flat surfaces, and matches that of the (102) plane of the bulk crystal[61]. There is also strong

evidence that the size, shape and degree of ordering within the domains of molecules on metal surfaces is influenced greatly by annealing of the substrate[65].

In its bulk form, PTCDA has two crystal structures, the α and β phases, whose characteristics are given in Table 1. The (102) plane of both these phases are almost the same at around 19.5Å x 12Å[66]. As can be seen from Fig. 5, the molecules within the structure alternate by 90° which is believed to be driven by the quadrupole moment within the molecule, i.e. δ- end groups attracted to δ+ charge on the centre of the molecule.

Table 1 Crystal structure of PTCDA[67]

	α-phase	β-phase
space group	$P2_1/c$	$P2_1/c$
a	3.74Å	3.78Å
b	11.96Å	19.30Å
c	17.34Å	10.77Å
β	98.8°	83.6°

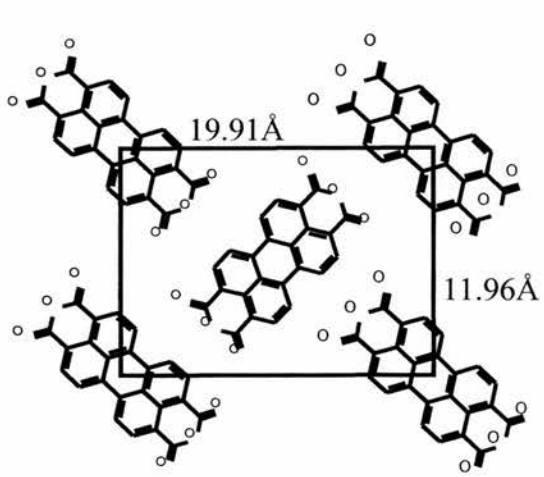

Fig. 5 (102) plane of β-PTCDA[68]

This structure has been recorded from single monolayers through layers many hundreds of nanometres thick[69,70], so the structure appears to be driven by intermolecular interactions and not through interactions with the different substrates used in the various experiments.

As PTCDA has oxygen functional groups, it is likely that it will form stronger bonds to the substrate than those molecules without such functionality. The bonds with metal surfaces in particular are strong enough to promote partial dissociation of the molecules[59]. XPS analysis of PTCDA on copper foil and tin disulphide shows that the relative intensities of the two O1s environments change as coverage increases[71,72]. In the bulk sample, a doublet peak in the ratio 2:1 is seen, the larger representing the carbonyl oxygen atoms (4 per molecule) and the smaller representing the anhydride oxygen atoms (2 per molecule). At sub-monolayer coverage, only a single peak is observed in the oxygen region, which based on its binding energy is likely to belong to the carbonyl oxygen atoms[69]. This can be explained in some way, by the molecule bonding through some of the oxygen atoms or loss of some of the oxygen atoms (Fig. 6).

PTCDA has been observed to lie flat on most surfaces so bonding would occur through each end. If the molecules were to stand up on a surface e.g. on Cu(211) it may have the suggested bonding at one end only and the unaltered C_2O_3 at the other.

Fig. 6 a) represents an electron donation from the surface contributing a negative charge at the oxygen atoms. This contribution could cause them all to become more equivalent so only a single XPS peak would be seen. As coverage increases the subsequent layers are bonded through inter-molecular interactions and remain intact with reduced contribution from the surface so the two oxygen environments diverge and two peaks become visible. Fig. 6 b) represents the loss of the anhydride oxygen and the formation of a covalent bond to the surface so only the carbonyl signal is visible in the XPS. The subsequent layers would not lose their anhydrides so the anhydride oxygen environment again becomes

visible. Fig. 6 c) suggests bonding through loss of one of the carboxylic groups. This has been seen to occur in the similarly functionalised phthalic anhydride[73]. Slight changes may occur in the C1s peak but they are masked by the significantly larger signal from the body of the molecule.

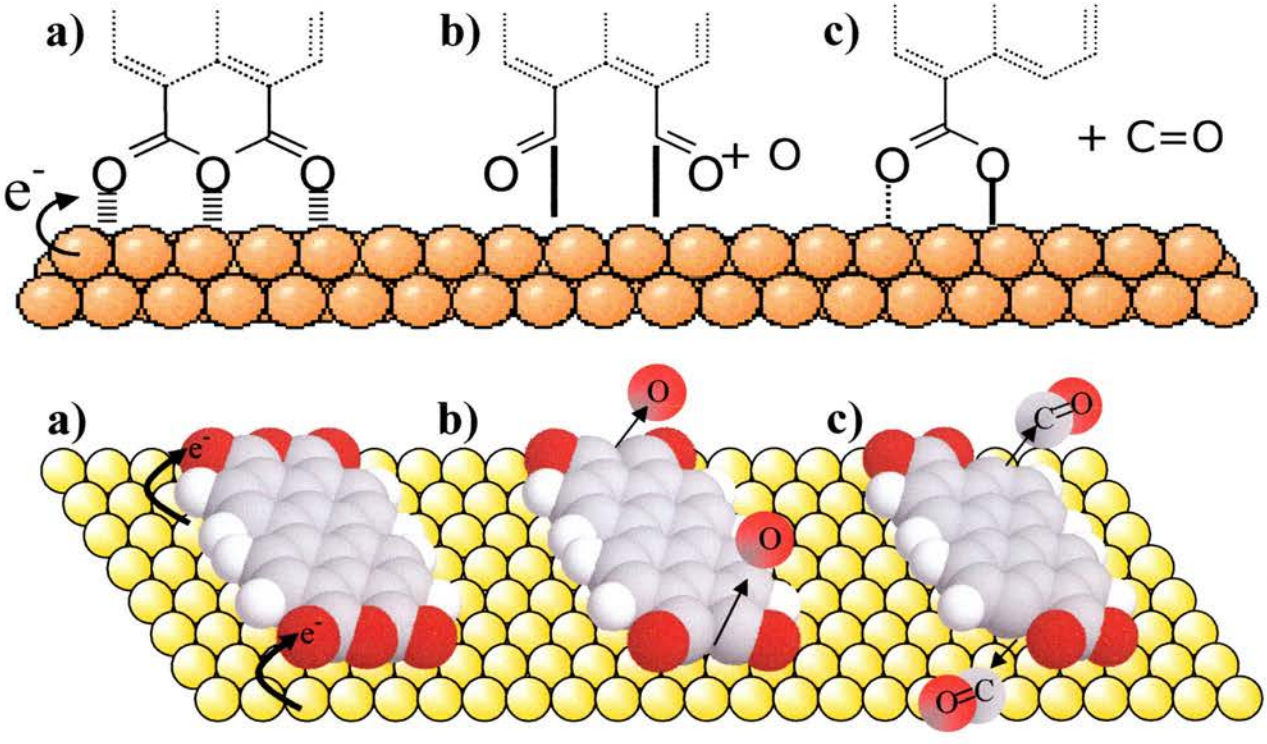

Fig. 6 Suggested methods through which PTCDA may bond to copper. Upper diagram shows bonding. Lower diagram shows probable orientation of molecules relative to the surface under each of the conditions. a) Oxygen atoms are made equivalent through electron donation from the substrate. b) Through loss of the anhydride oxygen, the molecule forms bonds to the surface. c) Suggests a similar mechanism to that seen in phthalic anhydride[73] where C=O is lost and bonding to the surface occurs through the remaining carboxyl group. In some cases, the molecule may bond to the surface through one end only in an upright fashion. In these cases, the end of the molecule not bonded to the surface would remain structurally unchanged.

Perylene

Perylene is structurally similar to PTCDA having the same core but without the anhydride and carbonyl functional groups. Perylene is also an organic semiconductor with a delocalised π-electron system, which has been used to manufacture a number of devices. Organic Field Effect Transistors (OFETs) based on perylene single crystals have exhibited room-temperature electron mobility of 5.5cm^2/V-s, five times that of the nearest organic competitor[74]. It has been investigated in a number of device applications but it has not been extensively investigated as a deposited thin film[75,76] although work on perylene micro-crystals has been done[77]. Its colour probably accounts for this lower interest. PTCDA is red and fits within the RGB device umbrella, perylene is yellow so does not and is therefore of less interest for optical applications.

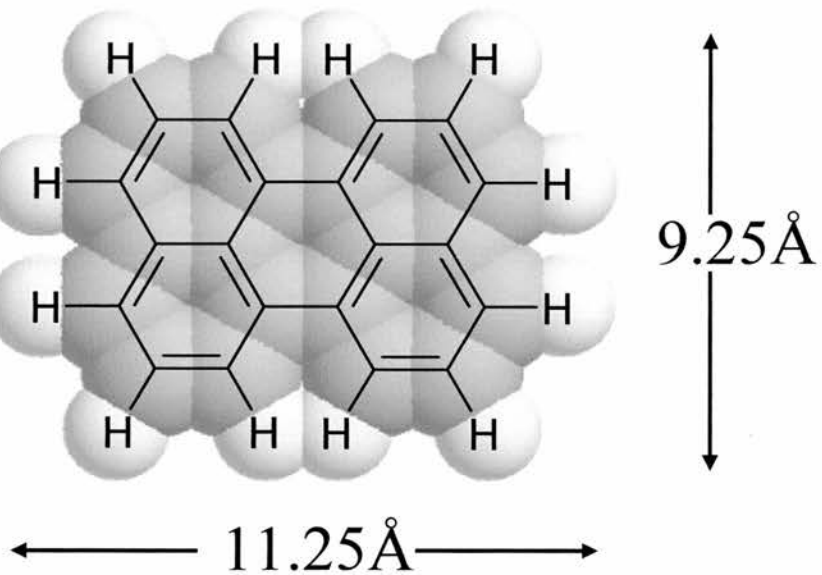

Fig. 7 Perylene: Molecular dimensions include Van der Waals radii. M_r = 252.31g

Early investigations into perylene suggested that its electronic structure is more like that of two naphthalene units with two C-C single bonds joining them[78] i.e. the de-localised π-

electron system is better considered as two parts which may have implications for the molecule - surface interactions. Subsequent modelling of the electronic structure suggests that this is not the case and the central bonds may elongate to prevent distortion in the planarity of the molecule[79]. This would give a single aromatic system spread across the whole molecule. The molecular structure and dimensions are shown in Fig. 7.

Perylene also occurs in two crystal forms, the α and β form (Table 2). The α-form has molecules paired in dimers in a herringbone structure. The β-form has a similar herringbone structure but is based on monomers instead of dimers as shown in Fig. 8.

Table 2 Crystal structures of α and β Perylene

	α-phase[78,80]	β-phase[81]
Space Group	$P2_1/a$	$P2_1/a$
a	11.27Å	11.27Å
b	10.82Å	5.88Å
c	10.26Å	9.65Å
β	100.55°	92.1°

The β-phase of perylene is only metastable at room temperature and above 140°C it converts to the α-phase. The two structures are similar, apart from the b dimension, which in the β-phase is approximately half that of the α-phase due to the structure only containing two monomers instead of two dimers.

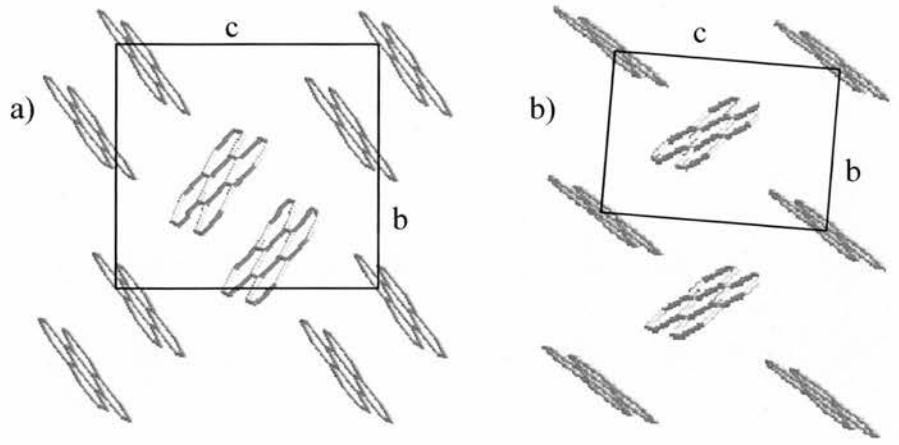

Fig. 8 a) Alpha perylene: $P2_1/a$, a=11.27Å, b=10.82Å, c=10.26Å, β=100.55° and b) Beta perylene: $P2_1/a$, a=11.27Å, b=5.88Å, c=9.65Å, β=92.1°

Compared to PTCDA, little work has been carried out on the structure of perylene adsorbed on surfaces. A NEXAFS study of perylene on Si(111)[82] suggests that the molecules deposited on the surface are all flat lying: layers up to ~50Å were grown. While PTCDA films are generally observed to grow in the bulk crystal structure, this cannot be the case for perylene on Si(111) as both the alpha and beta phases have molecules that would be significantly tilted to the surface if the bulk structure were grown. Assuming that the structure grown is not amorphous then it must be a new structure regardless of the preferred bulk plane orientation with respect to the substrate. Grown on Cu(111), the perylene molecules are aligned along the <110> directions of the surface[83]. As expected this give three separately ordered rotational domains due to the six-fold symmetry of the (111) surface. The molecules are suggested to align with the long edge of the molecule along the <110> direction, although the relatively poor resolution of the STM images and the almost square shape of the molecule make it difficult to confirm. The choice of the Cu(110) surface for our experiments addresses this problem as there can only be one domain if molecules align along the <110> direction with a rectangular unit cell.

Tetracene

Tetracene has a slightly different structure to the previous two molecules although it retains the D_{2h} symmetry. The four benzene units form a long straight molecule (Fig. 9). As it is of similar molecular weight and functionality as perylene, it is expected to behave similarly in terms of substrate interactions and deposition temperature. It also has a similar de-localised π-electron system that the other molecules have.

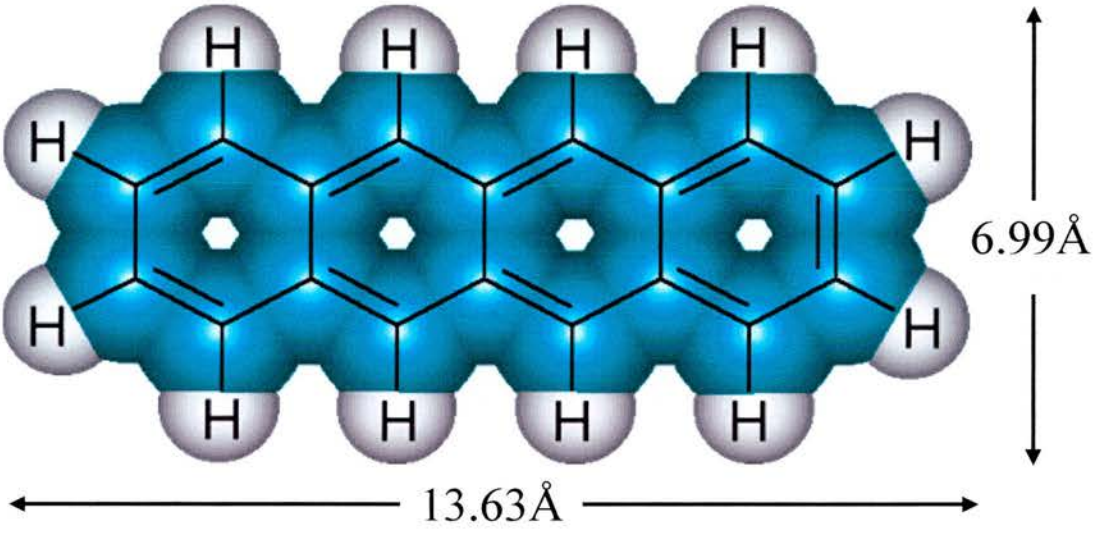

Fig. 9 Tetracene: Molecular dimensions include Van der Waals radii. M_r = 228.29g

Like perylene, relatively little work has been done on tetracene adsorption[84,85,86] compared to PTCDA. The polyacenes as a family have been investigated as isolated molecules and bulk solids for a number of years[87,88]. As mentioned before, anthracene was the photo-conductor in the first ever Xerox machine, indicating the molecules have optical and optoelectronic properties that may be of interest.

The most studied of the family is pentacene, the five-ringed analogue of tetracene. On Cu(110) it has been shown to have an extremely high degree of ordering, aligning along

the <110> direction and forming long, uninterrupted rows in the <001> direction[89]. The molecular spacing is governed by a combination of the molecular size and the copper row spacing. The molecules are only 7.2Å apart which is only slightly bigger than the quoted molecular width of 6.5Å (6.99Å by my Hyperchem calculations) i.e. the molecules try to close pack but the structure is relaxed slightly by the important molecule - substrate interactions. Pentacene has also been used in electronic devices such as TFTs (thin film transistors) although these use the bulk crystal, not thin films[7,90].

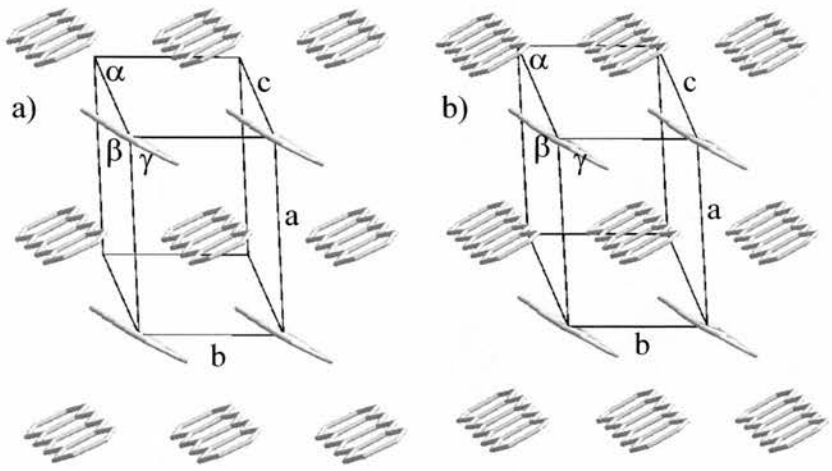

Fig. 10 a) Tetracene and b) Pentacene bulk crystal structure (crystal data from refs[91,92] and is shown in Table 3)

As can be seen in Fig. 10, the bulk crystal structures of the two molecules are almost identical as would be expected from two such similar molecules. Due to such similarities, tetracene and pentacene would be expected to display similar characteristics when deposited onto a surface. It should be noted that as perylene, but unlike PTCDA, tetracene has no plane common to all the molecules in the bulk crystal structures. This increases the likelihood of thin film growth leading to a novel structure and properties.

Table 3 Crystal structures of tetracene and pentacene[93]

	Tetracene[91]	Pentacene[92]
Space Group	P $\bar{1}$	P $\bar{1}$
a	7.98	7.90
b	6.14	6.06
c	13.57	16.01
α	101.3°	101.9°
β	113.2°	112.6°
γ	87.5°	85.8°

Ultra-High Vacuum (UHV)

The majority of techniques to be used in this project involve Ultra-High Vacuum (UHV). UHV is used to ensure that the samples under investigation are kept as clean as possible for as long as possible. It also allows low energy and ion based techniques to be used without interference from gas phase scattering. UHV chambers are large, Austenitic stainless steel structures usually constructed with flanges for the attachment of view-ports and analytical apparatus[94]. The flanges are sealed with gaskets of oxygen free copper, as the vapour pressure of rubber is too high and would prevent a good pressure being achieved due to continuous out-gassing.

Vacuum chambers are pumped using a variety of techniques to provide as good a base pressure as possible. The initial pumping stages are carried out by rotary pumps to a pressure of 10^{-3} - 10^{-4}mbar. Once these pressures are reached, the systems can be pumped by turbo pumps (high speed, rotary vane pumps) or diffusion pumps. These allow a chamber to reach UHV pressures - around 10^{-10}mbar. Rotary pumps and turbo pumps all contain moving parts that can interfere with scanning probe methods through the presence of vibrations. To overcome this, ion pumps and titanium sublimation pumps are required, as they have no moving parts[95]. A good base pressure is considered to be 10^{-10} - 10^{-11} mbar. To reach this pressure by pumping alone would take many weeks due to the extremely slow pumping speed of certain contaminants (principally water). To remove water in a time-scale that is convenient, it is necessary to bake the chamber. Baking overnight at temperatures of over 100°C is sufficient to remove the water from the system. Any

increase in temperature will facilitate the removal of water from a UHV system. At higher temperatures (over 200°C), damage may be done to components of spectroscopic instruments within the systems. A balance must therefore be struck between a high enough temperature to remove water at a satisfactory rate but low enough to prevent damage. If the organic samples are to be baked *in situ* to improve purity, caution must be taken to remain below the sublimation temperature to prevent contamination to the system or complete removal of the material. In our systems, we typically bake at 120°C to 150°C.

As UHV chambers are extremely finely engineered, problems can arise. Principally, leaks from atmosphere (due to improperly sealed gaskets or faulty valves) or "dead" (unpumped) spaces can lead to surface contamination such as oxygen. As will be discussed later, this extra surface modification can give rise to interesting structures of adsorbed molecules

X-Ray Photoelectron Spectroscopy (XPS)

XPS is a method of identifying what atoms are present in a surface and in what proportion with other atoms present. It can also provide some structural data. Individual photons of a specific energy are generated by firing a beam of electrons of many keV at anodes made of a particular metal. The most commonly used are aluminium (1486.6eV) and magnesium (1253.6eV). It is important to have two different anodes as it allows one to distinguish photoelectron peaks from Auger peaks (photoelectron peaks move as their energy is relative to that of the photon that excited them, Auger do not as they are caused by a decay process that is not dependent on the photon energy - when displayed as kinetic energy: the reverse is true if displayed as binding energy). Using two anodes allows easy identification of Auger peaks and also allows photoelectron peaks to be analysed at a second position if the first overlaps with an Auger peak.

The beam of photons is passed through a thin window of aluminium foil to remove stray electrons. The photons are then directed onto the sample, where they penetrate many hundreds of nanometres into the surface. This leads to emission of electrons from the core and valence shells of the atoms in the surface (Fig. 11). These excited electrons can only pass through a few nanometres of the sample before losing sufficient energy and being re-absorbed, making XPS an extremely surface sensitive technique. The kinetic energy of the electrons that are emitted from close enough to the surface to escape without loss of energy can then be detected by the analyser. The vacuum level is the "zero kinetic energy line" i.e. the point at which there is no longer an interaction with the atomic nucleus. The vacuum level tends to be 3-6eV above the fermi level or HOMO[96].

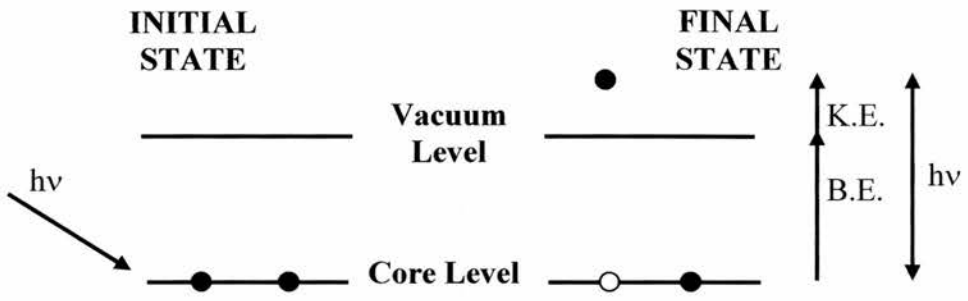

Fig. 11 Energy levels involved in XPS[96]. Photon (hν) of specific energy excites core electron. It requires Binding Energy (B.E.) to reach the Vacuum level. Remaining energy is measured Kinetic Energy (K.E.).

As a very specific energy is required to remove electron from a specific core level (Equation 1), the exact identity of the atom can be determined from well established tables. As the energy of electrons varies a little depending on the environment of the atom, multiple peaks or small shifts in binding energy can give a little information on the bonding present within the sample.

Equation 1[95]

Kinetic Energy (K.E.) = hν - Binding Energy (B.E.)

The conservation of energy expressed in Equation 1 states that the binding energy is the exact energy required to remove an electron from its initial core level to the vacuum level and the kinetic energy is what is left from the photon energy put into the system. So by scanning an energy region of 1200eV to 5eV with a short dwell time on each specific energy, a spectra of all the separate kinetic energies can be displayed. Since kinetic energy depends on hν and the primary characteristic of a core level is the binding energy,

Equation 1 is employed to present the spectra as electron intensity versus binding energy. Auger emission is a two electron, one hole process, where one electron is emitted in a primary process leaving the hole. An electron from a higher orbital decays, fills the hole and a second electron is emitted[95]. Auger peaks tend to be wider than photoelectron peaks and in groups due to the multiple combinations of decays and emissions that can occur. As this process is not dependent on the energy of the photon electrons, the peaks do not shift in kinetic energy depending on the anode used.

As the energy of valence electrons is less well defined (They are shared between atoms therefore they are not atom specific), they are not seen as sharp peaks, but are smeared out across a wide range. This makes them a lot less useful for elemental qualitative and quantitative analyses by XPS.

In this project, XPS has been used to provide an indication of layer thickness by comparison of overlayer peaks with substrate peaks. Secondly, peak shape of the bulk sample compared with that of the initial layers might give indications of the bonding process of the molecules to the surface. Film thickness can be determined in two ways. The first requires a significant difference in the molecular structure of the first layer (e.g. PTCDA losing the anhydride oxygen atoms on copper). As the second layer grows, differences should be seen in the peak positions and shapes. The second involves plotting peak intensity versus time. At thickness increases, if growth is on a layer by layer basis, the intensity gradient should decrease with time. The onset of a new layer of growth should correspond to a gradient change, allowing thickness to be calibrated. As layer thickness increases, binding energies of peaks can shift to higher energies as electron contributions from the substrate decreases. This can also give indications of film thickness.

XPS Transmission Function

To increase the accuracy of quantification from XPS spectra, the transmission function of the spectrometer was calculated under the same conditions that the experimental results would be collected. This allows inconsistencies in the specific photon energies of our system to be calibrated to allow accurate quantification of samples. The XPS of gold (Au 4f7/2, Au 4f5/2, Au 4d5/2, Au 4d3/2, Au 4p3/2, Au 4p1/2 and Au 4s peaks), copper (Cu2p1/2, Cu2p3/2, Cu3s, Cu3p1/2 and Cu3p3/2 peaks) and silver (Ag 3s, Ag 3p1/2, Ag 3p3/2, Ag 3d3/2, Ag 3d5/2, 4s and 4p3/2 peaks) were recorded as they are easy to clean (and keep clean) and they have peaks across the entire binding energy range. The wide range of peaks is required to cover the entire binding energy range to provide a more accurate calibration. For each individual element, binding energy was plotted against the peak intensities after allowing for cross section effects and the best straight line was fitted through them. This straight line was then normalised so that the binding energy of 286eV equalled 1 (corresponding to the C1s peak as it has a relative sensitivity factor of 1). This was repeated for the other two elements. From the three straight lines, a best fit is generated to give the transmission function (Fig. 12, Equation 2).

Equation 2

Transmission Function Correction = 1.40399 - (0.00141 x Binding Energy)

The binding energy of any XPS peak can be fed into this equation to produce a correction factor. The peak area is then divided by this correction factor to produce a more accurate result. Once divided by the photo-ionisation cross sections (relative sensitivity factors) an accurate percentage composition should be produced.

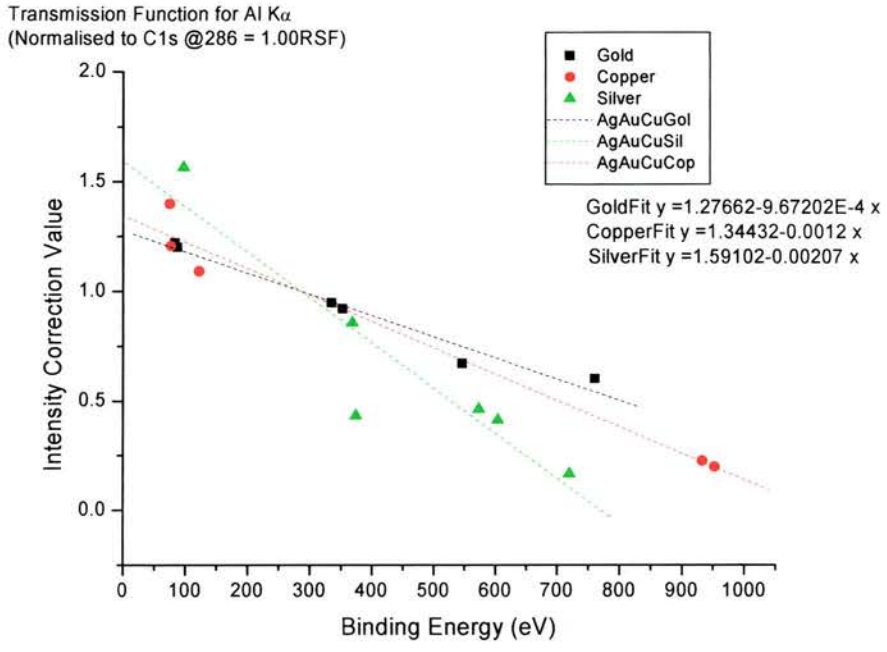

Fig. 12a XPS Transmission Function: data. Gold, Silver and Copper peaks are used to calibrate the spectrometer. Data is fitted with best straight line for each data set.

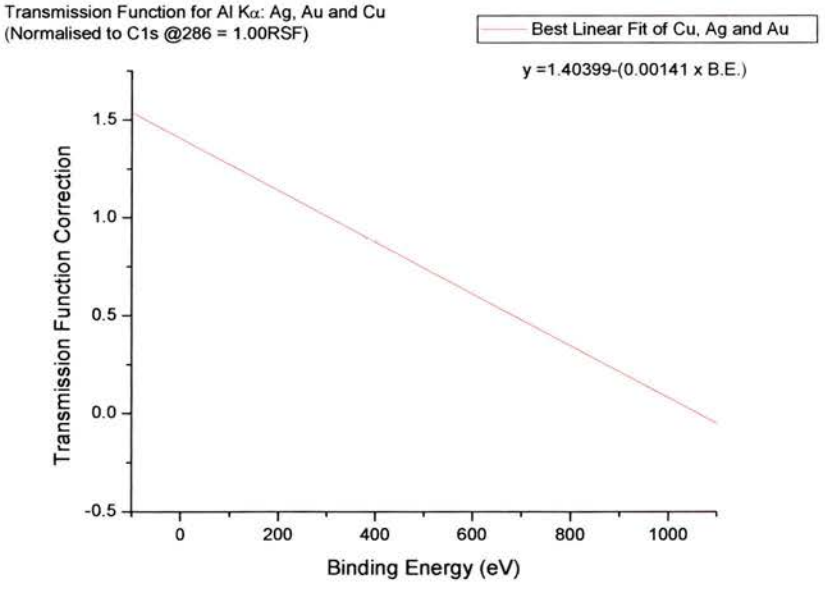

Fig. 12b XPS transmission function. The best straight-line fit through all the best straight-line fits of the Gold, Silver and Copper data gives the Transmission Function. y= 1.40399 – (0.00141 x B.E)

Low Energy Electron Diffraction (LEED)

Low Energy Electron Diffraction (LEED) is one of the most widely used tools in surface science. It can be used simply to provide spot positions which relate to the size, shape, and orientation of the unit cell of the surface, or intensity/voltage curves can be related to computer simulations at known electron beam incidence to give exact atomic positions. A focussed electron beam, of well-defined energy, is aimed onto a surface and then scattered by the atomic cores present. Well-ordered surfaces give good constructive interference of the scattered electrons at well-defined directions. The scattered electrons are then accelerated by a charged phosphorus hemispherical screen so they have sufficient energy to produce diffraction spots when they strike it[97] (Fig. 13).

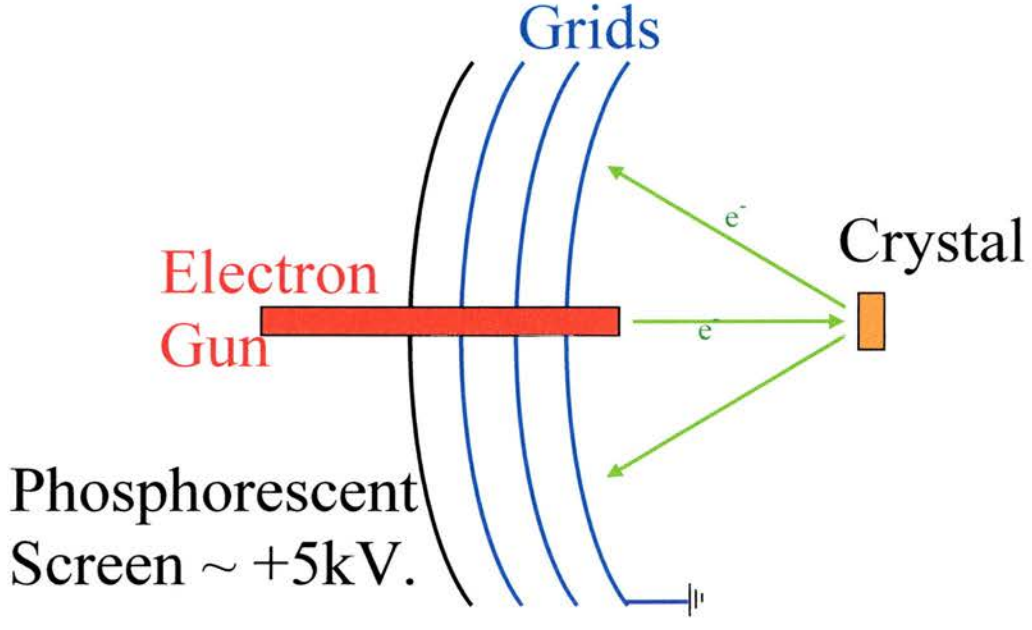

Fig. 13 Low Energy Electron Diffraction (LEED) schematic

The voltage of the two grids in front of the screen can be varied to tune the scattered electrons to provide a more defined LEED pattern. The negative voltage of the grids are set slightly below that of the electron beam to prevent any inelastically scattered electrons

reaching the screen. If the negative voltage of the grids is higher than the negative voltage of the scattered electrons, the electrons are deflected, reducing the brightness of the background[98].

As the electrons scatter from an ordered surface, at certain angles, the path difference of the scattered electrons differs by an integral number of wavelengths (Fig. 14).

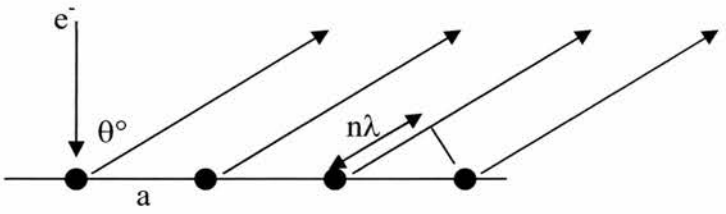

a = inter atomic distance
n = integer
λ = wavelength

When $n\lambda = a \sin \theta$, diffraction spots are seen.

Fig. 14 Scattering of electrons on a one-dimensional chain[96]. When n is an integer, the wavelengths of the scattered electrons constructively interfere leading to diffraction spots on a LEED screen. When n is not an integer, the waves destructively interfere and no spots are seen.

At angle θ, where n is an integer, the electron beams constructively interfere leading to spots on the LEED screen The angle that leads to an offset of one wavelength is known as the first order spot, two as second order etc. LEED is sensitive of ordered areas of around 100Å due to constraints of the electron beam (aperture and beam focussing). The more highly ordered the surface, the sharper the spots will be. If looking at an adsorbate or clean crystal surface, domains over 100 Å will produce spots that are sharp. Depending on the level of coverage, the overlayer spots may be seen in conjunction with the substrate spots

or may obscure them completely. If there is disorder or the domains are under 100Å, then the spots will become more diffuse or will not be seen at all (high coverage, low order will obscure substrate spots). A highly ordered surface will also give good contrast between the spots and the background[97]. If the ordering is poor the background will be much brighter. LEED can be used prior to carrying out experiments to ascertain whether or not the substrate to be used is clean and has large, ordered domains. It can also provide an extremely quick method of establishing whether or not an ordered structure has been produced before carrying out more time consuming experiments such as STM. If an ordered LEED pattern is recorded then the geometry and spacing of the overlayer spots with respect to those of the substrate are vital in deducing the unit cell parameters.

Vibrational Spectroscopies: Reflection/Absorption Infra-Red Spectroscopy(RAIRS) Transmission Infra-Red and Electron Energy Loss Spectroscopy (EELS)

Vibrational spectroscopies are extremely important in many forms of analytical science as they can identify the sorts of bonds that exist within or between molecules. This becomes even more important on a surface due to the surface selection rule (Fig. 15)[96]. Reflection Absorption Infra-Red Spectroscopy (RAIRS) and Electron Energy Loss Spectroscopy (EELS) both rely on the premise that atoms within every molecule are vibrating in a number of different ways and directions (in-plane, out-of-plane etc).

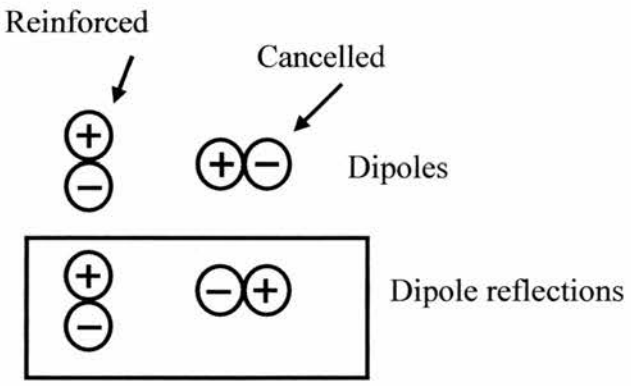

Fig. 15 Surface Dipole Selection Rule. When a dipole is perpendicular to the surface, the reflected dipole causes an overall reinforcement of the initial dipole. If the dipole is parallel to the surface, the reflected dipole is the opposite of the original so cancels it.

On a metal surface any dipole close enough to have an interaction will induce a dipole in the substrate that is best thought of as an image (i.e. the induced dipole is the reflection of the original). The image dipole arises from the response of the metal valence electrons to

the external dipole and is particularly efficient at vibrational frequencies that are well below the metal plasmon frequency. If the dipole is perpendicular to the surface, the dipole and its mirror image have the same directional vector and are therefore are reinforced. If the dipole is parallel to the surface, the mirror image has the opposite directional vector and cancels out the real dipole.

In EELS, an electron beam of a specific energy is fired at a sample in UHV and the kinetic energy of the scattered electrons are measured by an energy analyser. The majority of the electron scatter elastically ($E=E_o$) and give rise to a large peak (the elastic peak) but a small number of electrons undergo a discrete energy loss (or gain) due to specific bond vibrational modes and can be seen as peaks at lower (or higher) energies. The EELS spectra obtained in this project have all been recorded with a specular geometry, i.e. incidence angle = exit angle. Due to the surface dipole selection rule, only vibrational modes whose dipole change is perpendicular to the surface can be seen and these bands are quite intense. dipole changes parallel to the surface are not seen. EELS also has an impact scattering mechanism where all bands can be seen but usually at much lower intensity than the dipole allowed modes. These modes are best observed away from the specular direction.

RAIRS causes a similar excitation of vibrational modes of molecules, but the energy comes from the absorption of infrared radiation. Older, dispersive systems used a beam that scanned the photon frequencies and compared the intensity as a function of frequency with that of a beam being passed through a reference cell at the same time. To collect a single spectra could take around four minutes for a transmission spectra or much longer for RAIRS, with relatively poor intensities. Newer IR spectrometers, Fourier Transform

Spectrometers (FT-IR) use only one infrared beam that contains all the information of the sample (Fig. 16).

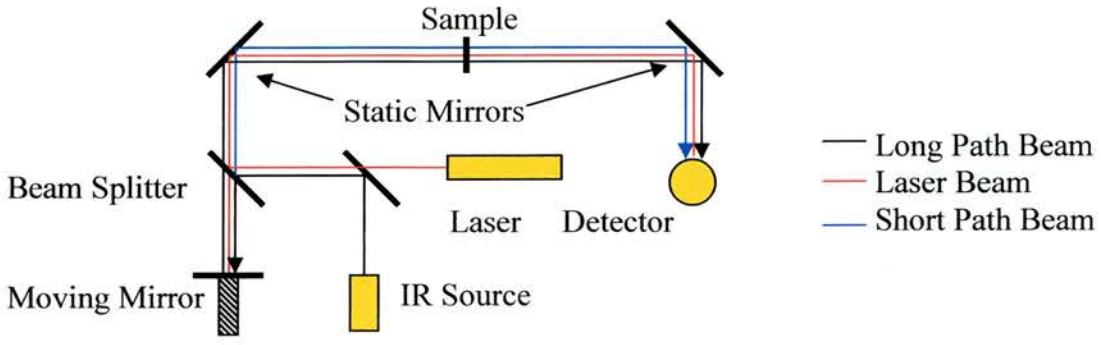

Fig. 16 Schematic of FT-IR spectrometer[99]. the IR beam is split with one beam traveling further via a moving mirror. The precise pathlengths are calculated using a fixed frequency laser allowing Fourier Transform to calculate intensity for each frequency.

The IR beam passes through a beam splitter, one beam going to the sample, the other to a moving mirror before going to the sample. When they recombine at the beamsplitter, they constructively or destructively interfere so intensity can be measured across the whole frequency range. As the mirror moves, the precise path length of the two beams can be calculated (using the fixed frequency laser beam as a reference)[100]. The spectrometer records the intensity at each known path-length and the computer processes this information using a Fast Fourier Transform procedure to calculate the intensity at each frequency and produce a single beam spectra. This allows a sample to be collected in seconds instead of minutes meaning many more scans can be run in the same time leading to significantly lower background noise levels and increased chance of detecting extremely small peaks.

For this project, it was considered useful to record the IR spectra of the various free molecules. To achieve a sufficient level of transparency, the molecules were ground with KBr to make a 10% mixture. This was then pressed into thin translucent pellets that were ideal for IR transmission experiments. As the pellets allowed a relatively intense signal to be collected, the DTGS (Deuterated TriGlycerine Sulphate) detector was used. It is not very sensitive to small intensities but retains sensitivity to a lower wavenumber(~400cm^{-1}). Transmission spectra were collected from 410 - 4000cm^{-1} over 128 scans. These spectra were reprocessed against a unique background of a signal recorded through the atmosphere in the analysis chamber using the same experimental parameters. The reprocessed spectra show all IR allowed vibrational frequencies in the molecules. These peaks were assigned by comparison with literature results[101,102,55] and are discussed in the relevant results section.

Once the spectra of the molecules has been recorded and assigned, Reflection/Absorption Infra-Red Spectroscopy (RAIRS) can be carried out. In RAIRS the molecules are deposited onto a surface and instead of the infrared beam being passed through the bulk of the sample, it is scattered off the surface at a grazing angle of ~4° (Fig. 17).

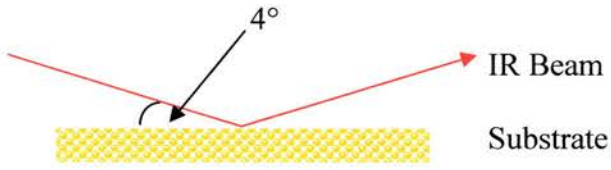

Fig. 17 RAIRS grazing angle. In our experiments, a grazing angle of 4° is used.

Calculations show the optimum angle to be 2°[103], but this may vary due to the exact properties of the metal substrate. At smaller grazing angles, the signal is masked by "background reflections" from the substrate so the IR signal is seen to drop off sharply.

The ideal spectrometer would carry out scans across a range of grazing angles from 2-10° but this is would be experimentally difficult achieve and impossible in our case. On Copper, 4° offers a good compromise between intensity and quality of signal. As the intensities from the molecules are tiny, the DTGS detector was unsuitable so an MCT (Mercury Cadmium Telluride) detector was used instead. It is only sensitive down to $700cm^{-1}$ but when cooled with liquid nitrogen, it is capable of recording extremely low-level intensities.

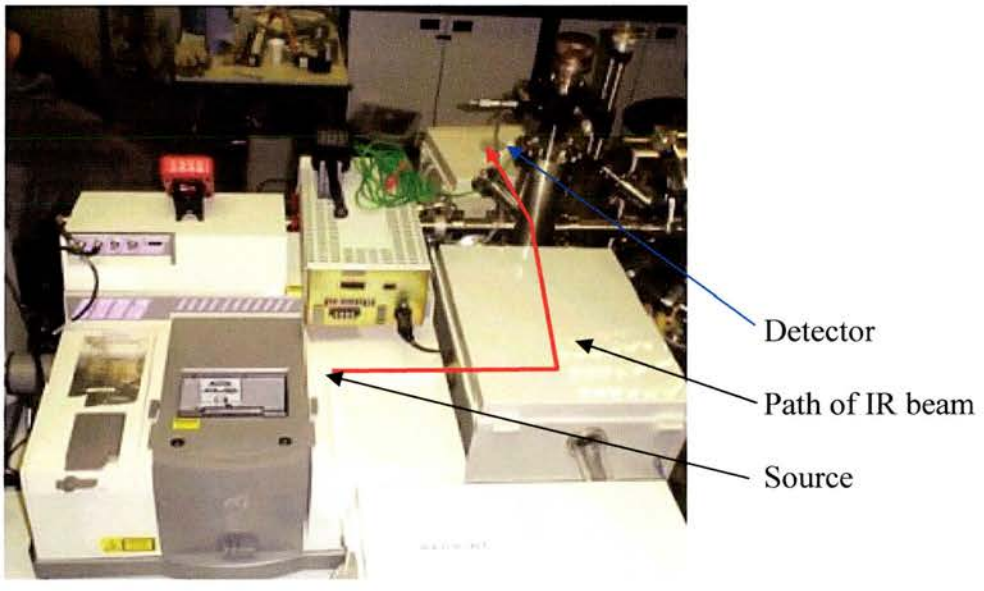

Fig. 18 RAIRS apparatus: Nicolet Magna 860 coupled with UHV chamber containing substrate and chemical deposition apparatus.

The pathlength of the IR beam in the apparatus used is only 100cm from the port on the side of the spectrometer (fig. 18). The shortness of this distance reduces the amount of signal degradation as the beam travels to the detector. The atmospheric pressure sections of the system are enclosed and mated to the UHV RAIRS with airtight seals and are purged with either dried air or nitrogen from a gas cylinder or liquid nitrogen boil-off. Purging the

system reduce stretching bands at 2300cm^{-1} arising from atmospheric CO_2 and the various water bands at 1300-1900cm^{-1} (O-H bending [region] coupled with rotation in gas phase [fine structure within region]) and 3500-4000cm^{-1} (O-H stretching bands)[104]. Purging of at least twelve hours was required if using dried air after opening the system until experiments were carried out. This time was greatly reduced if nitrogen was used.

The substrate was mounted in a section of UHV chamber with access to standard analytical tools such as LEED, mass spectrometry and STM. The sample in the RAIRS can be heated to 500°C or cooled with liquid nitrogen or helium to extremely low temperature. The sample, when in position to be analysed by the RAIRS, is in direct line of sight to the dosing apparatus. These combined features allow experiments to be carried out involving both temperature dependent and coverage dependent experiments. As the signals from RAIRS are extremely weak, it is preferable to spend a significant amount of time optimising the signal collected from the surface by fine-tuning the exact position of the sample. When the experiments are run, 256 scans were collected for each single beam spectra. All the spectra are processed against a background spectra collected under the same conditions at the start of the experiment.

Scanning Tunnelling Microscopy (STM)

STM was first developed in 1981 by Binnig and Rohrer at IBM who later went on to win the Nobel Prize for Physics for its invention[105]. Whilst being one of the newer surface science techniques, it is also one of the fastest growing and most useful. Until its invention, there was no way to easily image a surface at the molecular or atomic level. STM can even produce information on subatomic structure of the surface under analysis. The wavelength of light ~300nm is the main constraining factor in standard optics. Anything smaller does not reflect energy from the light and is not optically visible. Electron microscopes are available but do not have sufficient resolution to provide the fine sub-atomic detail that STM can achieve.

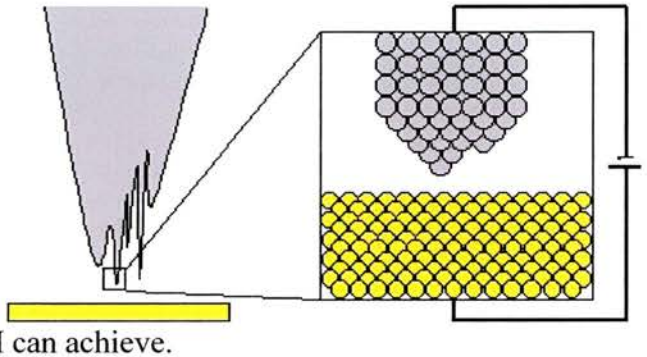

Fig. 19 STM tip (macroscopic and microscopic views). An STM tip, typically tungsten, is produced by electrochemical etching in KOH solution. The resulting tip should be atomically terminated to produce STM images.

STM works by creating an image using the electronic structure of the surface. A tip, generally tungsten (Fig. 19), is manipulated across the surface by piezo-electric motors and a current is passed through it to create a circuit. Piezo-electrics allow extremely small (sub-

Å) movements to be made that combined with current changes allow a picture of the surface to be produced[106]. For STM to succeed, the substrate under investigation must be a conductor or semiconductor so that current may flow.

An STM tip is produced be electrochemical etching of a tungsten wire with a solution of sodium or potassium hydroxide (~2M although exact concentration is not critical). The tungsten wire is placed through the centre of a tungsten loop and immersed in the hydroxide solution. A power supply is connected to the wire and loop and a current is passed through the circuit. The wire being etched is the positive electrode and the loop around it is the negative electrode[107]. Tungsten atoms enter the solution as W^{4+} ions, the $4e^-$ then react with water to provide $4OH^-$ and $2H_2$ (g). A visible sign that etching is successfully taking place is the evolution of gas bubbles at the positive electrode. Over time, the wire can be observed to becoming increasingly thin at the point around which the loop is situated. Eventually, the weight of the wire and tip holder into which it is mounted cause the wire to stretch and snap. This should produce an atomically terminated tip.

An STM can be run in either constant current mode or constant height mode. In constant current mode, the tip is moved in an out from the surface as it scans to maintain a constant current between the tip and the surface. A computer translates these movements into an image. In constant height mode, the tip travels back and forth without moving perpendicular to the surface. As the topography of the underlying surface changes, differences in the current passing between the tip and substrate should be observed[106]. It is these changes that are translated into an image in this mode. For this project, all STM images were collected using the constant current mode.

The resolution of the images can be altered by changing the gap voltage (the bias applied to the surface), the feedback setpoint (tunnelling current), and the loop gain (slows the feedback loop and reduces tip oscillations). However, good resolution images can only be

achieved with a high quality tip. An STM tip must be terminated with a single atom so that the current flows through an extremely localised point. If the tip has a few atoms at the same height then the current flow will be spread across this area and it will be impossible to distinguish surface features. In rare cases, a double tip can be produced where the tip has two distinct single atom points at the same height but they are sufficiently far apart that they can both produce high-resolution images. The effect is a shadow image.

In experiments of PTCDA on Si(100) conducted in St. Andrews[108], distinct duplications can be seen to the side of each of the islands (Fig. 20). This is explained by having a double tip a few tens of nanometres apart. The second tip seeing what the first did shortly after. It is extremely rare that images of this resolution would be collected to illustrate this point so clearly.

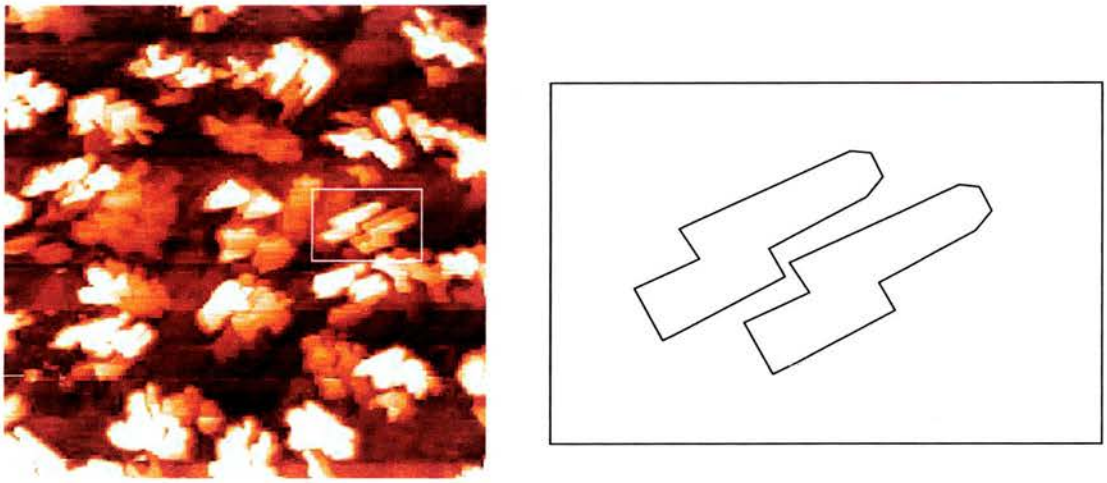

Fig. 20 STM of PTCDA on Si(110) recorded with "double" tip. The dual image, as indicated by the outline, indicates that there must be two termination points on the tip in use leading to two points on the surface being scanned simultaneously.

As STM works by imaging via a flow of current, induced by voltages typically of 0.01 - 2V, it is not the nuclei of the atoms involved that are seen but the associated electron

orbitals. The tip can be set to a positive or negative bias. If negative, electrons flow from the tip into the sample so the image formed is of the empty states of the sample, if positive it is of the filled states. If molecules are being imaged, it may not be apparent which part of the molecule is being imaged or what orientation it is in. Molecular orbital calculations of adsorbed molecules and in some cases even of free molecules can be used to establish where the HOMOs and LUMOs are within the molecule and therefore the structural orientation.

If at any point, current can no longer flow the computer has no reference to control tip height. This can occur for a film deposited onto a substrate that is sufficiently thick to insulate against current flow. This can cause the tip to crash into the substrate resulting in damage to the surface, tip or piezo-electrics.

In this project STM was used to image thin organic films in the range of sub-monolayer to ~20ML.

As STM images are analysed on computers, there are some constraints as to how the images are processed which introduce errors into the measurements. The images are displayed as a set number of pixels, which in turn define the points the computer uses to provide measurements e.g. a measurement from pixel a to b may be 1.87nm but a to one pixel further away from b may be 2.14nm. This margin for error or spatial resolution can be quantified as the total width of an image divided by the number of pixels in that width. This in turn affects how measurements are taken from the images. If the dimension of a feature is taken then it has this standard error. It follow therefore that if the measurement is recorded as an average over ten of the features in a line, then the error would also be divided by ten, making the result far more accurate.

Auto-Correlation of STM Images

Auto-Correlation of an STM image takes each peak of an intensity map and plots it in relation to all other peaks. This then provides an image that emphasises the periodic information that was hidden by random elements within the original image. These auto-correlation graphs tend to allow measurements to be averaged over a greater number of features decreasing the error in measurements and therefore far more useful data for construction of an accurate structural model.

Mass Spectrometry

Mass spectrometry is one of the most useful and versatile tools available to the surface scientist. It can be used in establishing UHV conditions - providing information on the initial levels of contamination within a system or indicating that there may be a leak if oxygen is present. If the chamber does have a leak then mass spectrometry is usually used in conjunction with a squirt of acetone on the flanges to isolate the location. It can be used to monitor out-gassing of chemicals for deposition or filaments within the chamber to ascertain when acceptable levels of contamination are present. Mass spectrometry can indicate whether a chemical has reached an appropriate deposition temperature or vapour pressure, as its fragments will appear in the spectra. It can also be used in desorption experiments to record molecules and fragments leaving the surface under the influence of heat to provide thermodynamic information on the formation boundaries of the initial monolayer and subsequent layers. All these investigations are carried out using the same simple apparatus.

A mass spectrometer works by producing ions of the parent molecule and ions of fragments of the molecule. The sensitivity available within these systems is sufficiently high that they can detect the smallest amounts (partial pressures of generally as low as $1x10^{-11}$mbar or $1x10^{-14}$ for a top of range system[109]) of contaminants (e.g. oxygen) that may interfere with the experiments or pick up desorption from sub-monolayer coverage of a surface.

The filament in the mass spectrometer ionises the molecules passing through it before they enter the quadrupole mass analyser (QMA)[110]. In this, there are four conducting rods, paired diagonally, that by switching the charge can accelerate the ions towards the detector. As the switching occurs, it has an increasing effect on the motion of the ion

causing it to undergo greater acceleration and therefore greater oscillation in its path of travel[97].

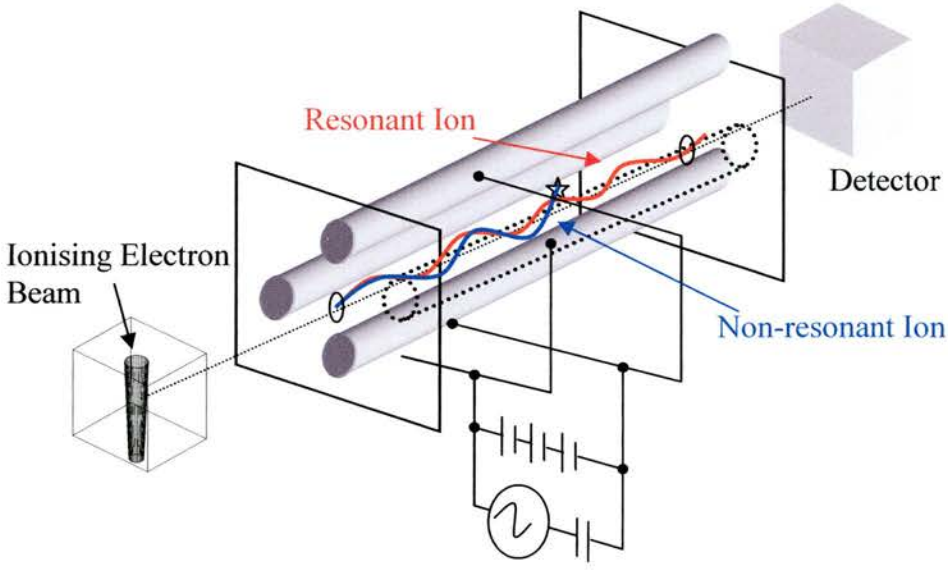

Fig. 21 Quadrupole Mass Analyser (QMA). After ionisation, the ions spiral down the quadrupole being accelerated at different rates depending on their masses. Only ions of a particular mass will reach the detector[110].

The amplitude of the oscillation of the ion increases until it hits the electrode and becomes neutral again. The lighter the ion, the fewer number of cycles before it hits the electrode. Ions that are not collected by the electrodes travel the full length of the QMA to the detector. The QMA therefore can be tuned so that only selected ions of the correct mass travel the full length of the quadrupole to the analyser. This allows both collection of a single mass or a collection across a wide range of masses, both of which are highly useful.

Temperature Programmed Desorption (TPD) – by fragment, pressure and vibrational mode

As discussed in the introduction of this thesis, the molecules under investigation tend to remain intact when deposited onto surfaces. XPS results of PTCDA on copper[111] indicate a loss of the anhydride oxygen to form covalent bonds with the surface that would be quite tightly bound. Subsequent layers are bonded by intermolecular interaction to the layer below and are significantly less tightly bound. Even if the initial layer is not covalently bonded, the interactions are usually measurably stronger than those of subsequent layers due to increased electron density on the surface, i.e. molecule-molecule interactions are usually weaker than molecule-substrate interaction. By desorbing any film by the application of heat, the weakly bound multilayers should desorb at a lower temperature than the monolayer. The transfer of molecules from the solid phase to the gas phase can be measured by a number of routes to provide structural or stoichiometric information.

By applying energy into the surface as heat with a controlled temperature ramp, an accurate correlation can be made between recorded signals and the temperatures at which they appear. By far the most common form of TPD is to record the molecular fragments produced by mass spectrometry. As the molecule may break up when desorbed (or the monolayer may fragment but the multilayer molecules may not), a number of signature peaks of the molecule are chosen and recorded for the entirety of the experiment. The area of a multilayer desorption peak is proportional to the number of layers present. The area of the monolayer peak (if a complete monolayer were grown) should remain the same irrespective of how thick the subsequent layer is. The ratio of these can be used to deduce the layer thickness (Fig. 22).

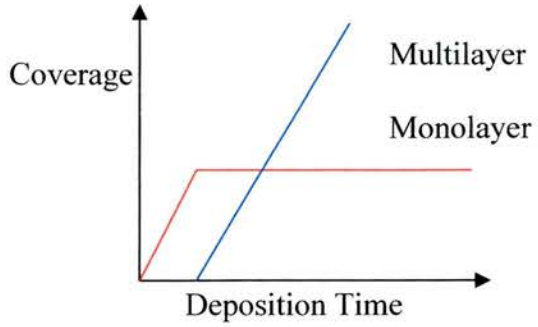

Fig. 22 TPD – Coverage or corresponding TPD signal as a function of deposition time. Under layer by layer growth conditions, peak corresponding to the first layer will grow then saturate. At the point of saturation of the initial layer, the peak corresponding to the overlayers will appear.

In cases where the mass spectrometer has difficulty detecting the molecular fragments, due to constraints in the detection limits since quadrupole/MS is less sensitive to heavy fragments, it may be possible to detect total pressure bursts at the multilayer and monolayer desorption temperatures. This may not be of use in determination of layer thickness but should accurately represent the desorption temperatures. In the event of the two desorption peaks overlapping, an alteration of the temperature ramp may separate them.

A third method is growth and desorption with continuous monitoring in RAIRS. The RAIRS spectra give structural information due to the presence or absence of vibrational modes. Following the intensity changes of these during film growth can indicate the completion of the monolayer and allow the determination of the spectra of a thick layer. If the substrate is then heated, the peaks get smaller as the layers desorb with multilayer peaks desorbing first followed by the monolayer peaks. If at any point during desorption, under the influence of a temperature ramp, the desorption ceases but peaks are still present, this indicates a significant change in the binding strength of the molecules. This is likely to be the point at which the entire multilayer has been desorbed, but not hot enough to desorb

the monolayer. Continued heating should see any remaining peaks removed (at the same higher temperature). Under the influence of heating, the peaks disappear as the molecules desorb.

There is evidence that fragments of the three molecules do remain on the surface. LEED investigations after TPD tend to show only substrate spots, but they are not as sharp prior to the experiments. With PTCDA on Cu(110), even after light Ar^+ bombardment and annealing, a subsequent film grew amorphously as opposed to the flat molecules that were observed before, indicating a significant level of contamination was still on the surface. Perylene and tetracene residues were easily removed, indicating that PTCDA is a far more tightly bonded molecule.

RAIRS TPD produces the most information of the three but is more difficult and time consuming to carry out but importantly it is not constrained by molecule size and related detection limit problems in a mass spectrometer. This makes the RAIRS method of most use in this project.

Luminescence

An integral part of this project is to investigate some of the properties of the films that have been grown. One of the main areas of interest in these molecules is that of display devices. For this reason we chose to investigate the light emitting properties of the films. Luminescence is the phenomena of a substance absorbing energy in some form and the re-emitting the energy as light (Fig. 23).

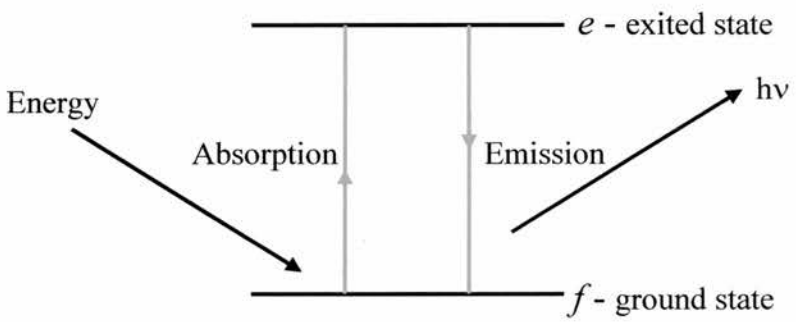

Fig. 23 Luminescence process[112]. The absorption of energy (light/heat/electrical) excites an electron to an excited state. As the electron decays to the ground state, energy is emitted in the form of light.

A molecule is excited from the ground state (*f*) to an excited state (*e*) by absorbing energy. The molecules then decays back to the ground state after time (t), emitting a photon of light as it does. The length of time that a molecule remains excited is important in defining the sort of luminescence involved. If t $\sim 10^{-8}$ seconds then the process is fluorescence, if emission is around a second or more, it is referred to as phosphorescence. In the range of 10^{-1} - 10^{-5} seconds it could be long fluorescence or short phosphorescence[112]. The process

can be established by temperature dependent studies (phosphorescence is temperature dependent, fluorescence is much less so).

The type of luminescence that a substance displays has an effect on what applications it is used for. If a substance has good phosphorescent properties then it would be better suited to ambient lighting applications e.g. back-lighting a mobile phone display. If it has good fluorescence then it would be better suited to a display device. We are not concerned specifically with what luminescent properties we observe, as applications for all sorts are available.

Photo-Luminescence

As the films studied in this project are grown in UHV, to remove them from the system to carry out property testing for device applications would compromise results with respect to the UHV characterised structure. Photo-luminescence, light produced by stimulation with light, was chosen as the first method due to the ease at which an *in situ* experiment could be set up. Samples were stimulated with a laser of known wavelength (InGaN diode laser - 408nm), which is in the ultra-violet (UV) region, just out of the range of human vision. This is advantageous as, when the laser is shone against a non-photoactive sample, nothing is seen at all. When shone against a photoactive sample, photo-luminescence could be clearly seen with the naked eye.

When a sample had been prepared, a fibre-optic cable for collection of the emitted light was moved so that it was ~5-10mm from the surface. The fibre-optic cable was mounted on linear drive so that it could be retracted during film deposition. The laser was aligned

externally from the UHV chamber through a glass view-port so that it pointed directly at the surface. The angle between the fibre-optic cable and the laser beam was ~45° but this could vary from system to system depending on the flanges available to set up the equipment (Fig. 24). To optimise the signal, the substrate was manipulated so that the normal was half way between the input and output so the angle of incidence and emission are equal (due to the physical constraints of some of the systems this is not possible so the closest compromise is used). With this set-up, the recorded spectrum contains a signal from the laser at 408nm. This is significantly lower than the wavenumbers of emission (500-700nm) so does not cause interference.

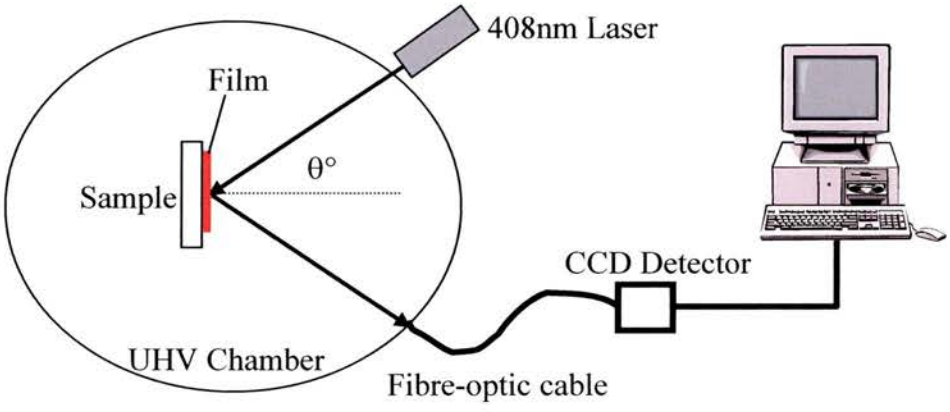

Fig. 24 Photo-luminescence schematic. UV Laser light was shone onto the substrate through a viewport. Emission was recorded via a fibre optic cable attached to a CCD detector. The resulting spectra was displayed and captured by PC.

The sample was irradiated by the 408nm laser and the light that was emitted was captured by a grating CCD detector for spectral display and recorded on a computer (Fig. 25). The set-up and capture times were extremely small, allowing these experimental recordings to be carried out extremely quickly. The photo-luminescence of a pre-grown film could be

collected in a few minutes. This allowed many data points to be collected during a film's growth with minimum disruption to the growth process, reducing possible contamination to the film and system.

The experiment could also be carried out *ex situ* allowing the comparison of films in UHV and those exposed to the atmosphere using the same equipment.

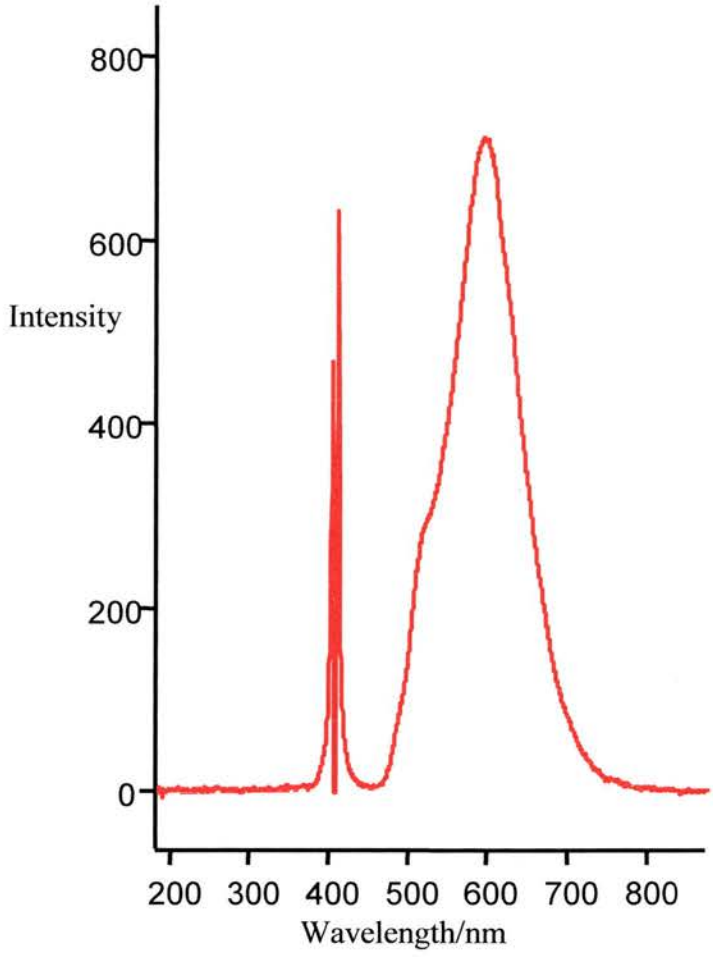

Fig. 25 A typical photoluminescence spectrum: Perylene on Cu(110). Peak at 408nm is UV laser. Photons in the range 470 – 730nm are the luminescence from a perylene thin film.

Electro-Luminescence

With the success of the photo-luminescence experiments, electro-luminescence experiments were attempted. Electro-luminescence is the stimulation of light by the application of an electric current. The experimental system was based on that of the photo-luminescence with some minor modifications to facilitate the stimulation of emission. The end of the fibre-optic cable was placed in a small glass sphere that had been coated with a thin layer of gold. Whilst the exact thickness of the gold was unknown, it was visible but translucent suggesting a thickness of 100-300nm. The glass sphere was isolated from the fibre-optic cable but was attached to an electrode. It was hoped that by moving the sphere (with the fibre-optic inside) into contact with the sample, a circuit would be formed. Passing a small current through this circuit would stimulate emission that could then be recorded (albeit at a lower intensity due to the gold film and glass) through the fibre-optic. Due to the input and output travelling through the same apparatus, it was possible to align it perfectly perpendicular to the sample, maximising any signal that may be achieved.

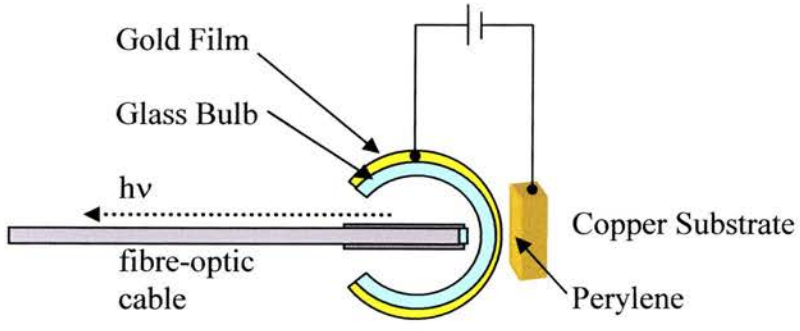

Fig. 26 Electro-luminescence experimental set-up. Gold film and copper substrate provide electrodes for perylene film. Emitted light was collected via fibre optic cable.

A thick film of perylene was grown on a Cu(110) substrate under the standard experimental conditions. Whilst its thickness was unknown, it was calculated to be in the order of a few tens on monolayers thick. LEED showed no spots, indicating a sufficient level of coverage. Photo-luminescence was checked visually with the laser, which confirmed the presence of a light emitting film. The sample was aligned and a digital voltmeter was attached to the gold sphere electrode and the sample mount electrode. The sample was slowly moved into contact with the gold sphere, confirmed by the continuity setting alarm. Resistance measured across the device was recorded at 11Ω. Low currents (10^{-2}A) and around 1.5V were passed through the device but the contact would break down. Localised heating of the sample at the point of contact causing the film to desorb probably caused this.

The experiment was repeated with liquid nitrogen cooling of the sample (~190K). After dosing of a similar thickness of film the experiment was carried out as before. Again, emission could be seen from the film when stimulated with the laser but, as before, the contact would break down when a current was applied albeit at a slightly slower rate than before. During both experiments, constant monitoring of the photo-luminescent output was being done. In both cases no change from the background reading was observed.

While this experiment did not produce any electro-luminescence, it did indicate a drawback of devices with metal - organic film contacts. The contacts are subjected to localised heating due to high resistance at the point of contact. This heating is likely to cause a breakdown in the organic film, destroying the contact. The device built for this experiment was extremely crude and had a number of aspects in it that should be improved to provide results but this falls out with the remit of this project.

Sample Preparation - Chemicals

The chemicals to be used were not purified further in any way prior to insertion into the UHV chamber. All chemicals used are commercially available: Perylene, Aldrich-99%, PTCDA, Acros-98% and Tetracene, Acros-98%.

PTCDA, having a sufficiently low vapour pressure was baked *in situ* which gave a significant period of out-gassing. It was also heated slowly to deposition temperature behind a closed gate valve to reduce the risk of surface contamination. Perylene and tetracene on the other hand have higher vapour pressures leading to a risk of losing the chemical through sublimation during the baking process. PTCDA was typically deposited at 220°C, perylene at 130°C and tetracene at 115°C. Because of this, the latter two chemicals were introduced to the systems after the bake-out was complete (but before the system had fully cooled to ensure a good base pressure could still be attained). These chemicals were out-gassed as the PTCDA was, but at a lower temperature than the deposition temperature to avoid vaporising the entire contents of the doser. Once degassed, the samples were monitored using mass spectrometry to monitor whether any water was coming off the chemical sample. If sufficiently low levels were observed then the sample was ready for deposition. Experimental results (specifically STM and RAIRS) show that this process of chemical preparation was more than adequate for the experiments to be carried out with no evidence of contamination to the films.

Deposition was originally going to be monitored by quartz crystal microbalance (QCM), but this was found to be insufficiently accurate at the low levels of coverage required. A second method of calibration was to be XPS, as discussed earlier, as changes in the intensity curve should occur at each separate layer. As will be seen later, this proved to be highly inaccurate. The most accurate method proved to be RAIRS desorption experiments

as they gave an obvious monolayer peak under desorption conditions which then allowed total coverage to be evaluated (Fig. 27). From this the doser could be calibrated in terms of ML/min and layers of specific thickness could be grown as desired. The coverage v time graph is not linear because with any of the analytical techniques used in this project, they can only measure spectra from a certain thickness of film. Once this thickness has been exceeded, the spectrometers can only measure the top portion of the film, so coverage becomes constant.

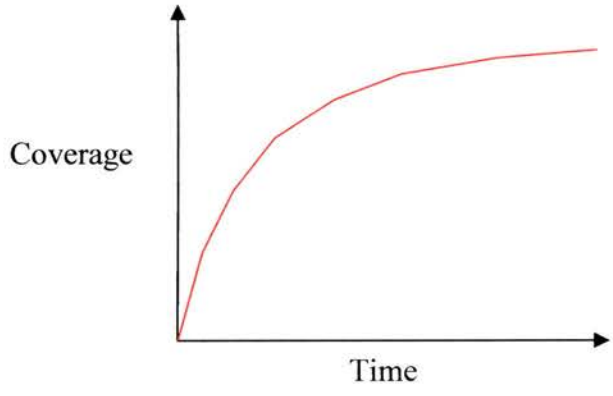

Fig. 27 Graph of Coverage v Time that can be calculated from RAIRS or XPS. As film thickness increases, the graph appears to plateau with time as techniques involved are surface sensitive i.e. can only penetrate a finite depth into the film.

Sample Preparation - Substrates

The copper substrates used were commercial crystals, one cleaved to reveal the (110) plane and the other cleaved to expose the (211) plane. Preparation of these samples involved, when required:

Mechanical polishing using various grades of diamond polishing paste, from 25 to 0.25μm, with oil and coarse or smooth polishing cloth. In UHV, the crystals were bombarded with Ar^+ ions at a typical voltage of 500eV for five to ten minutes and annealed to 500°C. This process was repeated typically for three to five cycles but longer if required. Occasionally overnight annealing at 200-300°C was used as well. In the various different UHV systems, where available, XPS, LEED and STM were used to assess the cleanliness of the substrate prior to experiments commencing.

Characterisation of Clean Surfaces

The two clean surfaces were predominantly characterised by LEED. As discussed earlier, the sharper the image, the larger are the domains of that surface and the higher the contrast between the spots and the background, the higher the order within the domains.

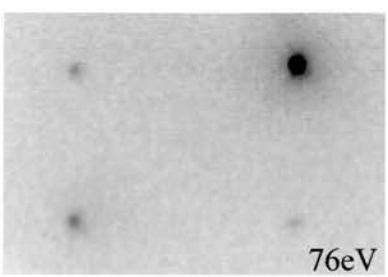

Fig. 28 LEED of clean Cu(110)

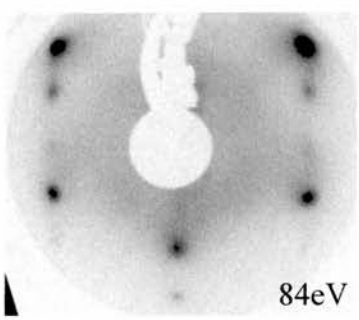

LEED of clean Cu(211)

The Cu(110) is a simple structure with unit cell dimensions of 3.62Å X 2.56 Å. In reciprocal space the long dimension of the LEED pattern represents the shorter side of the rectangular unit cell in real space but the ratio of the long dimension against the short dimension remains the same.

The Cu(211) surface is altogether more complicated. The LEED pattern from the surface has both weak and intense spots that arise from interference between electrons scattered by different atoms within the substrate unit cell.

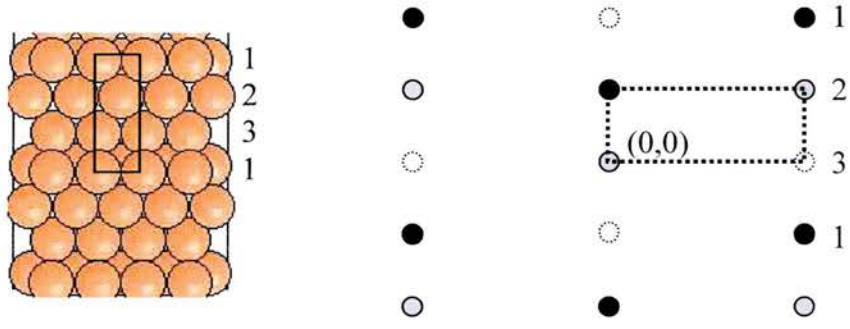

Fig. 29 Cu(211) unit cell and model LEED pattern

Measurements from the LEED pattern indicate that the unit cell is that shown in (Fig. 29). This pattern of spot intensities arises from third order splitting of beams characteristic of the (111) terraces.

Oxygenated Cu(110) Surfaces

During the course of the project, due to a few imperfections in the UHV systems being used, the copper surfaces became inadvertently oxygenated. On closer inspection, this gave rise to some interesting results which in turn lead to the substrates being deliberately exposed to oxygen to control the experiments.

The structure obtained when the Cu(110) surface is exposed to oxygen is the p(2x1) structure[113] (Fig. 30).

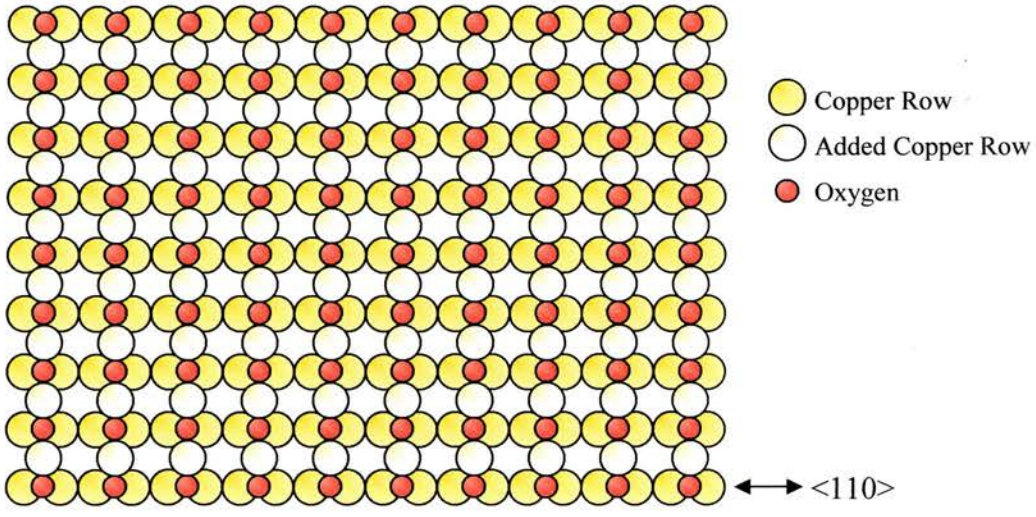

Fig. 30 Oxygen on Cu(110): Added Row structure - p(2x1): Unit cell = 3.62Å x 5.12Å

An oxygen atom sits on the short-bridge site between two copper atoms on the <110> direction. Copper atoms then add into the structure where the oxygen sits in a relative long bridge site. Three models have been suggested for the growth mechanism, a missing row model, a buckled row model and an added row model. A comprehensive STM study has dismissed the first two models and shown that the third mechanism is most likely[114]. Growth of the copper rows is more rapid on smaller terraces, implying an influence of

copper atom migration from the step edges, eliminating the buckled row model. There is also no evidence of missing copper rows next to the oxygen chemisorption sites so the missing row model can be discounted.

The structure obtained at low coverage appeared to produce islands of 2x1 oxygen, which were characterised by both LEED and STM. The islands grow in the <001> direction with the thickness and length influenced by the coverage[115]. High coverage forms thicker, longer islands, typically ten oxygen rows wide and hundreds of nanometres long. When the surface was deliberately exposed to oxygen, multiple structures were observed at high coverage.

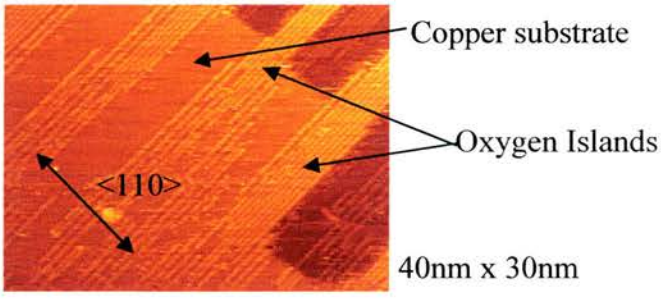

Fig. 31 A typical image of oxygen islands on Cu(110). The lines shown are rows of alternating copper and oxygen atoms, perpendicular to the close packed <110> substrate direction. Close packed oxygen rows are two substrate copper atoms apart (5.12Å). Where a gap between rows is visible the spacing is three copper atoms (7.68Å).

While many attempts were made to resolve this new structure, insufficient data and poor resolution STM images made this difficult. Investigations of these surfaces showed the visible rows to have spacing of 1.5 to 2 times the width of the 2x1 oxygen structure. These structures are likely to be p(3x1) and p(4x1) structures of the copper added row structure (N.B. Gaps in p4x1 structure fill up upon increased exposure to oxygen to become p2x1).

These structures have not been individually investigated but have been observed and briefly discussed in previous studies[116,117]. At extremely high oxygen exposure, a c(6x2) structure has been observed[118,119,120] which is similar in structure to the cuprite (Cu_2O) bulk crystal lattice. Again this is unlikely as the c(6x2) forms structure a structure of hexagonal spots, never rows.

Due to these varied and differing structures obtained, it was found that quick formation of oxygenated surfaces by introduction of pure oxygen directly into the UHV system was extremely difficult to control. Exposure to a leak from a "dead" volume over a longer time, e.g. overnight, produced a far higher quality oxygen p(2x1) structure.

Dosing Apparatus

The organic molecules under investigation in this project were deposited using a home built dosing unit. The apparatus consisted of a variable power supply, so both current and voltage could be adjusted during deposition to optimise conditions, a container holding the chemical to be deposited, a heating element and a thermocouple. It was not so important that the thermocouple give an accurate reading of the actual temperature but it should be reproducible so the same reading, corresponding to a specific deposition rate was achieved under the same conditions over different experiments.

Fig. 32 shows the initial doser design. Commercially available UHV feed-throughs with a standard CF38 flange, consisted of three 130mm copper rods and a K-type thermocouple with ceramic insulation were used. One of the copper rods was extended by 5cm for increased structural integrity (Third copper rod is redundant or can be used for increased strength). An 80mm long glass tube (7mm inner diameter, 10.5mm outer diameter) was sealed at one end and tapered 10mm from each end. A lug was attached to the sealed end for connection of the thermocouple. The glass tube had a tungsten filament (15coils) wrapped around it with the open end attached to the extended copper rod and the sealed end attached to one of the shorter rods. The tube was filled with sample and a small amount of stainless steel mesh was used to ensure no chemical could fall out if the doser was inverted.

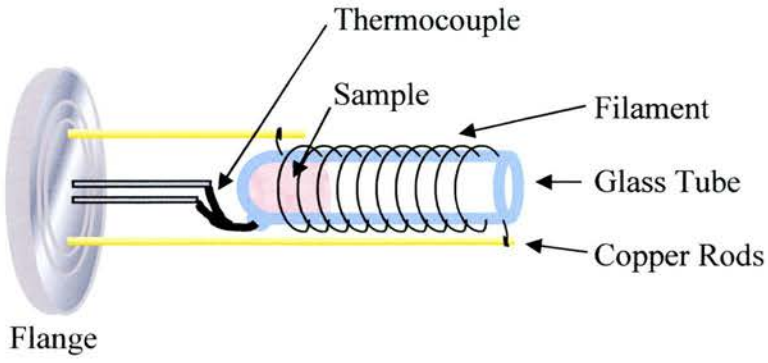

Fig. 32 Dosing apparatus (not to scale!). Sealed glass tube contains chemical for deposition. Thermocouple is mounted to a lug on the outside of the tube. Filament is coiled tightly around the tube to provide heating.

As the thermocouple was mounted externally to a glass lug, the reading obtained was a substantial underestimation of the sample temperature. Difficulties in attaching the thermocouple junction also lead to movement and poor contact between the thermocouple and the doser. The design of the doser was evolved to overcome this problem. The thermocouple cable was routed down a two bore ceramic tube, which was then sealed into the tapered end of the glass tube with liquid ceramic. This new design allowed the thermocouple junction to sit within the bulk chemical giving extremely high reproducibility and accuracy of the readings.

The only draw back of the Mk.2 version was that its construction made it extremely difficult to clean so a new one would have to be constructed for each new material. The final design used a glass tube (2mm inner diameter, 7.5mm outer diameter) (Fig. 33). The thicker glass with narrower cavity allowed much more uniform heating of the chemical. A slight tapering of the tube all that was required to hold the thermocouple in place and prevent back dosing (depositing chemical backwards to the flange instead of outwards to the substrate). This design could be easily cleaned and reused with different chemicals.

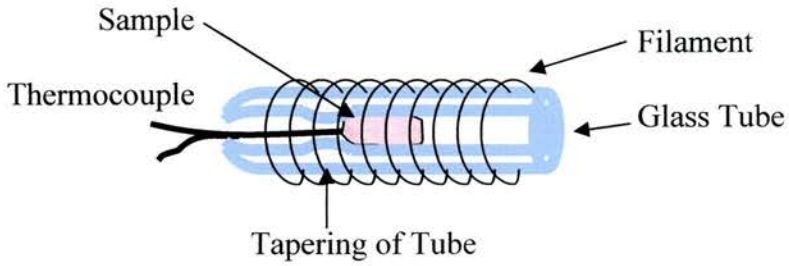

Fig. 33 Modified doser without feed-through mounting. Thermocouple is inserted into base of glass tube to give reading at the sample. Tapering of the tube provides a good fit for the cable. Filament is tightly coiled as before.

Organic Molecular Beam Deposition

Initially it was planned that experiments would all involve direct dosing of chemicals onto the substrates under investigation. As coverage increased, kinks should be visible in surface sensitive intensities of spectral data at the transitions between separate layers (assuming layer by layer growth). The doser was pointed with the aperture aligned straight at the substrate at a distance of six to twenty centimetres (depending on the physical constraints of the UHV system being used). As PTCDA has a sticking probability of one, it was considered sufficient to turn the single crystal substrate away from the molecular beam until the PTCDA sample was sufficiently degassed and a significant molecular flow had been reached. The sample was then turned to face the dosing aperture for a set length of time before being turned away. This had a few drawbacks with risk of surface contamination from the out-gassing and from deposition in other parts of the chamber. The systems were modified so the dosers were behind gate valves in side inlets that had their own pumping systems. This allowed the dosers to be out-gassed and warmed up with no risk of contamination to the clean surface. Once the doser had stabilised at the required temperature, the pumping of the inlet was ceased and the gate valve to the chamber was opened. The sample was turned to face the doser for the required time before the gate valve was closed. This allowed optimal direct dosing.

This method was sufficient for PTCDA, as after dosing, little PTCDA remained mobile within the UHV chamber due to the extremely low vapour pressure. For perylene and tetracene, as their vapour pressures are higher, the molecules continue to desorb from and re-adsorb on the chamber walls from a previous deposition process. This leads to background dosing. Substrates that had been cleaned but left in the chambers with the molecules present could be analysed after a few hours (or less!) and evidence of low

coverage structures of the molecules could be seen. The advantage of this process is that the deposition rate is extremely slow allowing the molecules plenty of time to diffuse across the substrate. This lead to the observation of highly ordered, low coverage structures that may have otherwise been extremely difficult to produce. Over time, usually two to four days, the molecules could be removed from the system by pumping so background deposition no longer occurred. Alternatively, baking of the system was required.

Gaussian 98® and Hyperchem™

In this project, due to the lack of relevant information available in the literature, it has been necessary to carry out computer optimisations of our molecules to provide information on the structure and properties of the molecules. The programs use semi-empirical methods, based on experimental data and *ab initio* methods which are based solely on mathematical principles. Both these methods use the Schrödinger equation and apply it to the entire molecule by making different approximations. Semi-empirical methods tend to be a little less accurate than *ab initio* methods but are substantially faster to carry out[121].

The simplest of these, Hyperchem™, has in the case of this project, been used solely as a tool for carrying out simple geometry optimisations which also provide the molecular dimensions. A single point optimisation calculates the total energy of the molecule in Kcal/mol and the electron charge distribution across the molecule (semi-empirical method)[122]. This is followed by a Polak-Ribiere algorithm geometry optimisation which allows the lowest energy conformation to be found. All the molecules under investigation in this project are planar and untwisted which provide an easy confirmation that the computer program has produced an incorrect result. Once the molecular dimensions have been calculated, literature results are used to calculate the Van der Waals radii of the molecules[35].

Gaussian 98® was used to calculate the frontier orbitals of the molecule and vibrational frequencies of the in plane and out of plane modes of the molecule by *ab initio* methods. The geometry must be optimised using the same level of theory and the same basis set to provide a valid result. In this project, B3LYP density functional theory is used with the 6-31g basis set. The program calculated the lowest energy geometry and dimensions of the molecule. It can then calculate the shapes of the molecular orbitals before calculating the principal axes of inertia, rotations, translations and finally frequencies of the possible vibrations[123].

Experimental Results

3,4,9,10-Perylenetetracarboxylicdianhydride (PTCDA)

The shape and properties of PTCDA has made it been one of the most widely investigated polyaromatic molecules in the adsorbed state. The molecule had already been investigated on a number of "flat" surfaces as discussed previously (PTCDA p11). Our initial experiments involved repeating studies carried out on a number of low index transition metal surfaces but also using Cu(211) on which adsorption of PTCDA had not previously been studied. When the unit cell of the Cu(211) surface is compared to that of previously investigated samples, it is seen to be much larger than that of (110) and (111) surfaces. The molecule is sufficiently large, that on the flatter surfaces, it covers four to six substrate unit cells, which means it is exclusively seen to lie flat. On the Cu(211) surface, the molecule will only completely cover one to two unit cells of the surface. As this changes the nature of the interaction between molecule and substrate it has been suggested that the molecules may stand upright or be significantly tilted. The large (111) terraces that are present in the (211) structure support this. If a molecule lay flat on these, it would be at an angle of 19.5° to the (211) surface plane.

A concern of the substrate, is that the Cu(111) face is the lowest energy face of a copper crystal. Any exposed crystal face has a tendency to drive itself towards this structure although for Cu(110) tendency is rather weak as it only has a slightly higher energy. As the Cu(211) has large (111) terraces, it was thought that over time, the (111) terraces might grow in width and the step height will grow from one to an increasing number of atomic steps. This would overall provide an environment where the already observed PTCDA structure on Cu(111) would form.

X-Ray Photoelectron Spectroscopy (XPS)

As PTCDA has an assumed sticking probability of one (due to its size and functionality), it was decided to attempt to calibrate the deposition rate using a peak intensity versus deposition time graph using XPS. Assuming layer by layer growth, as coverage increases by one monolayer, a small change in gradient of the intensity v time graph should be seen. Each change in gradient should represent the formation of a subsequent monolayer as its completion would attenuate electrons from lower layers although, in practice experimental uncertainties usually limit this observation to only a few layers at best

A second use of XPS, which is only relevant to PTCDA of the molecules under investigation in this project, is determination of the bonding to the copper surface. Studies of PTCDA on other flat surfaces[124] have shown that the XPS spectra of the initial stages of coverage differ from those of a bulk PTCDA crystal sample. Both the carbon 1s (C1s) and oxygen 1s (O1s) peaks are shifted to slightly lower binding energies at low coverage. The oxygen 1s region shows two peaks in the bulk sample but only one in the initial coverage on certain metal surfaces. The higher binding energy and smaller of the two peaks is missing which, due to its size must represent the two anhydride groups. The larger peak, twice the size and representing the four carboxylic groups is present, which suggests the two anhydride groups have been removed or significantly chemically modified so that they are shifted under the carboxylic peak and masked. If this effect is seen for PTCDA on copper then a mechanism for bonding may be deduced. The lower binding energy of the sub-monolayer molecules results from the electrons being less tightly bound to the atoms. This is a sign that the molecules have a negative charge as a result of charge transfer from the surface. This can be explained by the following:

Koopmans' theorem states that B.E is equivalent to $-\varepsilon_{orb}$ (i.e. the negative of the orbital energy). This initial state approximation is not entirely correct as, once an electron is lost from the nucleus, the remaining electrons "relax" to increase stability. In the case of adsorption at a metal surface, an ion can be further stabilised by electron contribution from the highly mobile electrons in the metal substrate and adjacent molecules. As film thickness increases, the ions receive fewer electrons from the surface so the binding energy is not lowered so much. As a result of this, binding energy will increase with increasing distance from the metal until there is no longer any electronic interaction with the metal substrate (Fig. 34).

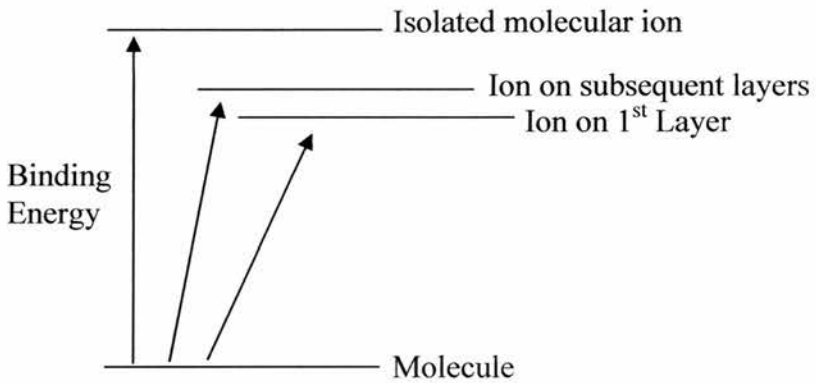

Fig. 34 Energy level diagram of binding energy stabilisation: final state approximation. Electrons from the surface stablise molecules on the initial layer, decreasing the binding energy. As film thickness increases, less stabilisation from the substrate occurs and binding energy increases. As stabilisation can occur from other molecules in the film, binding energy is never as high as that of an isolated molecule.

A second possibility for the shift in the binding energies of the peaks in the XPS spectra could be due to the phenomenon of chemical shift. As the electrons are excited from the core levels of an atom, how that atom is bonded to neighbouring atoms has a profound effect on the binding energy. If the PTCDA molecules remain fully intact on deposition

onto copper, then chemical shift is not an issue as energy changes must result from the final state approximations discussed previously. If however, the molecule loses one (or both) of the anhydride oxygen atoms (as discussed in Fig. 6 – p16 & 17) to form a bond to the surface in the initial monolayer, this will affect the electronic characteristics of the remaining atoms. As the multilayer molecules are likely to remain intact, this would result in chemical differences between molecules of the first and subsequent layers. As the balance of molecules shifts from one to the other (as film thickness increases) then the peaks arising from specific atoms could be expected to shift in binding energy. As will be seen from STM images later (p 82) it is likely that both these explanations contribute to the observed chemical shift.

A sample of PTCDA was desiccated overnight and baked for 24hours at 100°C. The sample was pressed into a pellet so the XPS spectra of the bulk sample could be recorded. The relative intensities of the bulk sample could then be compared to the thin film spectra to give indications of structure and bonding. The areas of interest for PTCDA are the Carbon 1s peak (the only core photoelectron peak of carbon) and Oxygen 1s peak (the most intense of the detectable oxygen peaks). The hydrogen is not seen as binding energy and photo-ionisation cross sections are too low.

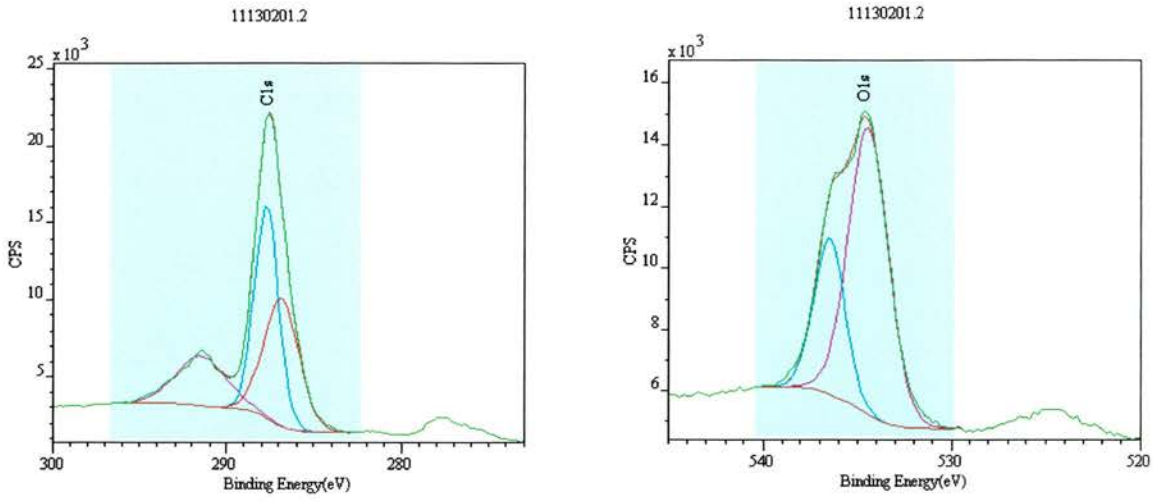

Fig. 35 C1s (287.6eV) and O1s (534.4eV) XPS peaks of bulk sample. Green lines show spectral peaks. Blue, magenta and red lines show fitted peaks. Blue shaded area is range covered by baseline. Spectra recorded at room temperature.

The C1s region (Fig. 35 left) shows a large peak at 287.6eV with a weaker band at 291.5eV. When the peaks are fitted (using CasaXPS software), they have a ratio of approximately 5:1 as expected from the molecular stoichiometry, which indicated that the large peak represents the perylene core of the molecule (fitted by two peaks indicative of subtle differences in the individual carbon environments) and the weaker feature represents the carbonyl carbons. The O1s peak (Fig. 35 right) consists of a doublet at 534.4 and 536.5eV. When the peaks are fitted, the 534.4eV peak has twice the area of the 536.5eV peak, which is in agreement with the molecular structure of two anhydride oxygen atoms and four carbonyl oxygen atoms. The ratio of the C1s peaks to the O1s peaks is important in ensuring the integrity of the structure and the purity of the sample is sufficient for experiments to be carried out. The peak areas which have been divided by the relevant relative sensitivity factors (R.S.F) in CasaXPS are then further corrected for by the transmission function described in the experimental section (TF=1.40399-(0.00141 x B.E.)). As the transmission function is calibrated to the C1s peak, the calibration factor for

carbon is one. For the O1s the correction factor is 0.65. Division of the peak area by this number and further comparison with the carbon peak areas gives a ratio of 3:1. The ratio of carbon to oxygen in PTCDA should be 4:1 in so there is poor agreement with this. The discrepancy may arise as PTCDA is known to form the tetra carboxylic acid on contact with water. This would decrease the ratio of carbon to oxygen towards 3:1. However, on sublimation in vacuum, PTCDA reforms from the acid to the anhydride.

When deposited in thin layers onto a surface, differences in the ratios of the peaks with respect to each other may give clues as to the method of bonding to the surface. A number of experiments were carried out to investigate this. For PTCDA on Cu(211), deposition was by incremental dosing on top of the previous layer - i.e. one minute coverage plus one minute coverage would equal two minutes in total. This assumes that there are no significant changes to the surface during the analysis and remaining time before the next layer was deposited. For each new experiment, an XPS spectrum was taken of the clean copper surface. This could then be subtracted from the thin film spectra to provide more accurate results thereby minimising the effects of background contamination. The "blanks" from day to day could also be normalised to each other, as they should represent equivalent surfaces, so the thin film data can be aggregated to provide a more statistically significant result.

For all experiments, the same deposition temperature was used. This provided a constant parameter during dosing by which all other changes are compared. Three experiments were carried out to produce a complete picture of dosing. One to five minutes coverage (Fig. 36), one to fifteen minutes coverage (Fig. 37) and one to sixty minutes coverage. At the rate of deposition chosen, by sixty minutes, a thick film, with no remaining substrate interaction should be present and the copper $Cu2p^{3/2}$ peak should be fully attenuated.

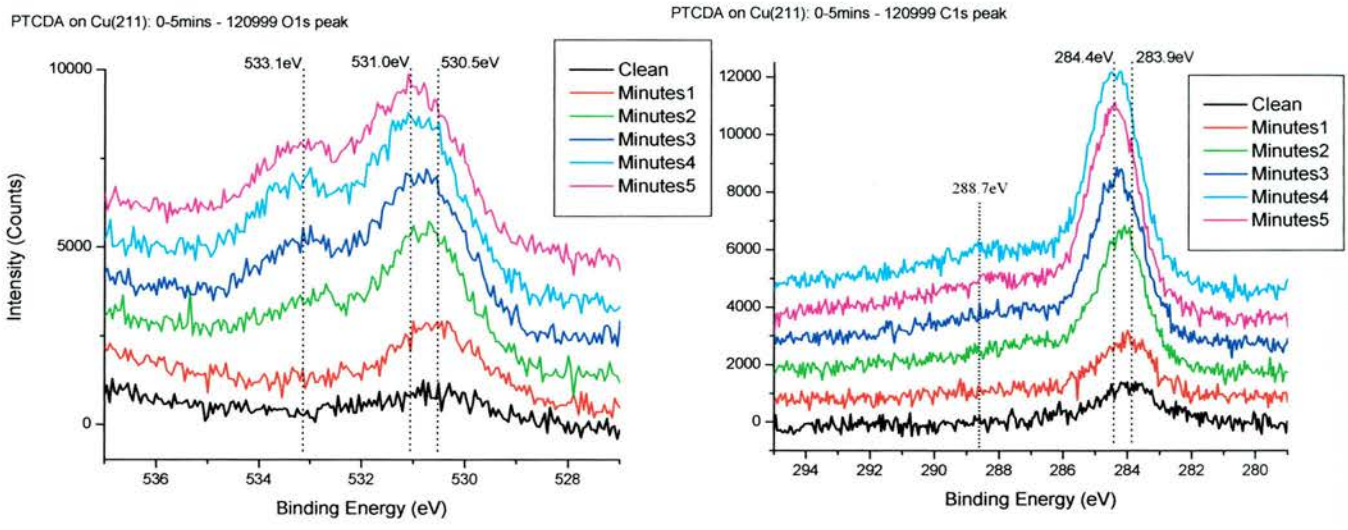

Fig. 36 O1s and C1s XPS spectra 0-5 minutes PTCDA on Cu(211). Peaks shift by ~0.5eV B.E as coverage increases. Initial coverage has no O1s at 533eV. This appears as coverage increases and coincides with the shift to higher binding energy. The B.E shift is also observed in the C1s spectra. Spectra recorded at room temperature.

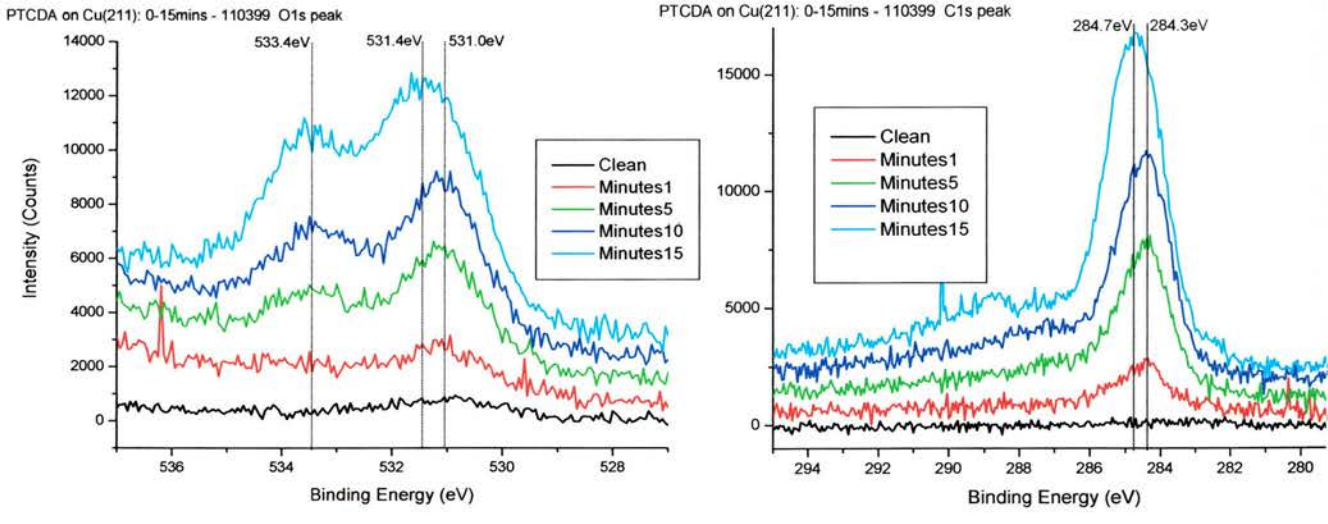

Fig. 37 O1s and C1s XPS spectra 0-15 minutes PTCDA on Cu(211). Peaks shift by ~0.5eV B.E as coverage increases. Initial coverage has no O1s at 533eV. This appears as coverage increases and coincides with the shift to higher binding energy. The B.E shift is also observed in the C1s spectra. Spectra recorded at room temperature.

Investigation of the O1s and C1s peaks shows that with increasing coverage, the peaks move slightly to higher binding energies by 0.5eV. This may be due to changing interactions with the substrate and associated changes in the molecular structure. The lower binding energy of core electrons in the initial layers indicates they are not as tightly bound as those of the thicker films due to the metal induced relaxation described earlier (Fig. 34). This implies that the structure is no longer receiving electronic donation from the substrate. As discussed previously, under these conditions the molecules have been observed to tend towards the bulk crystal structure.

The O1s peak displays an interesting effect that is indicative of the bonding to the surface. In the bulk PTCDA XPS spectrum, a doublet peak is observed at the O1s position. At extremely low coverage, only one peak is seen at 530.5eV (N.B. this corresponds to the 534.4eV peak of the bulk sample. The shift in binding energy is due to "charging" of the bulk sample that is affected by the differing electronic properties of the materials under investigation. Perfect earthing of the samples would prevent this but is not always possible due to constraints within the system. The thick PTCDA pellet itself has some insulating effect preventing proper earthing. As this is the larger of the two peaks in the bulk sample, it is assumed to represent the four carbonyl groups. The anhydride oxygen atoms are either not present, or are sufficiently chemically different to those of the bulk that they have been shifted to a lower binding energy and are being masked by the carbonyl peak. This suggests one of three possible methods of bonding shown earlier (Fig. 6, p14). The first is that the oxygen remains intact in the first monolayer but charge transfer takes place from the substrate to the PTCDA molecules. This smears the electron density across the two carbonyl and one anhydride oxygen atoms making them all equivalent. As coverage increases and the second layer begins to grow, the second peak appears to grow up from

the baseline, not appearing from behind the first peak, which suggests this method of bonding for the initial layer is unlikely. The second method is similar to that seen in phthalic anhydride on Cu(110)[125], where C=O is lost leaving a COO^- attached to the surface. While the C1s peaks of the XPS spectra are not sufficiently intense in the region required at low coverage to confirm this, later STM results show the molecule to be fully symmetrical in the first layer indicating that such bonding cannot be possible in this case. The most likely method of bonding is therefore due to the loss of the anhydride oxygen atoms and the formation of oxygen - copper bonds to the surface. As the second layer begins to grow, the molecules remain intact so the second oxygen environment appears in the XPS spectra. It is not fully understood where the removed anhydride oxygen atoms go in this process. On other metals[24], it has been suggested that the oxygen atoms combine with surface hydride species to form volatile molecules that are displaced from the surface by PTCDA and removed from the system by pumping. This cannot be the case for copper, as surface hydride species do not exist at room temperature under UHV conditions. It is likely that the oxygen atom forms a strong copper oxide species close to the molecule from which it originated. With oxygen on copper, the p(2x1) added row structure readily forms. As this is not seen, it is suggested that the PTCDA molecules prevent sufficient copper mobility for this structure to form.

Table 4 Literature[126] values for the peaks (0-5mins) observed are:

Binding Energy (B.E.)	Assignment	Relation to PTCDA
533.1eV	C-O-C	Anhydride Oxygen, O1s
531.0eV	O=C	Carbonyl Oxygen, O1s
288.8eV	C=O	Carbonyl Carbon, C1s
284.4eV	C	Perylene Core, C1s

The values in Table 4 agree with the bonding that would be expected within the molecule. The peak positions for the thicker film shift upwards by ~0.4eV due to less relaxation within the film. As the layer thickens, the molecules receive fewer electrons from the surface so the molecules are more neutrally charged so binding energy increases slightly. As the shift in the C1s and O1s is of the same amount (0.5eV) in the multilayer, this implies that the reduced relaxation affects the whole molecule equally, therefore the molecule must be fully intact at this point in the film growth. With stoichiometric and literature agreement of the peak assignments, it is possible to infer that the initial layer of the molecule loses the anhydride oxygen to bond directly to the copper surface. As coverage increases molecules that are not in contact with the copper physisorb on top of earlier layers and are bonded by π-π and Van der Waals interactions. This does not involve the loss of the anhydride oxygen hence it reappears in the XPS spectra.

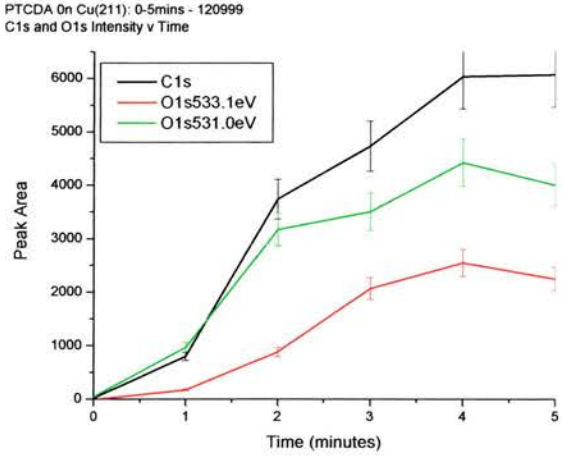

Fig. 38 Peak area v time: PTCDA on Cu(211) 0-5mins. Gradient increases at ~1min corresponding to the onset of the second oxygen environment and overlayer of PTCDA.

If peak intensity is plotted against time (Fig. 38), the onset of the 531.0eV peak corresponds with a change in gradient in the coverage v time graph. At sub-monolayer coverage, as the molecule must lose its anhydride oxygen atoms to form a bond with the copper, there is a relatively low probability of this happening so the sticking probability is less than 1. Once the first layer is complete or sufficiently complete for the second layer to start forming and the molecules bond via Van der Waals interactions, the sticking probability increases so the rate of coverage increases.

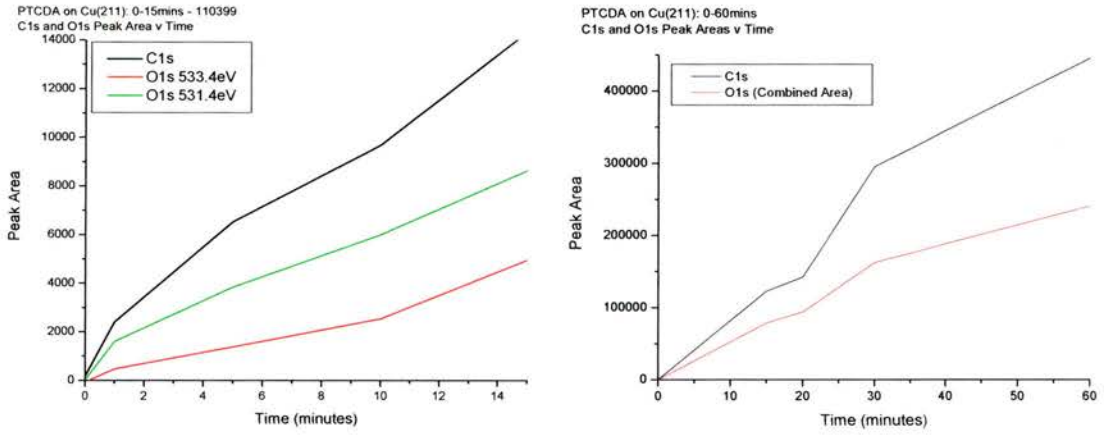

Fig. 39 Peak area v time: PTCDA on Cu(211) 0-15mins and 0-60mins. After initial monolayer, growth is linear. No decrease in gradient is observed as would be expected for a thick film due to depth exceeding Inelastic Mean Free Path of the scattered electrons. This indicates that the coverage does not exceed ~10 ML.

As coverage increases (Fig. 39) it does so in a linear fashion. This implies that the structure that forms after the initial monolayer does not change significantly for many 10's of layers (60 minutes deposition is thought to provide approximately 30-50 ML). This agrees with the widely reported phenomenon that PTCDA tends to grow in the bulk crystal structure when deposited on flat surfaces.

The gradient change observed at 1 minute in Fig. 38 but not seen in Fig.39 is further indication of coverage being approximately on monolayer per minute. Due to slight differences in the deposition conditions, the coverage at one minute could have been recorded at point one on Fig. 40 for one experiment and point 2 in another. When plotted with other experimental points from the experiments, two different graph shapes would be produced. The first would match the shape seen in Fig. 38, 0-5 minutes coverage the second would correspond to Fig. 39, 0-15 minutes coverage. This gives further evidence that under the conditions used for these experiments, the initial monolayer takes around a minute to grow. Once growth of subsequent layers has begun, coverage increases in a linear fashion. Fig. 40 therefore shows an ideal model for coverage v time of PTCDA on Cu(211).

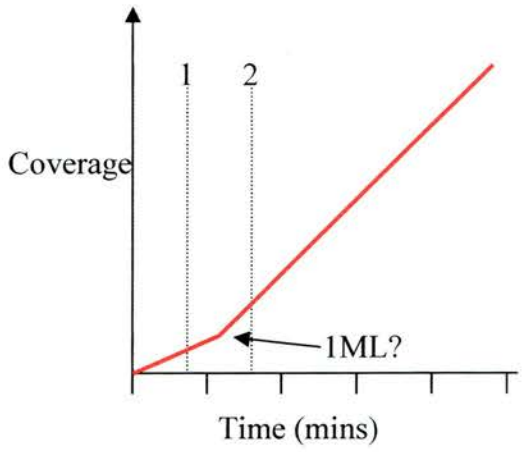

Fig. 40 Possible coverage v time graph of PTCDA on Cu(211). Initial growth (sub-monolayer) is slower than the overlayer growth of PTCDA on Cu(211). This is likely to be due to the molecules diffusing to find an exact binding site (see STM results). The overlayer molecules do not have to diffuse so far to fing the correct site so are more likely to stick, hence the linear growth. As the 1ML point or gradient change occurs at ~1minute under the deposition conditions in use, conditions may occur where there is sufficien error in the measurement that the coverage v time graph appears like Fig. 39 (0-15mins) with a steeper gradient than the overlayer growth.

STM of PTCDA on Cu(211)

PTCDA was deposited onto Cu(211) and studied by STM to investigate its bonding and structure. The substrate was held at around 120°C during deposition to facilitate molecular diffusion. A partial monolayer was grown to investigate whether or not any indication of the bonding method could be seen. No novel LEED patterns were observed but substrate spots were largely obscured.

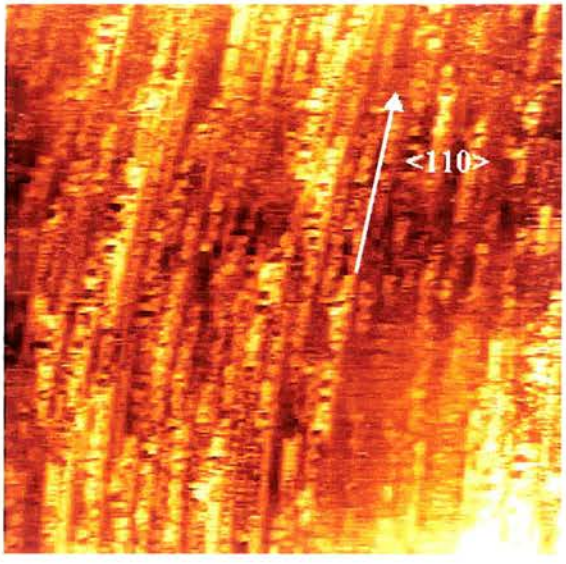

Fig. 41 Sub monolayer PTCDA on Cu(211): 41 x 41nm: Tunnelling conditions - gap voltage: -0.264V, feedback set: 2.796nA, loop gain: 0.52%

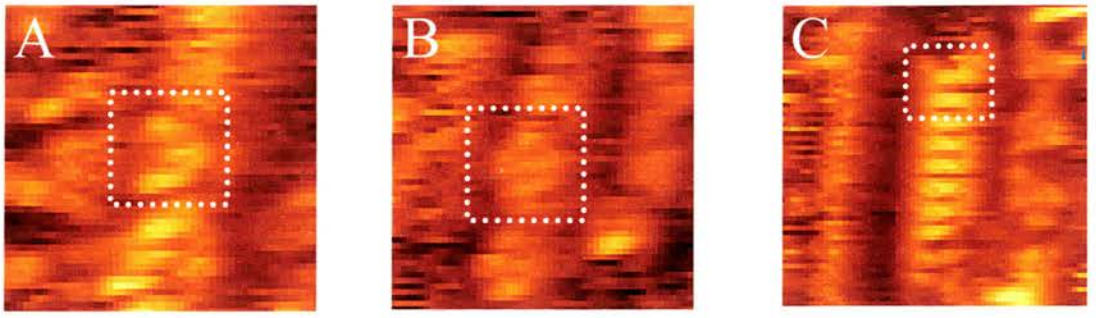

Fig. 42 Individual molecules on Cu(211) taken from fig.41: 5 x 5nm: tunneling conditions as per Fig. 41. A shows PTCDA bonded through one side only. B shows PTCDA with equal bonding on both ends. C shows contamination by perylene.

Initial investigations (Fig. 41) clearly show that the molecules align along the <110> close packed copper direction. The spacing between the molecular rows is typically ~18Å which corresponds to the width of three copper rows in the <111> direction of the Cu(211) surface. The PTCDA molecules are too large (13.86Å x 8.64Å) to be spaced by only two copper rows if they are perpendicular to the <110> direction of the Cu(211). The fact that they do occupy a commensurate position at the third row distance indicates that at low coverage there is a strong molecule - substrate interaction. Closer investigation of these images shows that there are three distinct sub-molecular structures (Fig. 42). Molecule B is typical of the "figure of eight" structures often observed previously e.g. Chizov et al[127]. The line profile across this molecule (Fig. 43 B) shows that it is lying flat and it is aligned with the two anhydride oxygen atoms (if they are still present in the molecule) along the <110> direction. As the "figure of eight" structure is visible, the molecule may be completely intact but this disagrees with XPS results. Molecule C is assigned to a short row of contaminant perylene molecules. The "two bar" internal structure of the molecule is one that is discussed in the later chapter concerning perylene adsorption on Cu(110). Sublimation of a sample of PTCDA produces small quantities of perylene. It is likely

however that the vast majority of perylene in the dosing apparatus would be sublimed at lower temperatures than the PTCDA and would be pumped away before the doser is opened to the deposition chamber. The lower strength with which perylene is bonded to copper would also allow it to be preferentially displaced by the strongly bonded PTCDA molecules as coverage increases. The most interesting of the three molecules is A. The molecule does not have the "figure of eight" structure of the molecule B that is associated with a complete, symmetrical molecule. This suggests that the structure of the molecule may have changed.

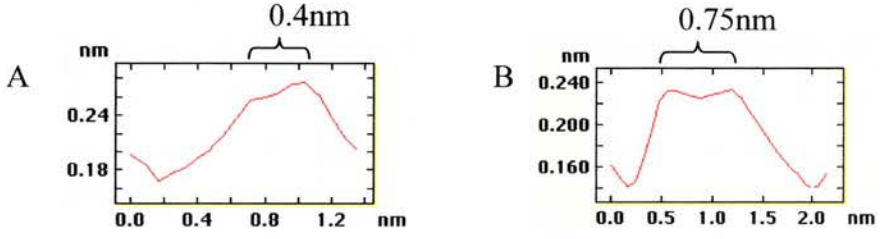

Fig. 43 Line profile of molecule A (Fig. 42 A) and molecule B (Fig. 42 B): Line profiles drawn perpendicular to <110>. The different widths of the upper features of the molecules show clearly that molecule A is tilted with respect to B as these would be similar if the molecules shared the same orientation.

The size and shape of the molecule, suggests that it sits on the surface perpendicular to the <110> direction. The line profile (Fig. 43 A) suggests that molecule A is not flat, but angled from the surface. It is therefore possible to suggest that this is evidence of the molecule bonding to the surface through the loss of the anhydride oxygen. If this is so, then the evidence suggests that it bonds through one end only, causing the molecule to be angled to the surface. It is not clear however whether or not the molecule is flat on the

terrace and protruding over the step edge, or it may be attempting to stand upright on the small terrace and leaning back on the step edge (Fig. 44).

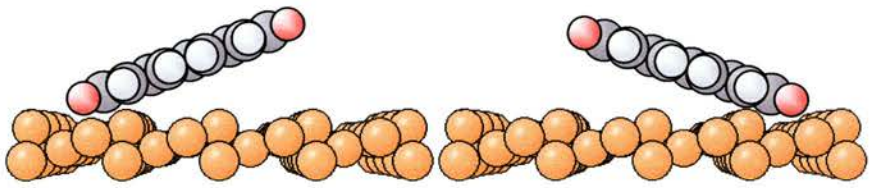

Fig. 44 PTCDA bonding through loss of anhydride oxygen when perpendicular to <110> direction: Left - PTCDA flat on terrace, Right - PTCDA upright from terrace but leaning back due to interactions with the step edge.

The fact that both completely bonded molecules and partially bonded molecules are present at sub-monolayer coverage casts doubt over the XPS results as a method of measuring film thickness as it is extremely difficult to assess the onset of the second layer of growth. The ratio of the two oxygen peaks at very low coverage does suggest that molecules containing only the carbonyl species are the only ones present or at least are in large excess. This would imply that the B type molecules (Fig. 42) are also bonded through loss of the anhydride oxygen atoms. The A type molecules, as they are tilted are likely to only be bonded through one end so one of the molecules two anhydride oxygen atoms are still present, albeit at half the concentration.

Coverage was increased to around one monolayer. LEED patterns were collected at 13eV but were of too poor quality to gain useful structural information although there was definitely some suggestion of ordered crystal structure. At the energies where the overlayer

spots could be seen, the substrate spots could not making it very difficult to calculate unit cell dimensions.

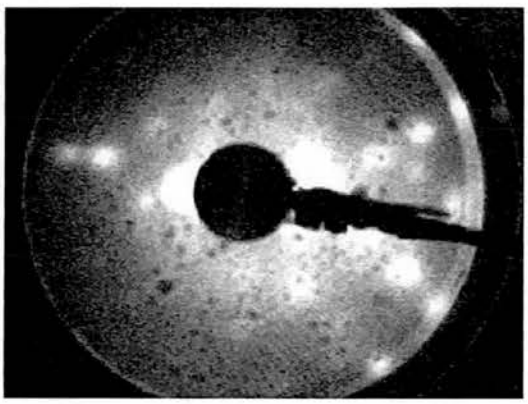

Fig. 45 LEED of PTCDA on Cu(211):13eV

The structures observed in the STM images show distinct similarities to the (102) face of the bulk crystal however, there are some differences. A feature of the (102) plane of the bulk crystal is that it has quadrupole coupling of the molecules (end of one molecule interacts with side of adjacent molecule). This is also seen on the Cu(211) surface but the structure is distorted by what is almost certainly interactions with the underlying copper surface. The molecules form pairs, with the end of one molecule facing the side of the next.

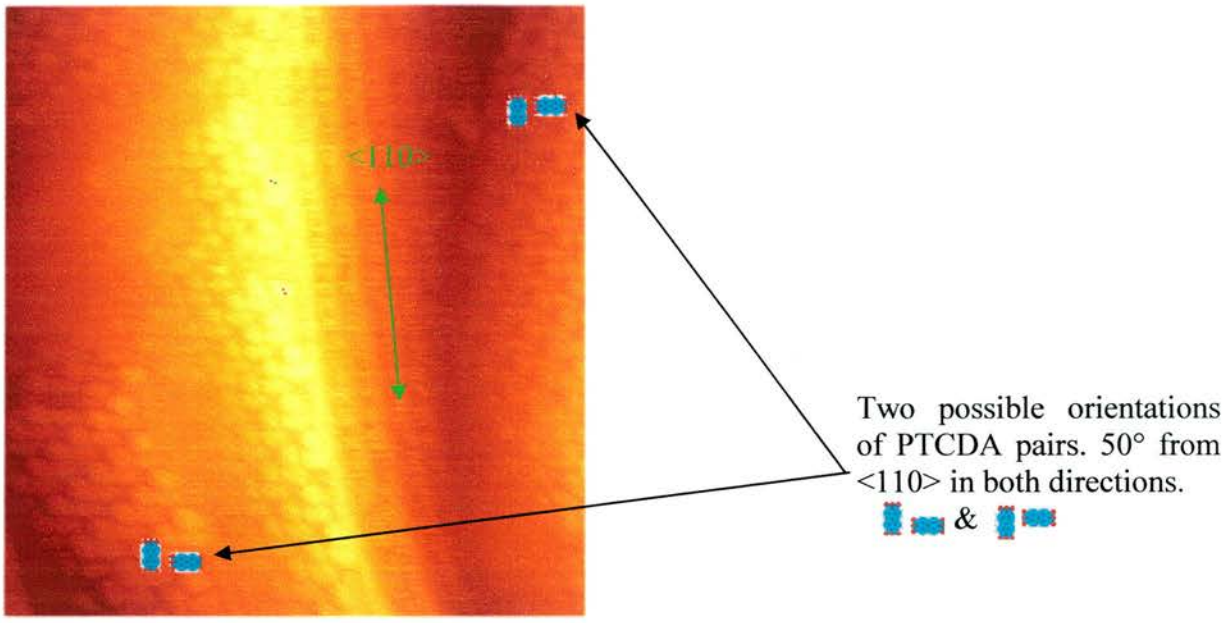

Fig. 46 PTCDA on Cu(211) 31 x 31nm: Tunnelling conditions – gap voltage: -0.758V, feedback set: 1.158nA, loop gain: 0.263%. Two structures of PTCDA can be seen in this image. They are mirror images of each other with the mirror plane perpendicular to the <110> direction (unit cells shown in fig. 47).

The molecules form the unit cell and its mirror image, as expected for this symmetry of surface. Fig. 47 shows how the structural features of the two domains can clearly be seen oriented ~50° from the <110> direction.

The model shown in Fig. 47 shows the positions of the molecules relative to the underlying copper rows for the two possible orientations. In this structure, all the molecules parallel to the <110> direction sit over equivalent sites and all the molecules perpendicular to the <110> direction sit over equivalent sites. If the structure were dominated by quadrupole coupling, then molecules of the same orientation would sit over one of two alternative sites (Fig. 48). As PTCDA has a strong interaction with the copper, it is unsurprising that the structure is influenced by the surface copper atoms.

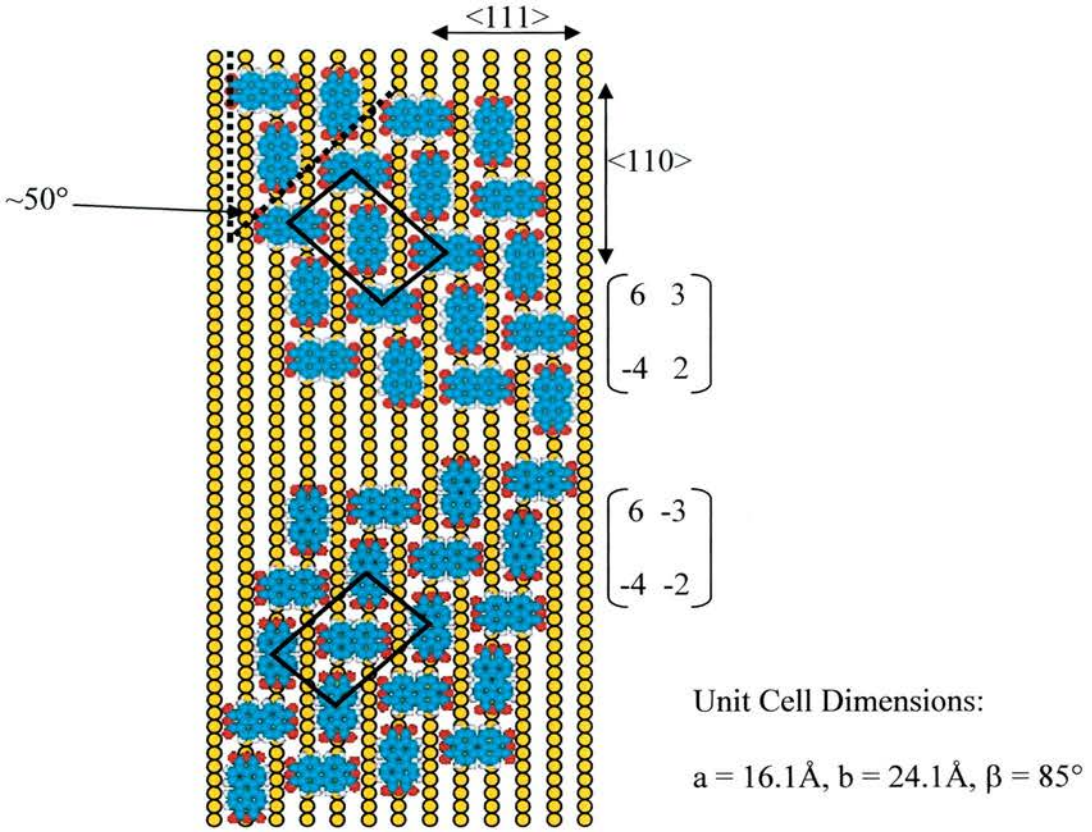

Fig. 47 Vector unit cell and dimensions of two PTCDA structures on Cu(211)

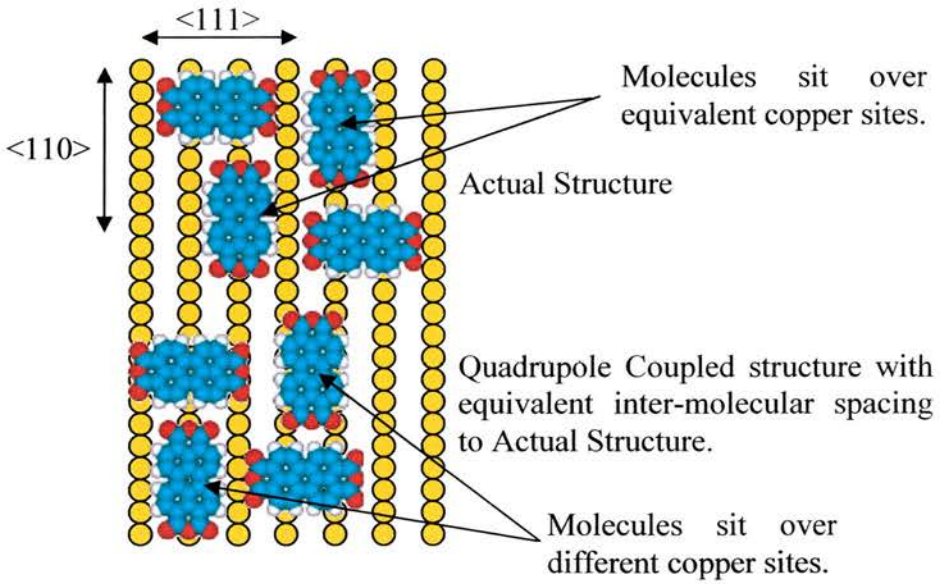

Fig. 48 Model of actual structure and quadrupole coupled structure compared. In the quadrupole coupled structure, molecules in the <110> direction are not aligned over equivalent sites if they have strong interactions with the copper rows. In the offset (actual structure) they do.

PTCDA on Cu(110)

After investigations on the Cu(211) surface, it was decided to deposit PTCDA onto Cu(110) as the structure seems to be driven by the interactions with the copper rows. The atomic arrangements of the rows of the two surfaces are the same, although if the terraces of Cu(211) are considered the symmetries are different, but the copper rows are only 3.62Å apart on Cu(110) instead of 6.27Å on Cu(211).

Infra-red Spectroscopy of PTCDA on Cu(110)

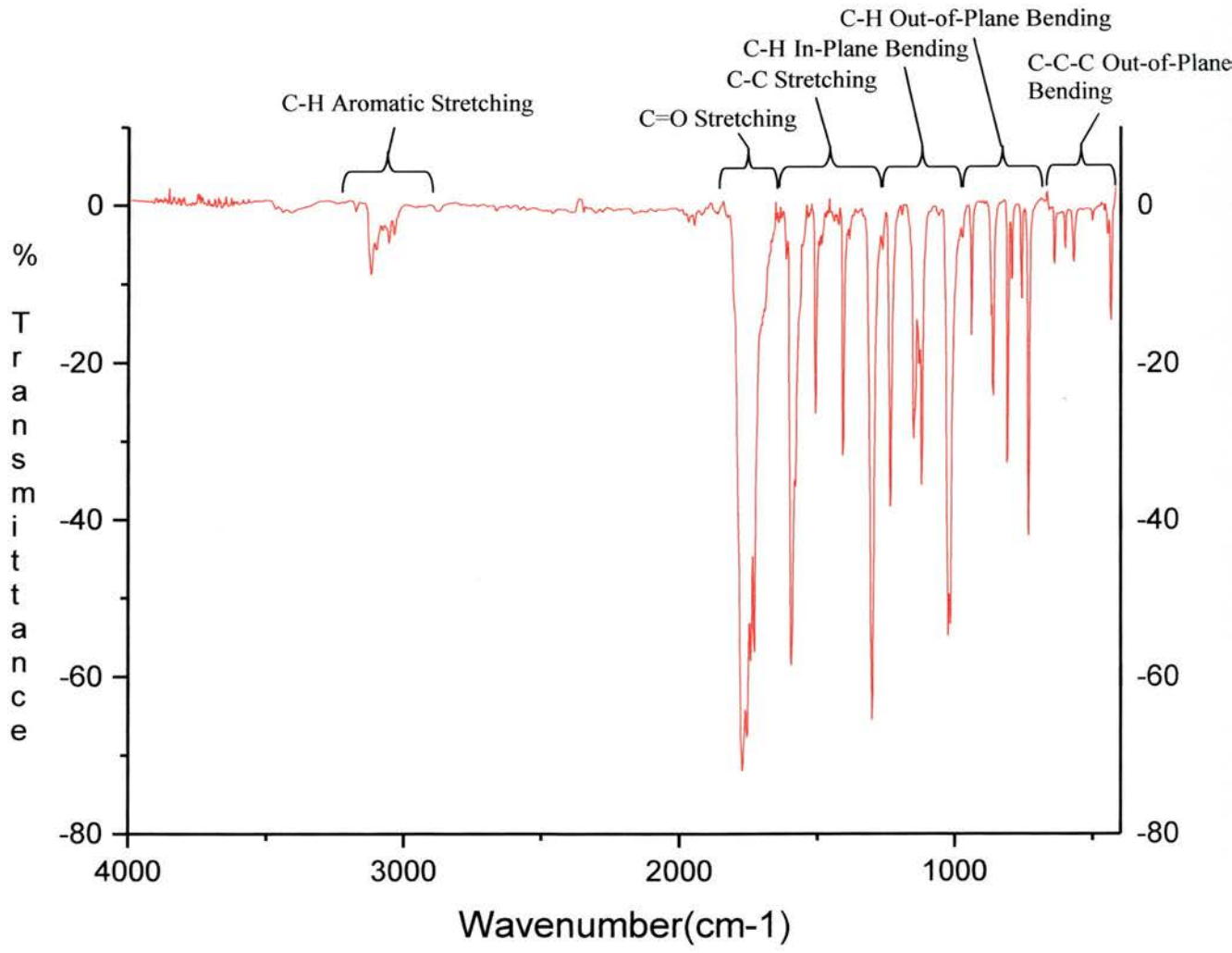

Fig. 49 Bulk IR spectrum of PTCDA in KBr. Peaks assigned from refs [128,129,130,131]

The infra-red spectrum of PTCDA in KBr was collected to provide the bending and stretching modes of the free molecule. The peaks were assigned by from literature values[128,129,130,131] (Fig. 50). There is a slight discrepancy between the papers as to the exact assignment of peaks. However, there is agreement that all peaks detectable by our RAIRS system below 900cm^{-1} are all out-of-plane modes.

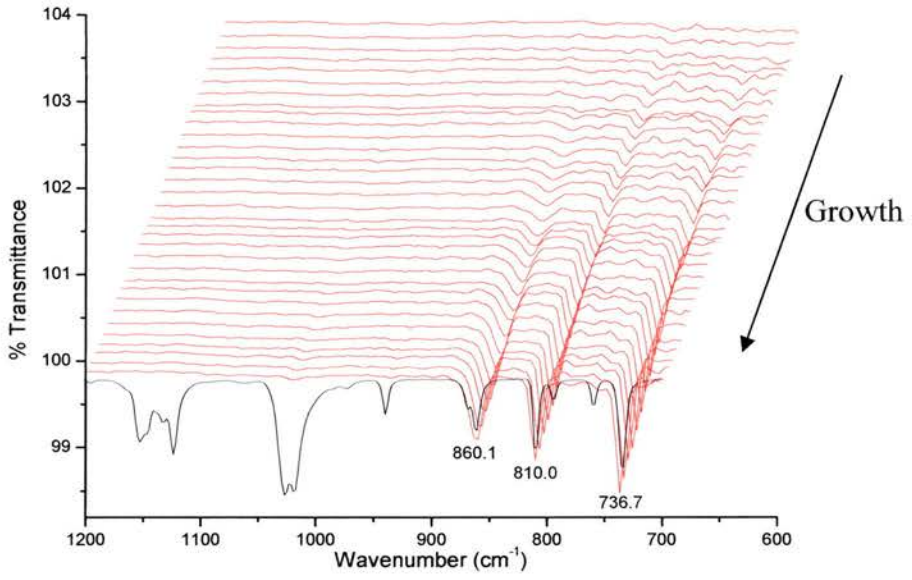

Fig. 50 700cm^{-1} to 1200cm^{-1} of RAIRS spectra of PTCDA on Cu(110) as a function of coverage. Black line shows overlaid free molecule spectrum - smaller peaks from this may not be visible in RAIRS due to lower intensity. Peak positions refer to RAIRS spectra.

Once the peaks had been identified, RAIRS was carried out and the results clearly show significant differences related to the molecular orientation (Fig. 50). The molecules were deposited onto the Cu(110) surface under controlled temperature conditions. Peaks visible in the free molecule spectra are clearly not visible in the RAIRS (Table 5). When compared to the peak assignments, the visible peaks all represent C-H out-of-plane

bending modes and the missing peaks all represent the C-H in-plane bending modes. This data shows that the molecule, as in many other examples lies flat on the surface. correlation tables[132,133] show a conversion of the B_{3u} symmetry modes of the free molecule to A_1 when the symmetry is reduced to C_{2v} on the surface. Only these vibrations with A_1 symmetry are visible.

Table 5 Comparison of vibrational modes of PTCDA "free" molecule and PTCDA on Cu(110)

Free Molecule and Symmetry[134]		PTCDA/Cu(110)	Assignment
732.8	A_g	736.7	C-H Out-of-Plane Bending or C-C Ripple
757.9	B_{3u}	-	In-plane mode
810.0	B_{3u}	810.0	C-H Out-of-Plane Bending or C-C Ripple
860.1	B_{3u}	860.1	HC-CH Wagging
939.2	A_g	-	C-H In-Plane Bending
1026.0	A_g	-	C-O-C Stretch
1122.4	A_g	-	C-O-C Stretch
1151.3	A_g	-	C-H In-Plane Bending

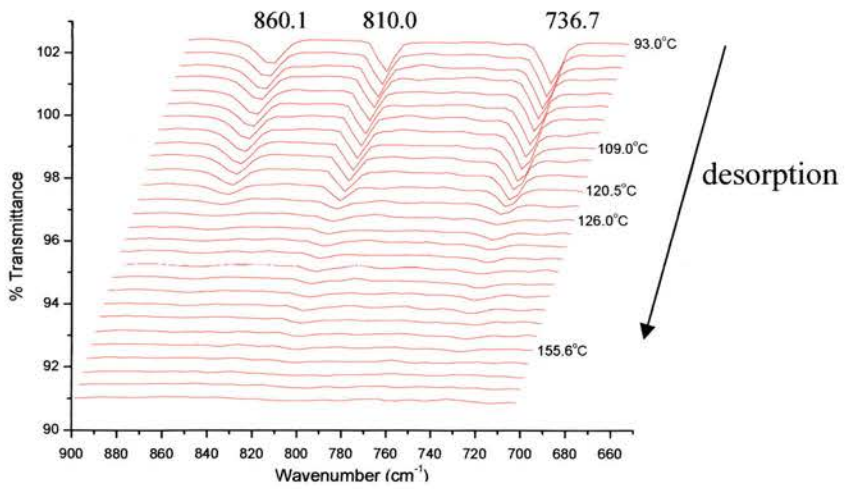

Fig. 51 Desorption of PTCDA from Cu(110): see fig.52

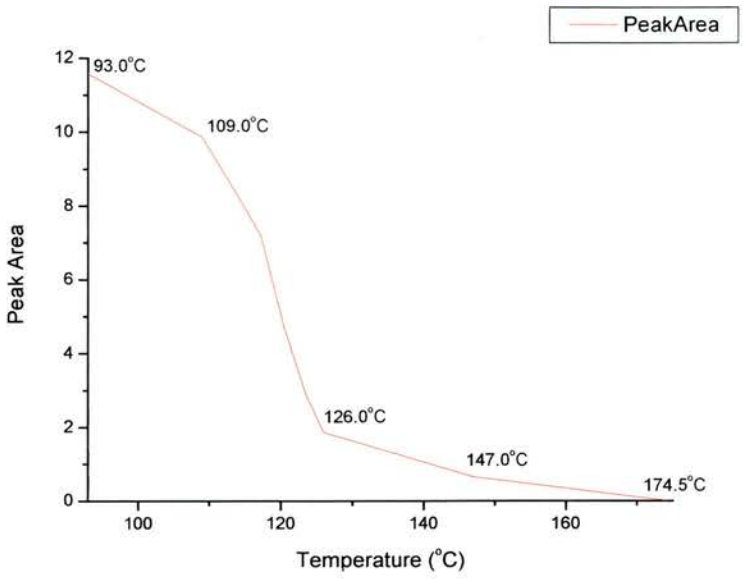

Fig. 52 Desorption of PTCDA from Cu(110): Area of 736.7cm^{-1} peak, C-H out-of-plane stretching mode v temperature (°C). Multilayer desorbs at ~126°C, monolayer desorbs at ~155°C.

The substrate was heated slowly to monitor temperature controlled desorption (Fig. 52 & Fig. 53). As temperature increased, the intensity of the major peaks can be seen to slowly decrease to 109°C where a sharper drop-off is seen until 126°C. Above this temperature only a single monolayer is present until around 155.6°C where this too is desorbed. Knowing these desorption temperatures, we can control the substrate temperatures during growth to determine the conditions so that the structures are optimised. This in turn should make it easier to characterise any structures that are recorded.

STM of PTCDA on Cu(110)

As Cu(110) does not have the terraces found on the Cu(211) surface, and the copper rows are closer together, a different structure is expected. The closer (3.6Å) copper rows should allow closer packing of the molecules. The structure observed (Fig. 56) appears to be perfectly quadrupole coupled with the molecules aligned with the anhydride groups along the copper rows and alternating with molecules perpendicular to the copper rows. Viewed over a large area, it is apparent that the structure has some interesting fine detail (Fig. 53).

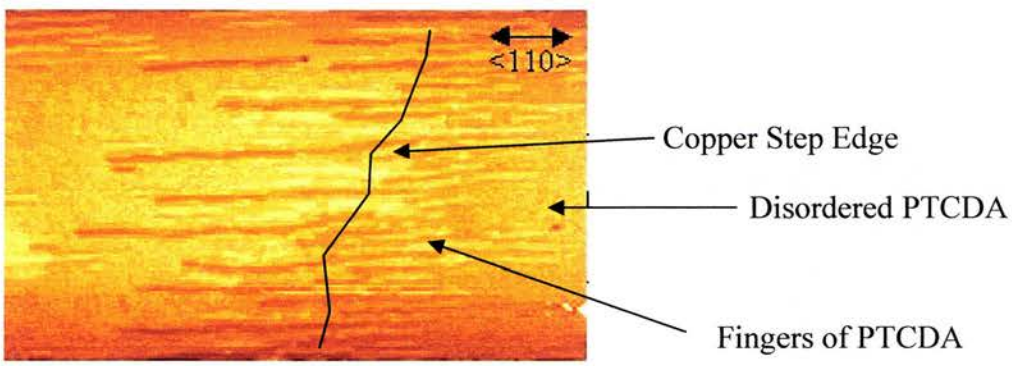

Fig. 53 PTCDA on Cu(110) 300 x 150nm: tunnelling conditions - Gap voltage: -0.19V, Feedback set: 0.915nA, Loop gain: 1.468%. Fingers of PTCDA grow along the <110> direction apparently propogating from copper step edges.

Initial inspection indicates that the PTCDA molecules grow outwards from the step edges in long fingers that follow the <110> direction. The presence of light fingers and dark fingers seems to indicate molecules at different heights and suggests multiple layer growth. The flat regions in between the fingers and areas at the ends of the fingers contain patches of molecules that appear to contain no order. These are more obvious in Fig. 54. It is also apparent from this image that the dark patches between the fingers are also filled with

ordered molecules. Height profiling (Fig. 55) suggests that they are a molecular layer lower down. Due to the level of exposure of the copper crystal to the PTCDA molecular beam, it in unlikely that sufficient molecules would have been deposited to produce almost two full ordered layers. Coverage should be approximately one monolayer.

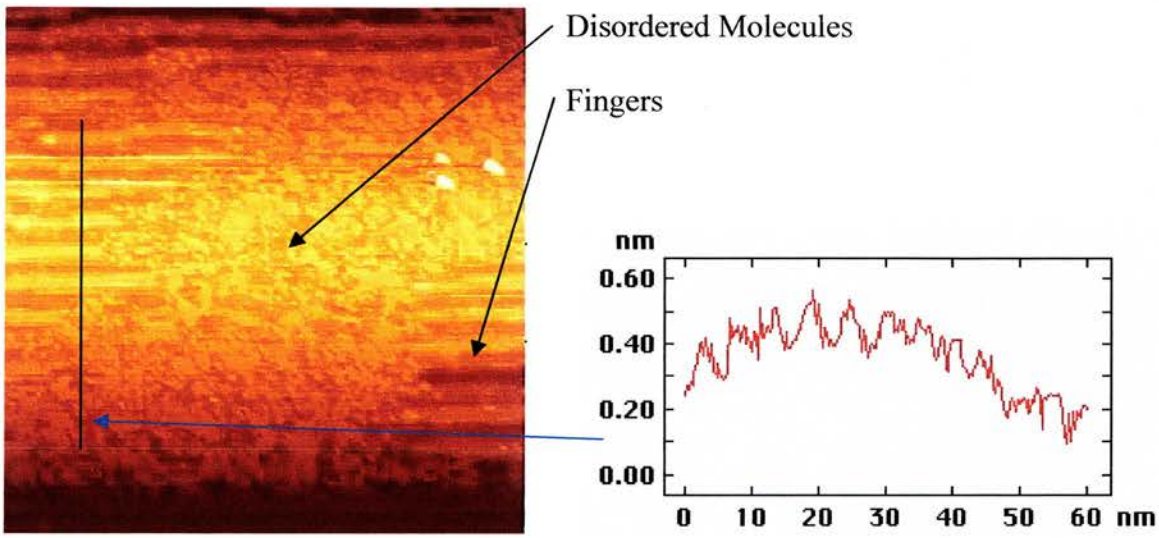

Fig. 54 PTCDA on Cu(110) 100 x 100nm and line profile: tunnelling conditions - Gap voltage: -0.19V, Feedback set: 0.915nA, Loop gain: 1.468%. Areas of the substrate not covered with molecular fingers appear to contain patched of disordered molecules. The line profile across the fingers shows then to be around 5nm wide and fairly uniform in width.

Magnifying these fingers shows that they are composed of PTCDA molecules in long bands of quadrupole coupled molecules (Fig. 55). In the disordered areas of molecules, bare patches can be seen which are likely to be the substrate copper. Considering this, the apparent height differences observed are likely to be misleading and caused by structural effects as discussed below. The structures observed are unbroken from the patches of bare copper to the brightest fingers. If multilayers were present, the steps between layers should be visible.

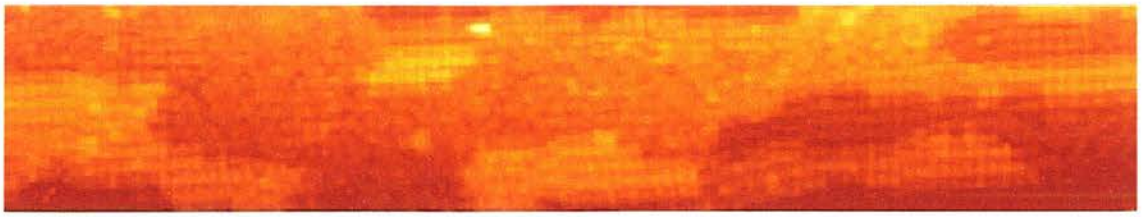

Fig. 55 PTCDA on Cu(110) 80 x 15nm. Closer inspection of the fingers show them to be made of rows of quadrupole coupled molecules. The fingers do not however appear to be a new layer of growth. Tunnelling conditions - Gap voltage: -0.21V, Feedback set: 0.915nA, Loop gain: 0.405%.

This phenomenon of fingers of PTCDA on the Cu(110) surface has been reported previously in the literature[135,136,137]. The lighter and darker molecules were described in terms of height differences and attributed to the PTCDA molecules rearranging the underlying copper atoms so that there is an added copper layer under the lighter areas. While real height differences are a common explanation for lighter and darker areas in STM images, it is not the sole possible cause. Lighter areas could also indicate that the molecules have a higher conductivity than those of the same height but darker. This could be caused by the differing underlying copper structure or by differing packing densities of the molecules.

Closer inspection of our data suggests the structure and its interactions with the substrate may be far more complicated. The molecular pairs along the <110> direction are about 23Å long which corresponds to nine close packed copper atoms and is close to the minimum close packed intermolecular distance of 22.5Å based on molecular Van der Waals dimensions (Hyperchem™ calculations – p13 and ref. 35) From earlier results, we have seen that PTCDA has strong interactions with the close packed copper rows but with the quadrupole coupling it appears to have comparably strong interactions with the

adjacent molecules. Measurements of the molecular separation in the <100> direction are consistently greater than 23Å and tend to be around 27 or 30Å. Even allowing for errors in measurement, these distances are too great to correspond to close packing of the molecules but are also inconsistent with a commensurate structure (as they would be around 25, 29 or 32Å) (Fig. 56A).

If the molecules were close packed then they would sit over different sites on the copper. If they were completely incommensurate then there would be no density fluctuations due to packing or underlying copper atoms. If the molecules proved to be commensurate but only over a number of unit cells, then the molecules may show a repeating density fluctuation due to the different sites the molecules sit over but the fluctuations would be far more regular than is observed. However, if the molecular spacing were dominated by interactions with the close packed copper rows, then all the molecules would sit over the same site of the copper and therefore no difference in electronic density would be seen and all molecules in the STM images would be the same brightness. If the copper rows do have a strong interaction with the molecules, but the molecules also have a strong inclination to close pack with each other, then there may be a complex combination of the two. If the molecules are attracted to each other, but they also pull the copper row to which they are also strongly attracted out of position, this will have an effect into the bulk crystal. The result of this could be differing tunnelling conductivities, which in turn would affect the "height" of the molecules when imaged by STM (Fig. 56).

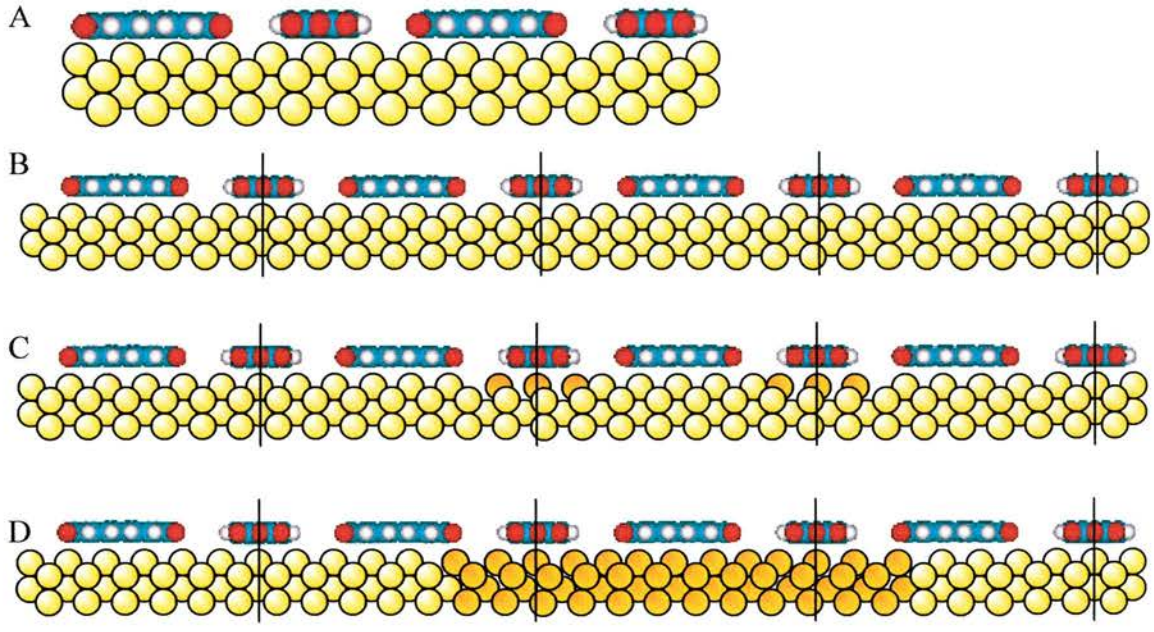

Fig. 56 Aspects of PTCDA bonding to Cu(110) surface: A) Quadrupolar coupling between PTCDA molecules but intermolecular spacing determined by commensurate interaction with "fixed" substrate atoms, B) Intermolecular spacing determined by intermolecular Van der Waals interactions leading to incommensurate structure, C) as B) but with local disruption of topmost Cu atoms leading to local site equivalence of PTCDA pairs, D) as C) but including deeper relaxation of Cu structure.

Perylene

Infra-Red Spectroscopy - Perylene

Perylene was mixed with KBr, ground and pressed into a translucent pellet. A transmission IR spectrum was collected (Fig. 57) and the vibrational modes were assigned by reference to the literature[138,139] (Table 6).

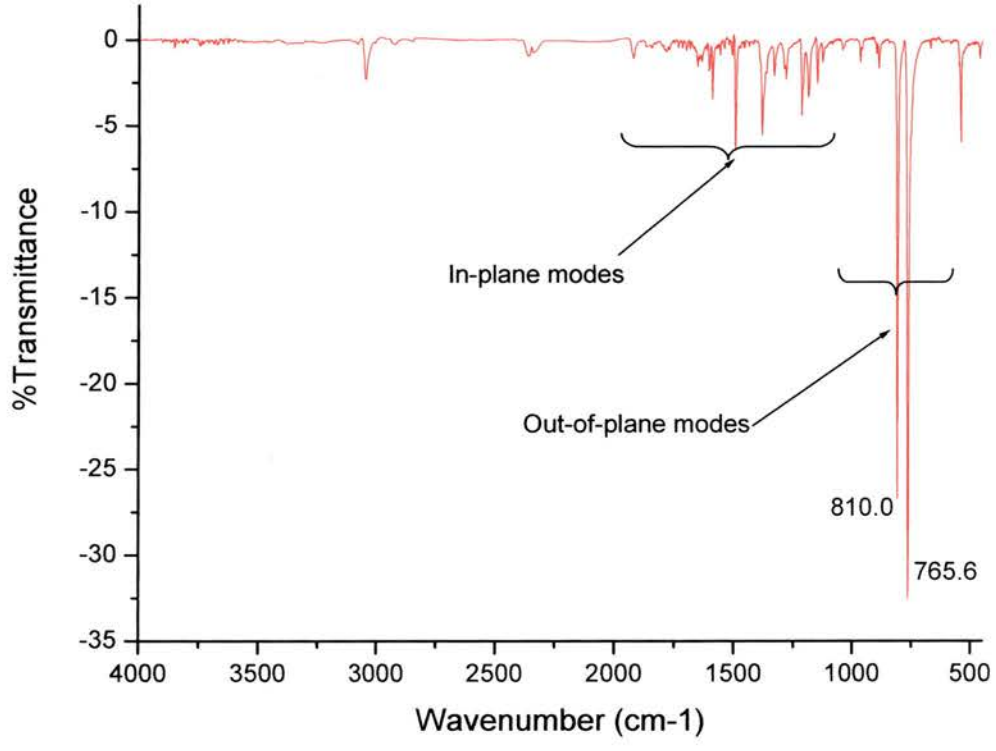

Fig. 57 Transmission IR of perylene in KBr highlighting in plane and out-of plane vibrational modes.

Table 6 Vibrational modes and symmetries of perylene (free rotational state) [138,139,140]

Wavenumber (cm^{-1}) and symmetry	Vibration
540.0 (B_{3u})	C-C-C Out-of-plane bending
765.6 (B_{3u}), 810.0 (B_{3u}), 889.0 (B_1), 966.2 (B_{2g})	C-H Out-of-plane bending
1041.4 (B_{2u}), 1126.2 (B_{1u}), 1149.4 (B_{3g}), 1186.0(B_{3g}), 1215.0(B_{3g}), 1280.5 (B_{2u})	C-H In-plane bending
1330.7 (B_{2u}), 1380.8 (B_{3g}), 1492.7 (B_{2u}), 1591.0, 1652.7 (B_{2u})	C-C Stretching
2339.3, 2362.4	Atmospheric C=O Stretching (of CO_2)
3047.0 (B_{2u})	C-H Aromatic stretching

Two strong modes are observed at 765.6 and 810.0 cm^{-1} which correspond to the C-H out-of -plane bending, all higher wavenumbers correspond to in-plane modes. *Ab initio* calculations of the frequencies of the vibrational modes of perylene were compared with the vibrational modes of the recorded spectrum (Fig. 58). The out-of-plane modes clearly match well those from the literature shown in Table 6. These two, large out-of-plane bands, should make it easy to resolve the orientation of the molecules on the surface. As a result of the surface dipole selection rule, if these bands alone are present then the molecules are flat, if they are absent then the molecules are upright. A different ratio of in and out-of-plane modes could indicate a tilted molecule or a mixture of several distinct structures. If the ratios remain the same as the transmission spectra then all molecular orientations are present and the sample is probably amorphous.

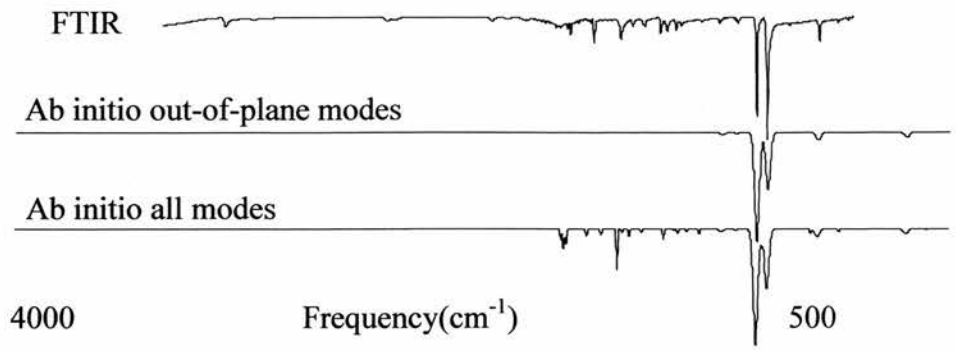

Fig. 58 Comparison of perylene transmission IR spectrum with Gaussian98 calculated spectra of all modes and out-of-plane modes only.

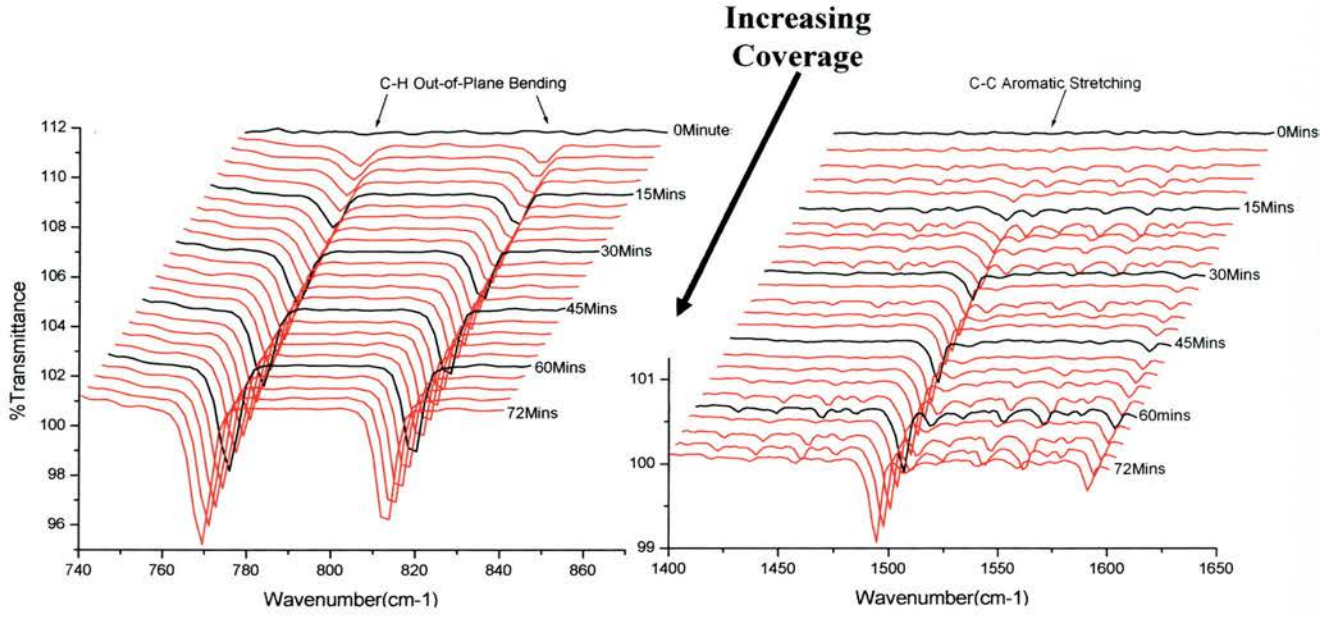

Fig. 59 Growth of perylene on Cu(110): 769cm^{-1} and 814cm^{-1} C-H out-of-plane bending modes

Fig. 60 Growth of perylene on Cu(110): 1494cm^{-1} C-C aromatic stretching

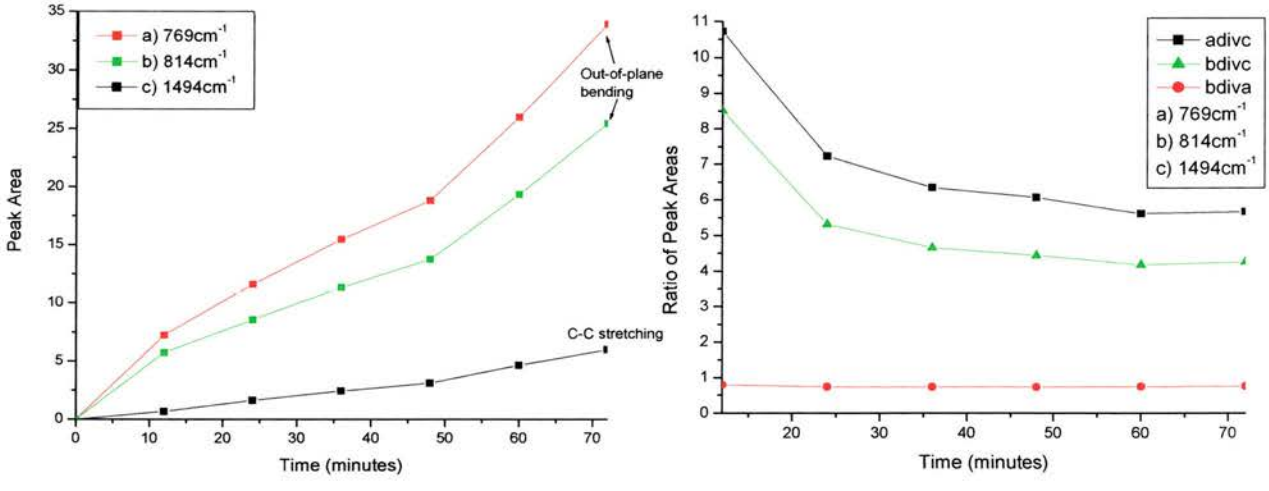

Fig. 61 Changes in peak area vs. time during continuous deposition of perylene

Fig. 62 Ratios of peak area vs. time. prior to 12 minutes, there is no visible mode at 1494cm^{-1}.

Deposition was carried out on a room temperature substrate with a relatively slow initial deposition rate. The only peaks noted initially are the two out-of-plane modes at 765.6 and

814.0 cm^{-1}(Fig. 59), indicative of the molecules lying flat on the surface. An investigation of the various symmetries shows that only the vibrations with B_{3u} (i.e.765 and 814cm^{-1} – 540cm^{-1} is below the range of the RAIRS detector) remain visible if the molecule is flat on the substrate (They convert to A_1 symmetry[132]). As coverage increased, the in-plane modes become visible (Fig. 60). The areas of several of the peaks are plotted against time to show the rates of evolution change over time (fig. 61). The ratio of the peak areas (Fig. 62) shows clearly that the out-of plane modes grow at a constant rate with respect to each other (the ratio of peak areas is constant). The in-plane mode at 1494cm^{-1} must be growing at a faster rate than the out-of-plane modes as the ratio of out-of-plane to the in-plane modes is decreasing as coverage increases. This suggests that initially, the perylene molecules are predominantly flat but as coverage increases, an increasing proportion of molecules are no longer flat, indicating that the overlayers are becoming increasingly disordered. This fits with the model of a highly orientationally ordered initial structure that is driven by substrate interactions. As the deposited layer thickens, the interaction between the substrate and the grown film becomes weaker and more disordered, allowing molecules to stand upright (or tilted).

Table 7 Data for Fig. 61 and Fig. 62

Time (minutes)	Peak Areas a) 769cm^{-1}	b) 814cm^{-1}	c) 1494cm^{-1}
0	0	0	0
12	7.22	5.73	0.67
24	11.60	8.54	1.61
36	15.46	11.34	2.44
48	18.81	13.76	3.10
60	25.98	19.32	4.63
72	33.93	25.43	5.98

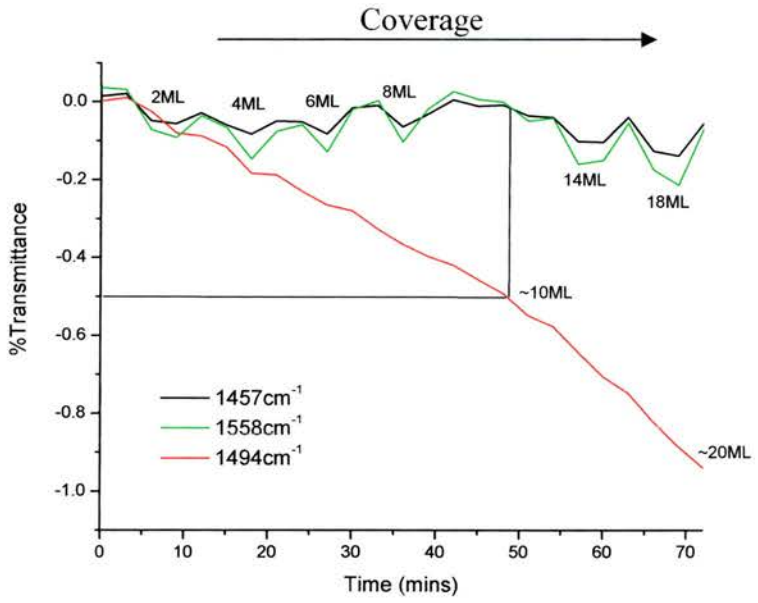

Fig. 63 Peak 1494cm^{-1} v Time: Adjacent peaks (visible in fig. 60) appear and disappear as coverage increases. Two of these are plotted v time. Calculated total film thickness is marked. This oscillation may be as a result of the "pinning effect" of the perylene growth. As this is a two layer process it may produce the oscillation.

Fig. 63 shows the variation in intensity of the weaker in-plane modes around 1500cm^{-1} as a function of deposition time. The small peaks can be seen growing to an intensity equivalent to around a monolayer and then disappearing and reappearing repeatedly (Fig. 60). If plotted against time (Fig. 63) then it is clear that these peaks are oscillating in intensity with a constant time interval. When the intensities are calibrated against the layer thickness (calculated via TPD), the sequence appears to follow a perfect two-monolayer pattern. As the experiment was done as both constant deposition and constant temperature it is impossible to say whether or not this is a real feature of the surface or a mechanical effect caused by the spectrometer. It is possible that this effect will be connected to the novel structures investigated by STM. There is evidence that the multilayer structure is driven by a "pinning" effect where the upper layer stabilises the lower layer. If this is a two-layer process then it may cause a structural distortion visible in RAIRS.

Desorption of Perylene from Cu(110)

As a continuation of the deposition experiment above, once the film had been grown, it was desorbed under the influence of a temperature ramp (RAIRS - TPD). The temperature was slowly ramped (~0.5K/min) to allow a slow desorption of the deposited film (Fig. 64). The peak intensity dropped off increasingly fast at 30°C before dropping off sharply between 39°C and 43°C. Small peaks remained until the temperature reached 57°C when they too disappeared. It is likely that these correspond to the multilayer and monolayer desorption temperatures. The behaviour of the 814cm^{-1} feature is shown in Fig. 65.

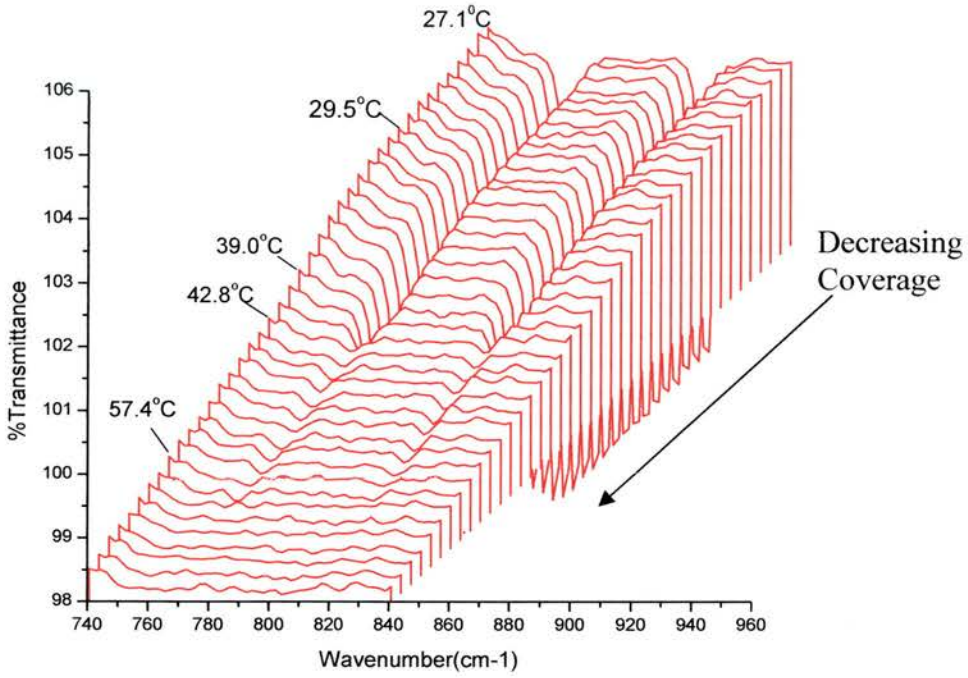

Fig. 64 Temperature Programmed Desorption of Perylene from Cu(110): RAIRS spectra in the range 740 - 840cm^{-1} collected during heating (0.5K/min). 769 and 814cm^{-1} peaks are out-of-plane bending modes. Multilayer desorbs between 39.0°C and 42.8°C, monolayer desorbs at 57.4°C.

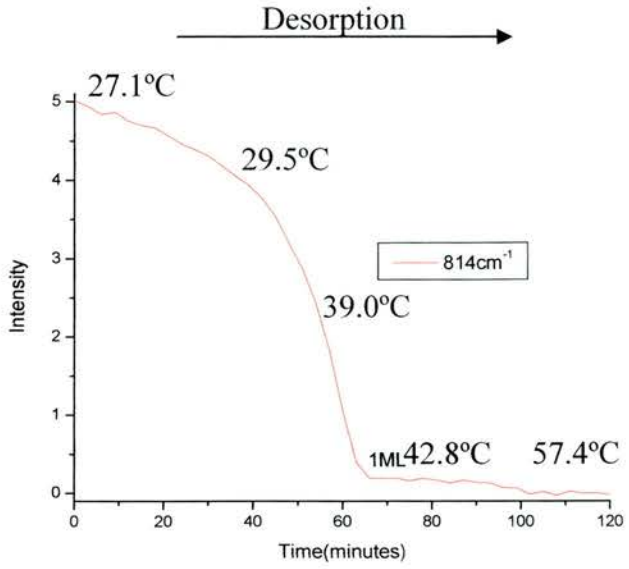

Fig. 65 Desorption of perylene from Cu(110): Intensity of 814cm^{-1} peak v time. Multilayer desorbs at ~40°C, monolayer at ~57°C

If it is assumed that the small peaks at 769 and 814cm^{-1} that remain between 43°C and 57°C are the monolayer peaks, then their areas can be used to approximate the thickness of the multilayer (Table 8). By this method, the initial multilayer can be determined as approximately twenty monolayers thick. This suggests that under the deposition conditions used, the first monolayer was completed in around 3.5 minutes

Table 8 Areas of multilayer and monolayer peaks

	Multilayer Area	Monolayer Area	Calculated Multilayer Thickness
769cm^{-1}	34.95	1.85	18.9 layers
814cm^{-1}	24.68	1.22	20.2 layers

Low Energy Electron Diffraction (LEED)

With the multilayer and monolayer desorption temperature calibrated from RAIRS - TPD, LEED studies were carried out to monitor any ordered structures that may be present (Fig. 66). The crystal was facing away from the perylene doser so that the deposition rate would be extremely slow (i.e. only from background deposition). This would allow the capture of subtle changes in structure as coverage increased. The substrate was held at 40°C to facilitate the diffusion of molecules over the surface to optimise molecular packing.

On initial exposure to perylene (1-5minutes), a slight halo was seen around the (0,0) spot, recorded at 28eV. As exposure time increased (10-20 mins), spots could be seen above and below the (0,0) spot. At 20 minutes, spots begin to appear at approximately ±37° relative to the "12 o'clock" position, and by 24 minutes, the vertically positioned spots have disappeared. As coverage increased further, the spots became sharper and the angles increase to 40-42°. Increased coverage caused the spots to disappear (possibly due to a disordered monolayer) but annealing to 100°C returns the sharp monolayer spots with an angle between upper spots of 80°. From earlier RAIRS-TPD experiments, the desorption temperature of the monolayer had been calculated at 57°C which is significantly below 100°C at which a LEED pattern (presumed to be the monolayer structure) for perylene was recorded. This may be due to the slow pumping speed of perylene from the vacuum chamber. This would account for spontaneous reformation of the monolayer LEED pattern when the substrate cools below the monolayer desorption temperature but should not allow a LEED pattern to be recorded above it. It is more likely that due to thermal constraints within the RAIRS chamber, thermal effects cause changes in the substrate (expansion, buckling etc) that affect the IR beam pathway and prevent the film being detected.

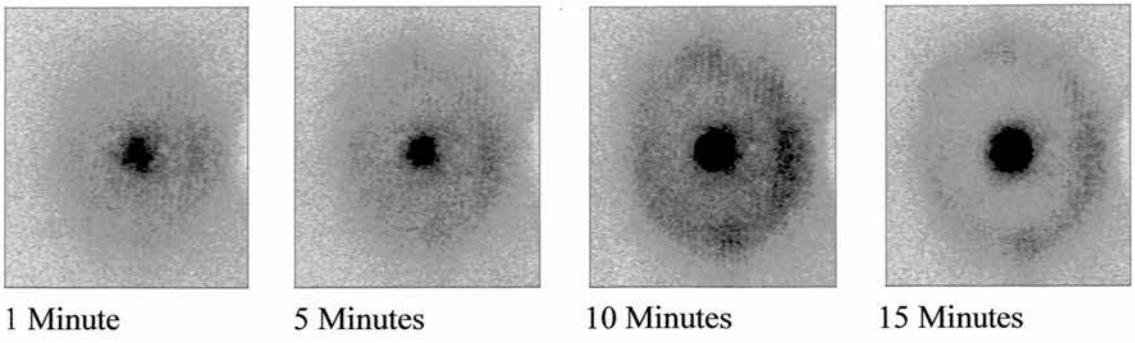

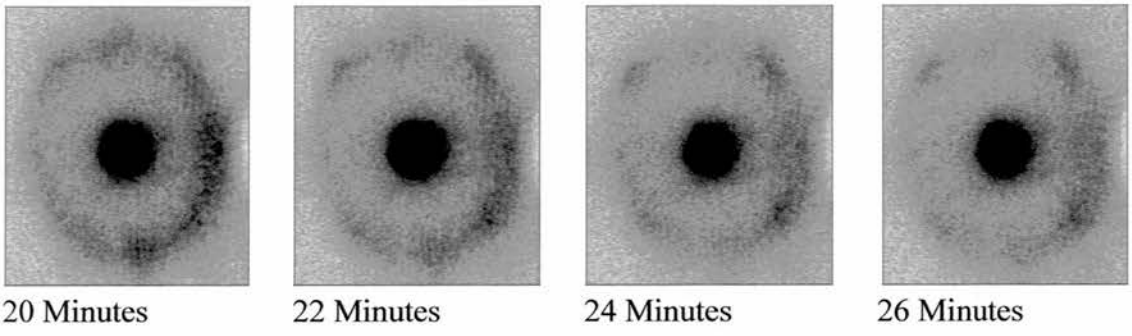

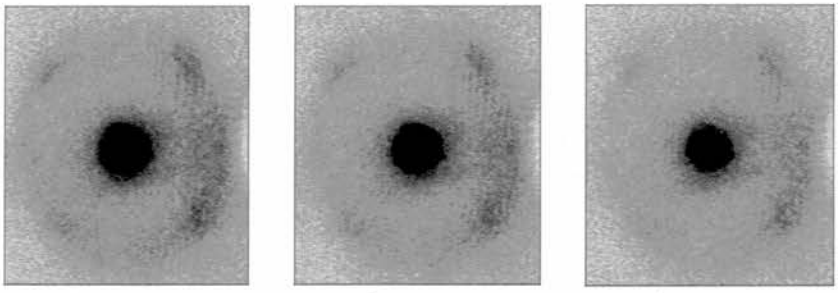

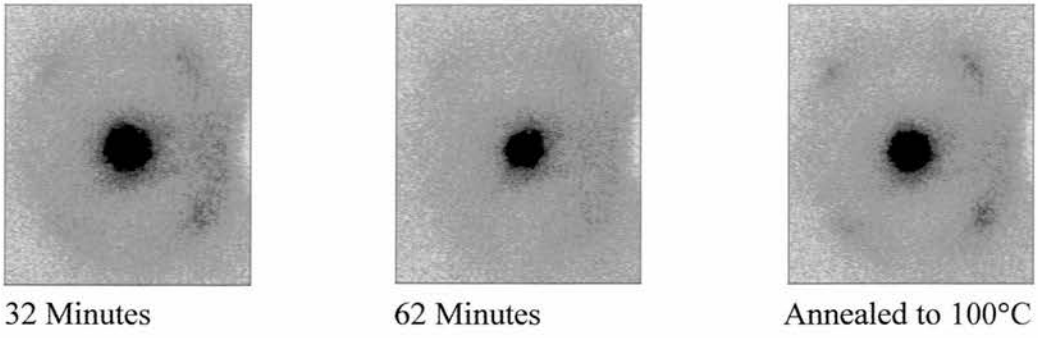

Fig. 66 LEED of perylene on Cu(110) under constant deposition conditions. After 62 minutes, sample was annealed to 100°C. All images collected at 28eV. Initial halo around 0,0 spot indicates a disordered structure with the molecules at the minimum intermolecular distance. As the structure becomes more ordered, spots resolve and the distances and angles become fixed at those of the unit cell.

Due to the discrepancy between the monolayer desorption temperature recorded in the RAIRS-TPD experiment and the LEED experiment a film was grown at 60°C. This should be above the lower recorded desorption temperature. The LEED pattern was recorded at 60°C to ensure that no structures were formed as the substrate cooled. The recorded pattern was different to that recorded at the lower substrate temperature. Six spots were now clearly visible instead of four with two in the horizontal positions. The angle between the two upper (and lower) spots had decreased to 65° (Fig. 67). Increasing coverage on top of this new structure (with the substrate at room temperature) then provided a significantly different LEED pattern and therefore structure (Fig. 68). The unit cell is now rectangular.

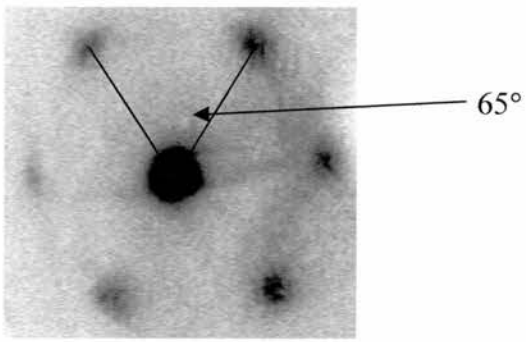

Fig. 67 LEED of perylene film grown at 60°C - 26eV. This corresponds to the β-phase that will be discussed later.

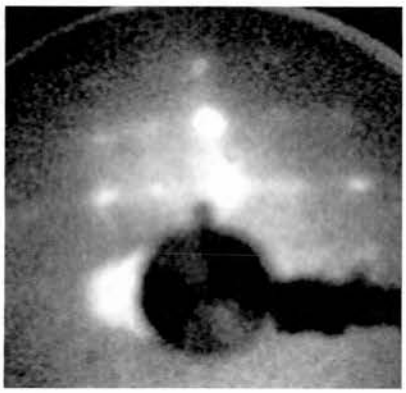

Fig. 68 LEED of thick film of perylene -19eV. This corresponds to the γ-phase that will be discussed later.

If the three structures are assigned α (Fig. 66), β (Fig. 67) and γ (Fig. 68) phases and unit cell dimensions are determined from the LEED pattern by correlation with the substrate spots the following is found:

Measuring the initial halo (Fig. 66) a dimension of 13.0Å is recorded. This corresponds to the inter-molecular distance that molecules would achieve if there was no orientational order of the molecules, i.e. they can orient themselves in any of the 360°

α-phase unit cell: a = 12Å ± 1Å, b = 12Å ± 2Å, β = 79° ± 3°(angle is an average of all LEED patterns)

β-phase unit cell: a = 10.8Å, b = 10.8Å, β = 65°

γ-phase unit cell: a = 20.7Å ± 0.2Å, b = 19.3Å ± 0.1Å, β = 90° (dimensions calculated from STM images as no substrates spots were visible for calibration)

Model LEED patterns are shown in Fig. 69.

As the initial structures are grown, compression can clearly be seen. This could correspond to closer packing of molecules as coverage increases. The γ-phase is significantly different and is likely to stem from a completely different structure.

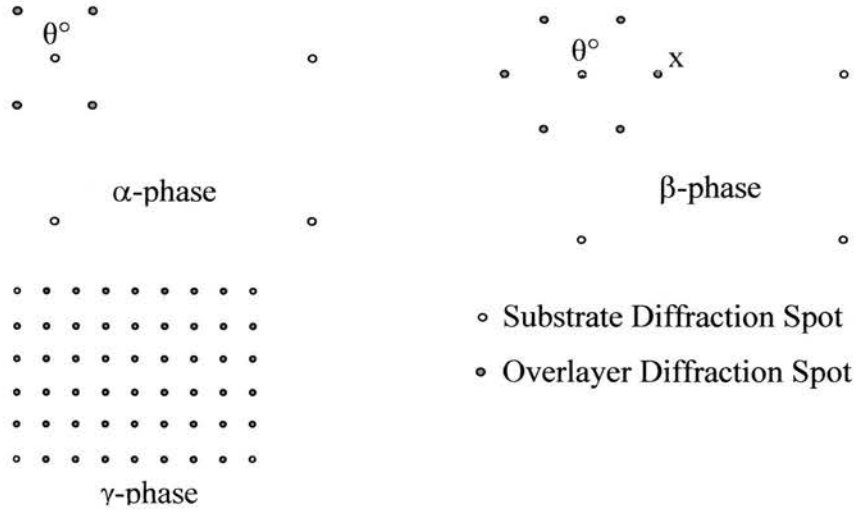

Fig. 69 Ideal models of α, β and γ LEED patterns. θ is smaller in the α-phase than the β-phase and the spots at position x are absent.

STM

RAIRS suggested the molecules were predominantly lying flat and the LEED studies indicated three distinct structures with differing unit cells. The experiments were reproduced in the STM in an attempt to image the films corresponding to the various phases.

Four distinct phases were observed in the LEED experiment, the halo, α, β and γ-phases. The halo represents an extremely low level of coverage of perylene on the copper surface. As it was expected to be extremely difficult to produce an extremely low level of coverage under normal deposition conditions, a lower sublimation temperature was used (~90°C) for only three minutes. The sample was dosed with the substrate at room temperature. The LEED pattern recorded was the halo seen in the initial images of the LEED experiment. Isolated molecules of perylene on copper are presumably weakly bound and easily moved by the STM tip and thermal diffusion. They can also be quite "transparent", where their electron density is similar to that of the substrate so there is little obvious contrast in the STM images. Molecular resolution can be difficult to find as molecules may be overlooked. When molecules are imaged, colour contract processing of the images makes them more obvious.

It is only once the molecules start forming clusters of three or four molecules that they become far more obvious. The STM image (Fig. 70) shows that the molecules can form both islands on the terraces and decorate the step edges. The subsequent images (Fig. 71) of repeated scan over the same area show the same cluster. This indicates that the island size and shape varies significantly between scans because of the mobility of molecules suggesting a structure of islands in equilibrium with highly mobile single molecules.

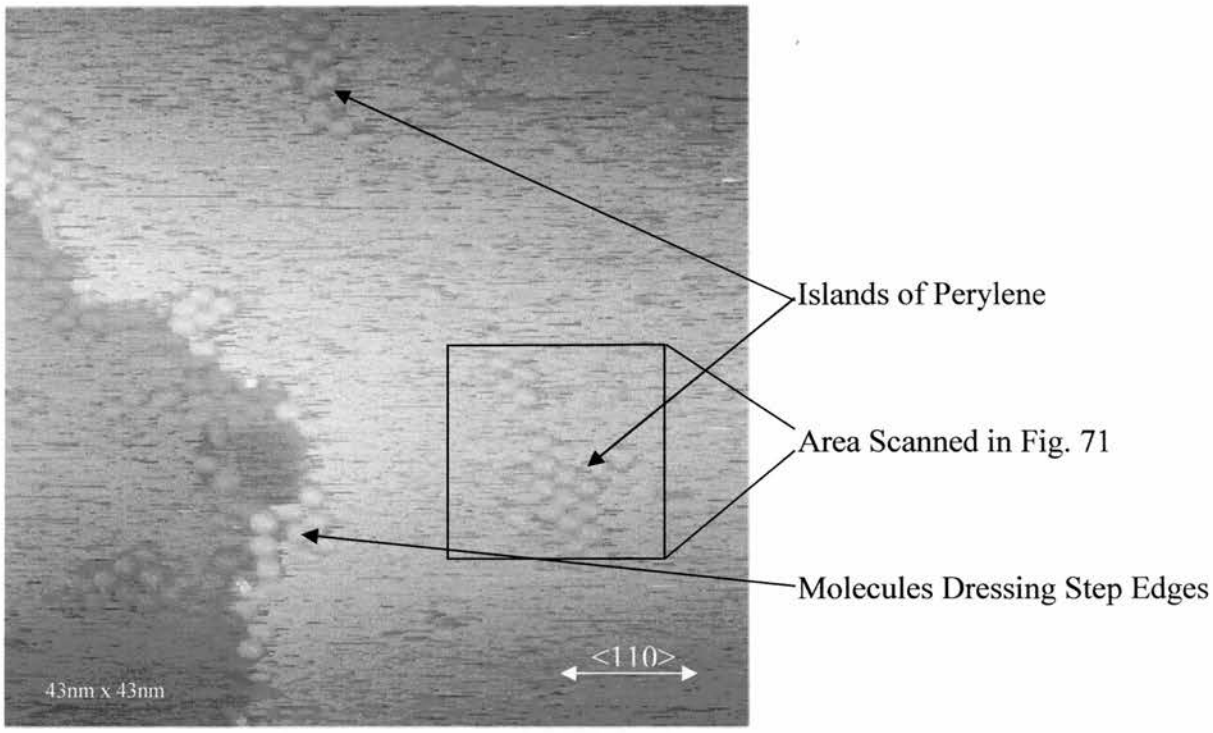

Fig. 70 Low coverage perylene on Cu(110). Tunnelling Conditions: -0.008V, 0.132nA, Loop gain 2.06%. Individual and small groups of molecules can be seen on step edge and in small islands on terraces

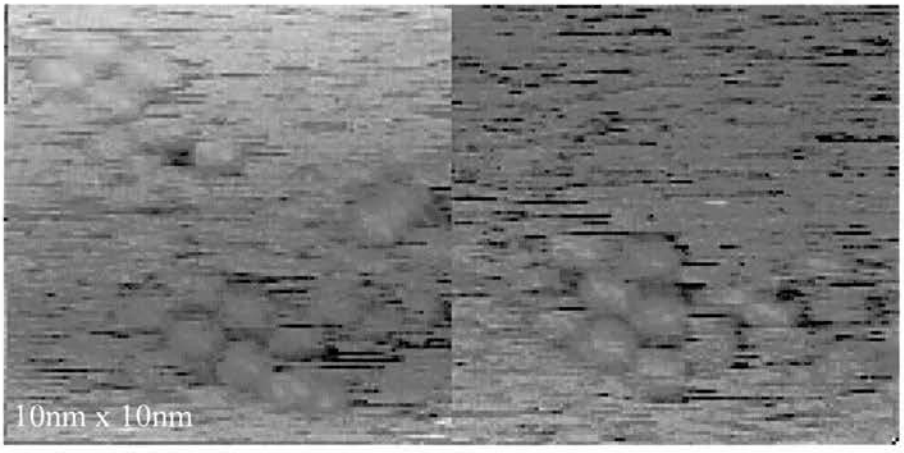

Fig. 71 STM images showing mobility of perylene molecules. Tunnelling conditions as fig.70. Island decreases with size with each subsequent scan. Molecules are easily removed.

Auto-correlation images based on such STM images agree with measurements from the "halo" LEED pattern and indicate a consistent inter-molecular distance of 1.3nm.

After these images were collected, the regions at the edges of the scan area were examined but no evidence of tip-deposited molecules were seen suggesting they had either undergone tip induced desorption or that they were just being moved again by thermal diffusion. Subsequent studies by Q. Chen[141] proved that the molecules are not desorbed, but are "shunted" across the surface by the tip. On an oxygenated surface (~50% oxygen 2x1), the copper islands at the sides of the image fill up first before propagating their structure into adjacent copper islands. The oxygen regions form a barrier that prevents the perylene diffusing away across the surface, so islands of molecules form far more easily. The tip interaction is best described as shunting as if it were a stronger interaction then it is less likely that the molecules would be deposited at the edge of the scan area, but would instead be dragged back across the image.

This stage of growth can therefore be described as molecules that are loosely bound to each other that form clusters of molecules that are 1.3nm apart but have no directional order, hence the halo instead of spots on the LEED pattern.

Coverage was increased to approximately one monolayer with the LEED showing that of the α-phase with compression from 1.3nm to1.1nm.

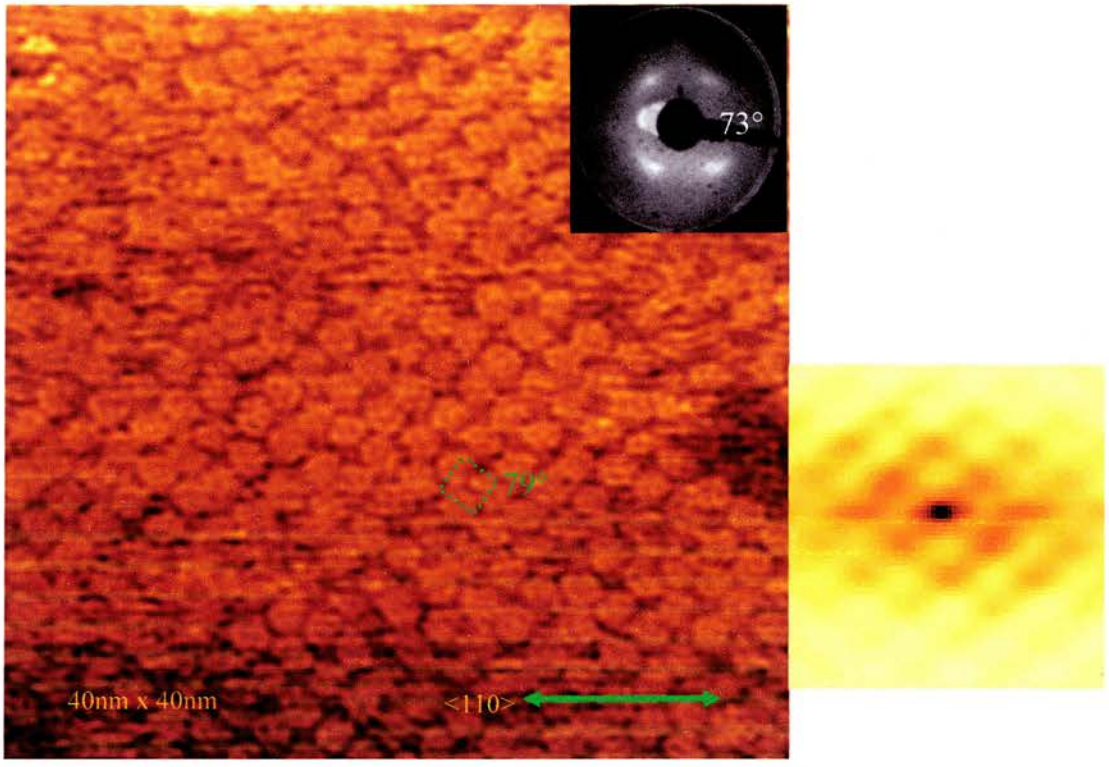

Fig. 72 One monolayer of perylene on Cu(110). Tunnelling conditions: -0.067V, 0.299nA, 8.73% Molecules can clealy be observed to form a full monolayer.

Auto-correlation functions of the images show them to contain a higher degree of order than is immediately apparent from the STM images (Fig. 72). From measurements using the auto-correlation of the STM image, it is seem that the unit cell dimensions agree with those recorded from the LEED pattern. As all the data fits, this structure can be assigned as the α-phase with dimensions of: $a = 12Å \pm 1Å$, $b = 12Å \pm 1Å$, $\beta = 79°$. The unit cell contains a single perylene molecule. This structure could be commensurate with a c(8x4) structure which would give precise unit cell dimensions of $a = 12.5Å$, $b = 12.5Å$ and $\beta = 70.6°$. The orientations of the molecules within this structure are unclear due to insufficient resolution in the STM images, however the inter-molecular spacing are large enough that

the molecules may have any orientation. This may be the influence that prevents the structure from optimising the close packing of the molecules. Continued deposition on top of the α-phase gives rise to the same LEED pattern and structures in STM. This implies that the β and γ phases must be temperature dependent.

Before the evolution of the α-phase, there was no evidence of any structure connected with the vertical spots on the LEED pattern (Fig. 73). This phase was seen after the formation of the structure that gives rise to the halo LEED pattern but shortly before the surface achieved its first monolayer coverage with the α-phase.

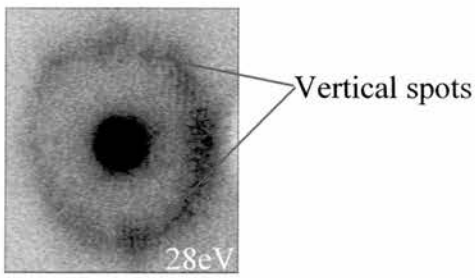

Fig. 73 Low coverage of perylene on Cu(110). LEED pattern represents a phase between the low coverage shown in Fig.70 and 72

This may indicate that before the final compression leading to production of the α-phase, a brief phase transition occurs to another structure that as yet has been unidentified in the STM. It is possible that this LEED pattern has some connection with the γ-phase structure that will be discussed later. It is suggested that the lower layers of the γ-phase are "pinned" by an upper layer. It could be possible that in the absence of an upper layer that the γ-phase begins to form but is too unstable without a second layer so reverts to the α-phase.

When α-phase structure was annealed to 70°C, the LEED pattern changed to that characteristic of the hexagonal structure which, when measured suggested a further small contraction had occurred. STM showed that significant changes in the structure have indeed occurred. Fourier transformation of the STM image produces a diffraction pattern that matched that of the β-phase LEED pattern.

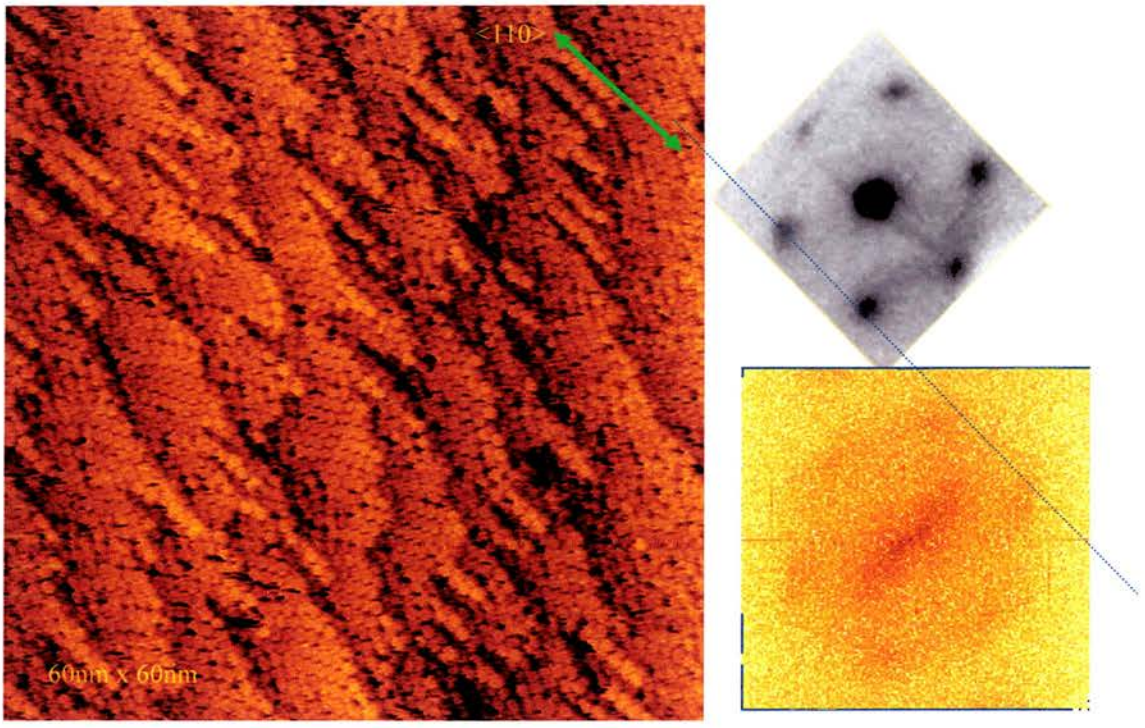

Fig. 74 Annealed monolayer of perylene on Cu(110), LEED (grey) and FFT of STM image. Tunnelling Conditions: -0.115V, 4.282nA, 6.97%Loop Gain. LEED and FFT of STM images are the same indicating that the structure observed in STM must be real.

The molecules on the terraces are now clearly aligned with each other and they share the same orientation (Fig. 74). This alignment accounts for the compression seen in the dimensions and angles of the LEED pattern. The LEED pattern and the apparent structure in the STM images have different symmetries. This can be accounted for by known distortions that can occur in STM images such as drifting of the piezo-electrics.

The LEED patterns must be correct so we can accurately say the unit cell dimensions for the β-phase LEED pattern are: a = 10.84Å, b = 10.84Å, β = 65°. This recognises that there are two separate phases of mirror symmetry that combine to produce one LEED pattern. Investigations of the STM images show that the molecules now all share the same orientation. Measurements taken from the STM images give a unit cell of a = 12.5Å, b = 8.5Å and β = 90° (Fig. 75). This structure is commensurate with the underlying copper substrate and has unit cell vectors of:

$$\begin{pmatrix} 3 & 1 \\ -2 & 3 \end{pmatrix} \text{ and } \begin{pmatrix} -3 & 1 \\ 2 & 3 \end{pmatrix}$$

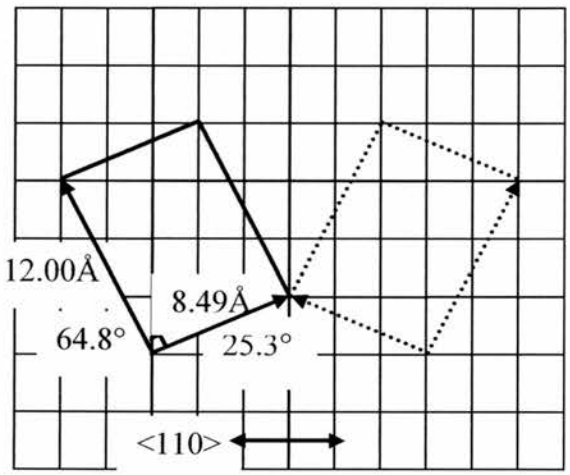

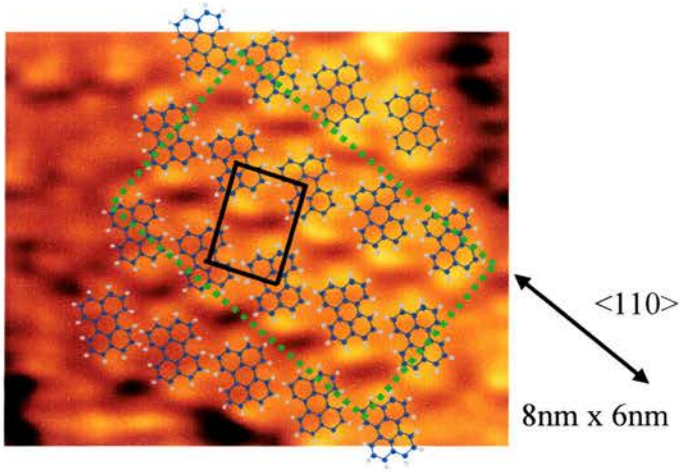

Fig. 75 β-phase of perylene on Cu(110). Tunnelling Conditions as Fig.74. Molecules are more highly regularly oriented than the α-phase

An interesting feature of this structure is the small fingers up to about ten molecules long that are starting to appear as the second layer of this structure (Fig. 76). These fingers were perfectly aligned with the underlying substrate along the <110>, close packed copper direction.

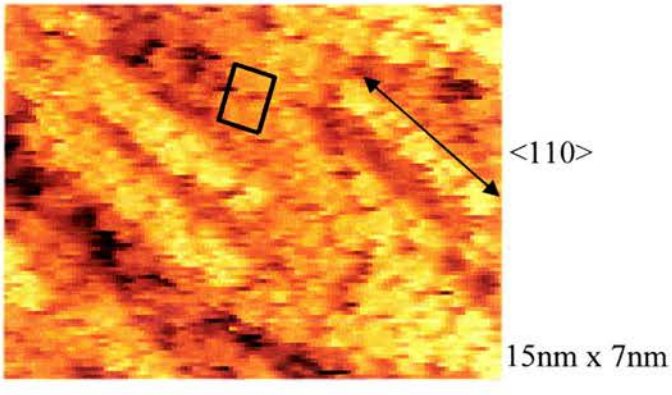

Fig. 76 Fingers of perylene growing on top of the β-phase (unit cell marked). Tunnelling Conditions as Fig. 74. Fingers are aligned with <110> direction whereas β-phase structure is not.

The orientation of the rows of fingers was confirmed by comparison of LEED patterns with visible substrate spots with the Full Fourier Transform of the STM images. As the overlayer spots are the same it can be confirmed that the <110> direction is that marked in Fig. 76. It seems odd that the structure follows the substrate so exactly with a layer of an incommensurate structure in between. There is however some evidence, discussed later, to suggest that the underlying layers undergo a rearrangement to align themselves with the overlying structure and substrate.

As the overlying "fingers" indicate the <110> direction, this can be defined on the new monolayer structure. The supercell (shown in green in Fig. 75) is maybe commensurate with the substrate and has dimensions of 36Å x 22Å (14 x 6).

Continued growth on top of this structure or continuous dosing on a clean substrate with annealing in the initial stage of growth, produced an intermediate stage where the two different crystal structures could clearly be seen on the same STM image. This showed a linear structure (γ-phase) that had grown from the "fingers" seen in the previous images (Fig. 74, Fig. 76) separated by patches of the previous crystal structure that is the annealed, one monolayer thick structure (β-phase). These structures are highly reproducible but are absolutely reliant on the annealing stage during the growth. This can be through forming the β-phase from the α-phase through gentle heating, or by producing the β-phase initially while cooling the substrate through the monolayer desorption temperature (~60°C) under molecular beam conditions or with sufficient molecules in the system to permit background deposition. The β-phase must be produced before the γ-phase can be produced.

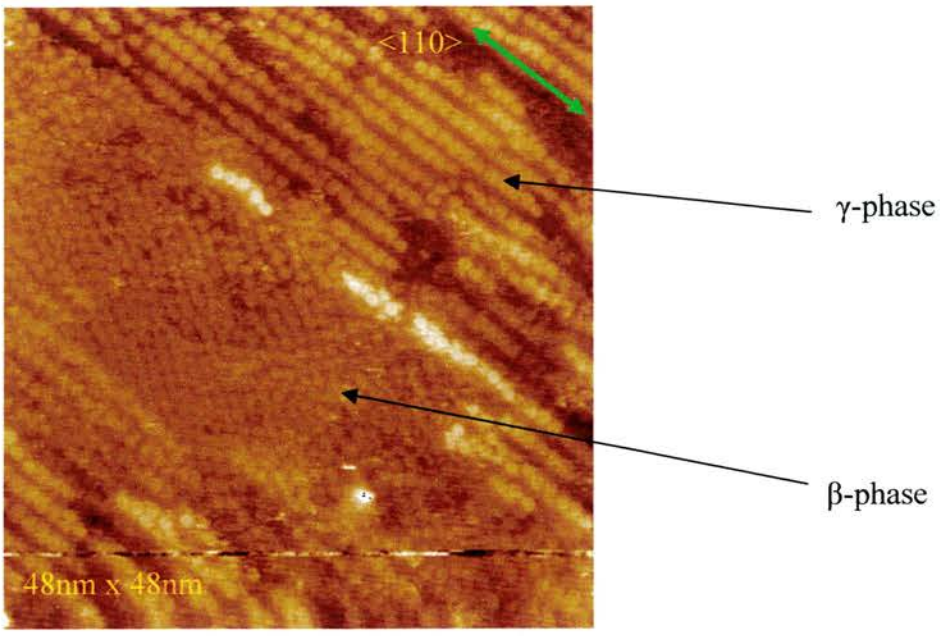

Fig. 77 β and γ-phases of perylene on Cu(110). Tunnelling Conditions: -0.016V, 0.725nA, 4.64% Loop gain. Annealing with sufficient deposition allows both phases to exist.

The LEED pattern recorded from this structure is, as expected, a combination of the β-phase and the γ-phase. The limited resolution of the STM images does not allow detailed examination of the molecular orientation within the linear structure, but information is available regarding the molecular spacing. The separations of the rows at this coverage are not uniform. Auto-correlation can be carried out on line profiles to extract the average spacing for perylene rows intersected by the line profile. Measurements ranging from 1.6nm to 1.9nm between the perylene rows were recorded. These measurements do not seem to relate in a commensurate way to the spacing of the underlying copper rows that run parallel to the perylene rows. The molecular distance along the rows is around 1.2nm, which corresponds approximately to the close packed intermolecular distance.

It is also significant that both crystal structures exist at the same height. This is evidence that, as coverage increases, the structure changes from one to the other as opposed to the γ-

phase growing on top of the β-phase giving strength to the restructured monolayer argument. From this image, others at the same coverage and those at higher coverage, there is some evidence of the growth mechanism. At the ends of the linear structures, the molecules on the layer beneath can be seen to be more disordered than the exposed molecules surrounding it. As in the lower coverage images, these disordered molecules are seen next to patches of the β-phase, under the growing γ-phase, it can be assumed that a rearrangement of the initial monolayer has taken place. Due to the constraints of current spectroscopic techniques, this is currently impossible to confirm.

Further growth on top of the transitional phase, produced an exclusively γ-phase crystal. The growth leads to the surface of a perylene crystal of ~20 monolayers thick (Fig. 78) being "smoother" than that of the copper substrate on which the crystal is grown. Line profiles drawn across the surface showed a height different of only 0.5nm over a distance of 2000nm. However, the surface was covered with small pits that seemed to reach down to the substrate. These were believed to be caused by contamination on the substrate that hindered the subsequent multilayer growth or electron beam damage from LEED investigations. These pits were used as an approximate method of measuring film thickness that compared well with RAIRS-TPD experiments.

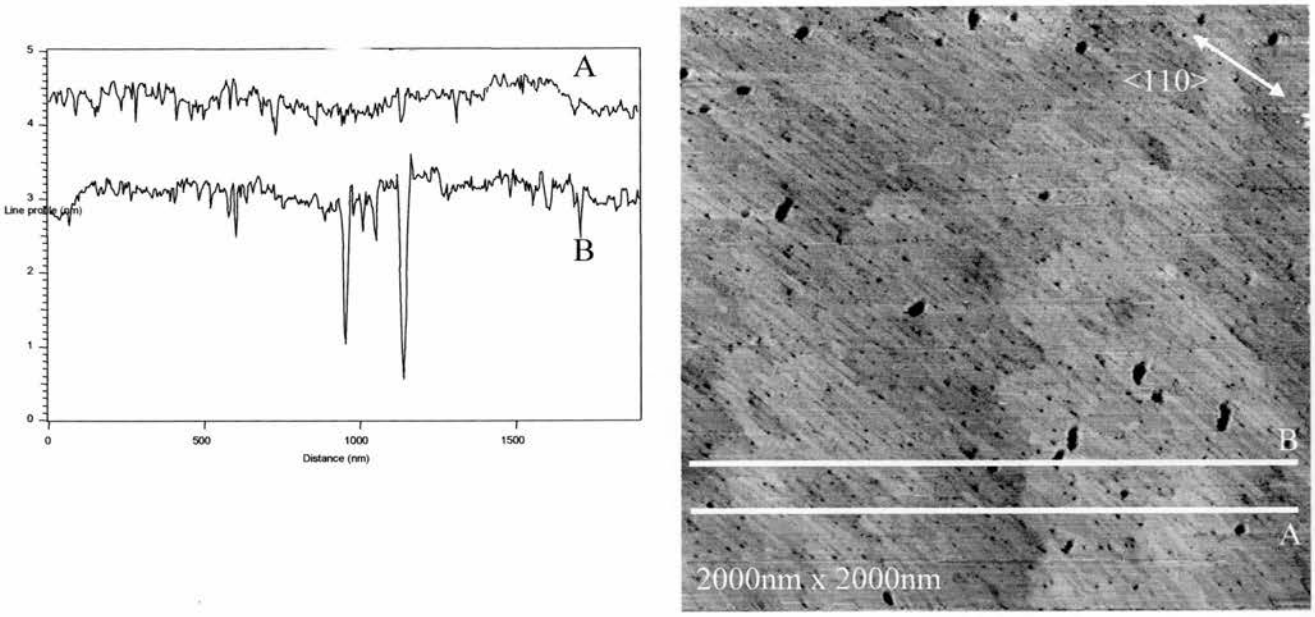

Fig. 78 Line profile across 2000nm perylene/Cu(110). Tunnelling Conditions: 0.006V, 1.862nA, 12.82% Loop gain. Line profiles show surface to be flatter than the underlying copper. LP across holes gives indication of layer thickness.

For the smoothing to occur, the molecules in the initial layers must have filled any roughness in the surface due to the high molecular diffusion observed previously, permitting uninterrupted crystal growth of the subsequent layers. This indicates that there are few substrate interaction that affects the process of growth of the thicker films, although there are indications that there are important interactions at lower coverage. The most obvious of these is the fact that the long perylene chains are aligned along the same direction as the close packed copper. If there were no interaction from the substrate then it would be expected that many more orientations would be seen, however, the crystal surface has the same symmetry as that of the underlying substrate (C_{2v}). The structure is basically described as highly ordered rows of perylene, with subsequent rows sitting over the gaps between rows of the level below (i.e. ABA stacking) (Fig. 79).

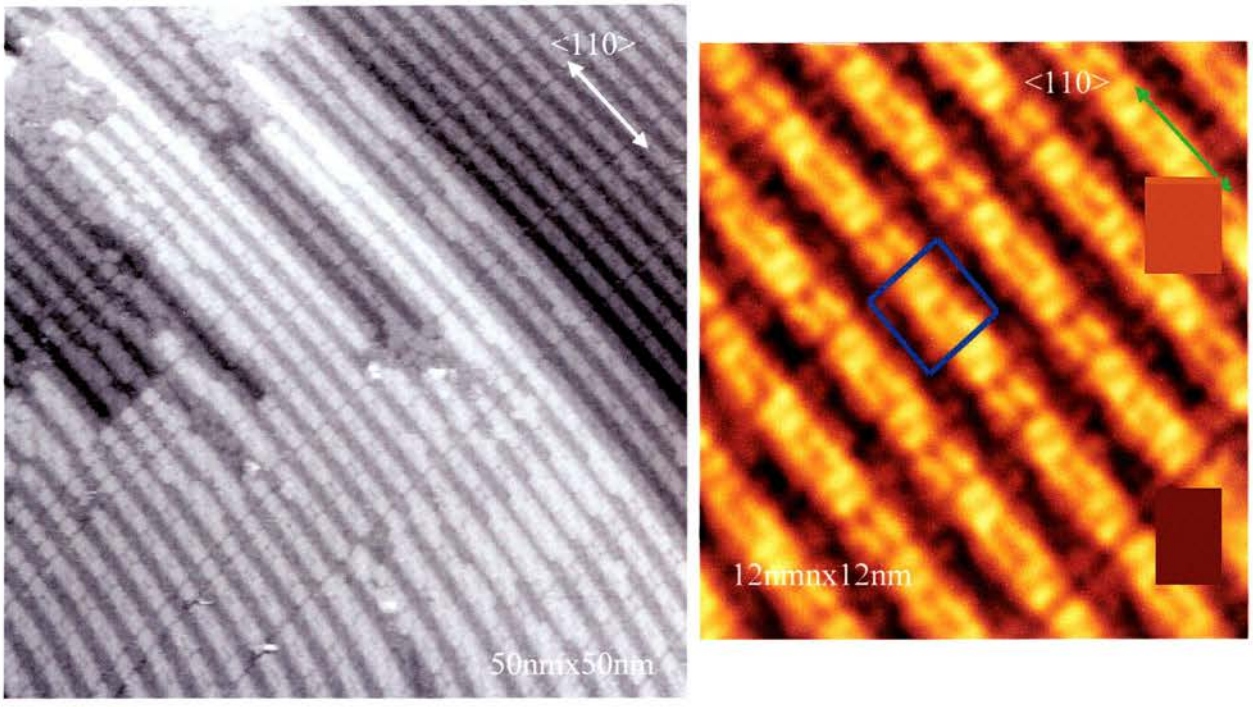

Fig. 79 Thick film (~20monolayers) perylene on Cu(110). Tunnelling Conditions: 0.007V, 0.468nA, 5.56% Loop Gain. Adjacent molecules in rows alternate orientation by 90°. Where they don't, a clear defect is seen. The molecules in the row below appear to be orientated the same as the molecules directly above them in top row.

Based on STM images and their auto-correlation images, the unit cell has dimensions of: a = 20.7Å ± 0.2Å, b = 19.3Å ± 0.1Å, c= 3.4Å and β = 90° (Fig. 82). As discussed above, the angle and symmetry of the unit cell match those of the substrate, so a rectangular unit cell is unsurprising. The unit cell length of 20.7Å corresponds to eight copper atoms along the <110> (close packed) direction. The unit cell structure is probably incommensurate in the b direction, however two unit cells are close to being commensurate with eleven copper rows. Over this distance, it is unlikely that this is a major driving force controlling the structure but it probably helps reinforce it.

Within this structure, the orientation of the molecules with each other is most interesting. Quantum mechanical calculations of the HOMO and LUMO molecular orbitals of the free molecule were carried out using Gaussian98 (Fig. 80). While the HOMO has orthogonal nodal planes perpendicular to the plane of the molecule, the LUMO only has the one intersecting the naphthalene units. Since the bias used for the STM images was very low it is likely that tunnelling from HOMO and to LUMO are important. This suggests that the low intensity, which bisects the molecular image, corresponds to the plane bisecting the naphthalene units as shown in Fig. 80. When the orbitals are superimposed, a node can clearly be seen along the centre of the length of the molecule. When this is compared with the STM images, it is clear that this relates closely to the molecules that are observed (Fig. 81).

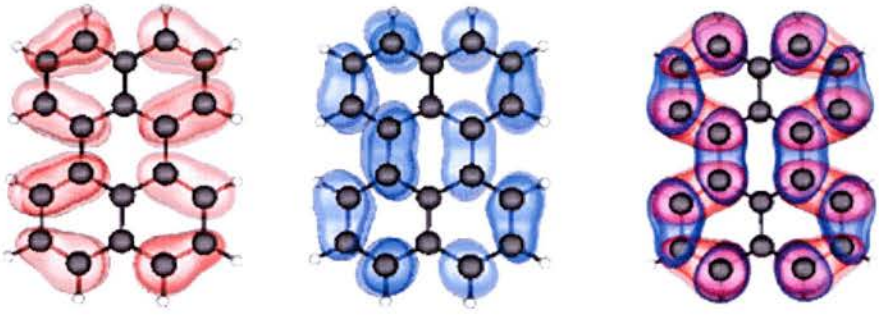

Fig. 80 Molecular orbital calculations of perylene free molecules. (Gaussian 98) When the two orbitals are overlaid, two features with a node are observed that match the STM images of the thick perylene film.

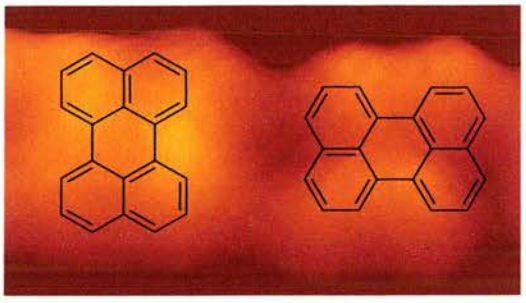

Fig. 81 Molecular models of perylene superimposed on STM image (taken from blue square in Fig. 79) based on MO calculations shown in Fig. 80.

Along the <110> direction, the molecules in each row show clear quadrupole coupling where adjacent molecules are rotated by 90° to each other. Defects do appear in the structure where two molecules will be oriented with their long edges parallel but adjacent molecules are never seen to appear short end on. In structures involving quadrupole coupling, the effect is expected to be three-dimensional, i.e. have the correct charge balanced orientation with respect to molecules above and below it as well as around it. This structure clearly breaks this rule. In the colour insert in Fig. 79, the molecules of the row beneath can be seen to have the same orientation as the row on top, in the grey section, the molecular orientation is seen to remain the same across three molecular levels. With this level of packing, the molecules in alternate rows must be packed at the optimum distance. These inter-row, inter-molecular interactions must have a strong influence on the structure. The patterns of the line defects support this view. In the rows along the <110> direction, where two adjacent molecules are seen to share the same orientation, not only does this same defect occur in every adjacent row in the same layer, but it also can be seen in the layers below. This causes distinct lines in the structure (in the <100> direction) which, appear to travel through the entire width of the image. It was not possible to define their actual lengths as zooming out to image a larger area reduced resolution sufficiently

that the lines were no longer visible. The implication of this structural feature is that they form distinct grain boundaries that are perpendicular to the <110> direction. There does not appear to be any structural defect that affects the structure in the <100> direction.

Fig. 79 also provides some insight into the crystal growth mechanism. Earlier results indicated that the γ-phase can only grow on the β-phase. Due to the orientation of the γ-phase a reconstruction of the initial monolayer would most obviously fit the growth mechanism. From the high coverage images and the orientations of the molecules within the structure, there is evidence that the upper layer stabilises the layer below which in turn propagates growth in the <110> direction. At the end of the rows shown in Fig. 79 (top left corner) the molecules of the penultimate layer appear to be highly disordered. Closer inspection shows these to be similar to the β-phase. It is unlikely that these areas of disordered molecules stop growth of the structure as this would prevent film thickness reaching 20 monolayers as observed. This suggests the structure grow through a reconstruction and "pinning" involving both the upper and lower structure.

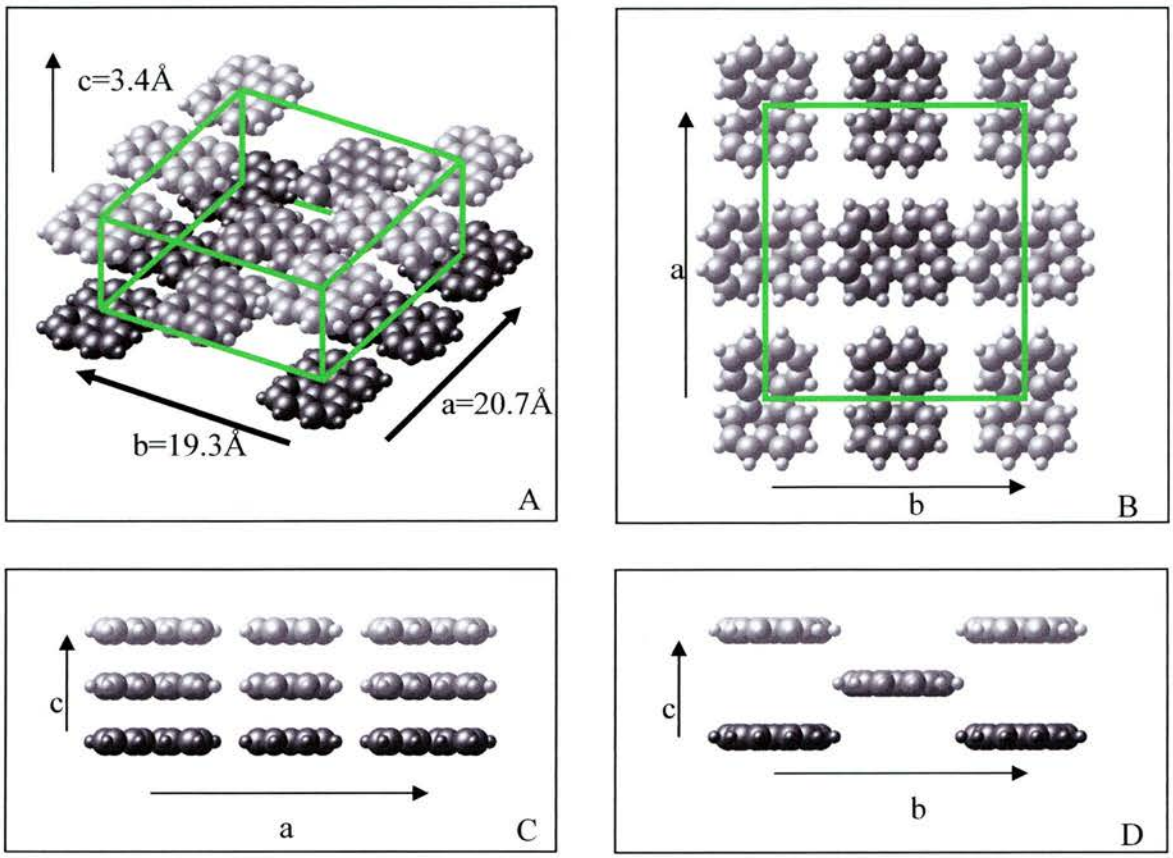

Fig. 82 Crystal structure of γ-perylene[142]. Centred orthorhombic structure, a=20.7Å, b=19.3Å, c=20.7Å, β = 90°

Photoluminescence of Perylene on Cu(110)

In situ photoluminescence of perylene on Cu(110) was also investigated to provide insight into the structure and growth. To obtain the photoluminescence spectrum for perylene, a small amount was dissolved in toluene and the spectrum was collected (Fig. 83).

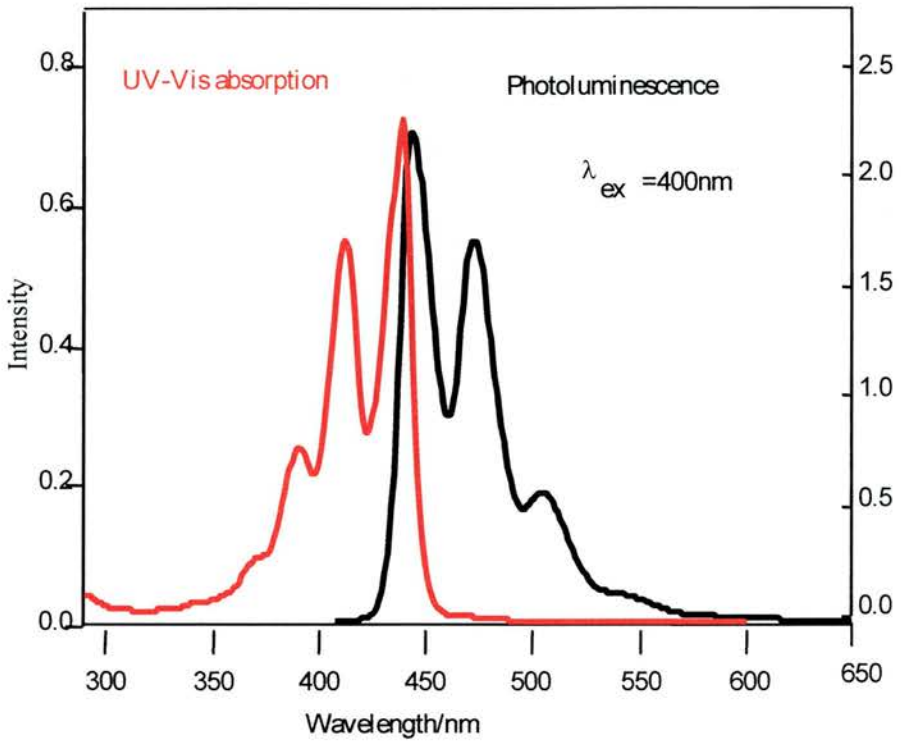

Fig. 83 Photoluminescence and UV-Vis absorption of perylene in toluene[143,144]

The spectrum clearly shows the principal absorption at 450nm which has been assigned to emission from monomeric perylene[145,146]. In contrast, the bulk α-phase of perylene contains dimers. When emission is stimulated in the solid, not only can the electron be excited to a higher level in the original molecule, but it can be transferred into a higher level of the adjacent molecule in the dimer. This causes positive and negative charges that attract causing an increased stabilisation of the dimer. This excited dimer is known as an excimer. As the excimer is more stable, the emitted photon has a lower energy at about

550nm[147,148,149,150]. As the γ-phase thin film has molecular packing that allows molecules in each layer to sit extremely close to molecules in adjacent layers, it was thought that a novel excimer interaction could occur. Due to the ABA layer growth of the perylene γ-phase any molecule can form an excimer with the molecule in the layer above it or below it (or both). Because of this, photons emitted from this sort of excimer would be expected to have energy lower than the 550nm emission of the standard excimer.

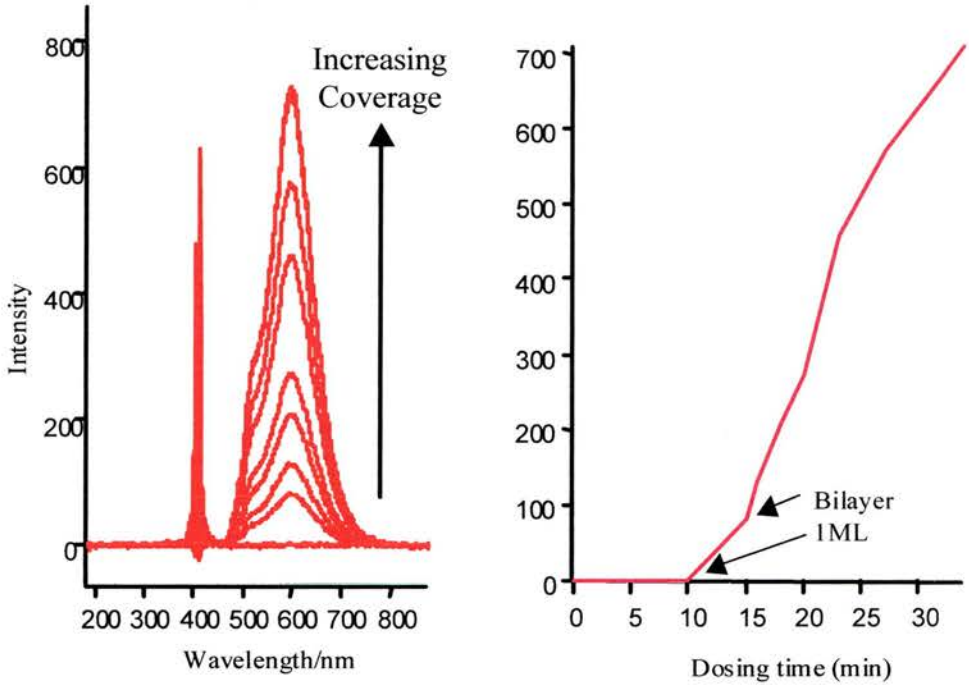

Fig. 84 Photoluminescence as a function of dosing time (minutes). Intensity increases linearly with increasing coverage.

As the spectrometer setup allows collection of spectra without hindering deposition, it was possible to collect the photoluminescence spectra as a function of time. As coverage increased, the intensity of the photoluminescence increased (Fig. 84). The peak at 410nm arises from the laser beam used to stimulate emission from the perylene film. Its wavelength is sufficiently removed from the region of interest not to interfere with results. The peak arising from the perylene film is indeed seen to occur at 600nm, which as

expected is lower than the normal bulk excimer signal at 550nm. The plot of photoluminescence versus dosing time show that there is a time lag before photoluminescence is observed. This is obviously coverage dependent. The initial monolayer probably takes a few minutes to form and is unlikely to provide a significant photoluminescence signal due to quenching of the excited state by the substrate. As coverage increases and the second monolayer is formed the photoluminescence appears. Until the completion of the second monolayer, this signal may still be partially quenched, hence the delayed onset of photoluminescence and noticeable kink in the graph.

The thick film of perylene was then desorbed while the luminescence was recorded. In between the collection of each luminescence spectra, the sample was moved into the EELS spectrometer to confirm film thickness (Fig. 85).

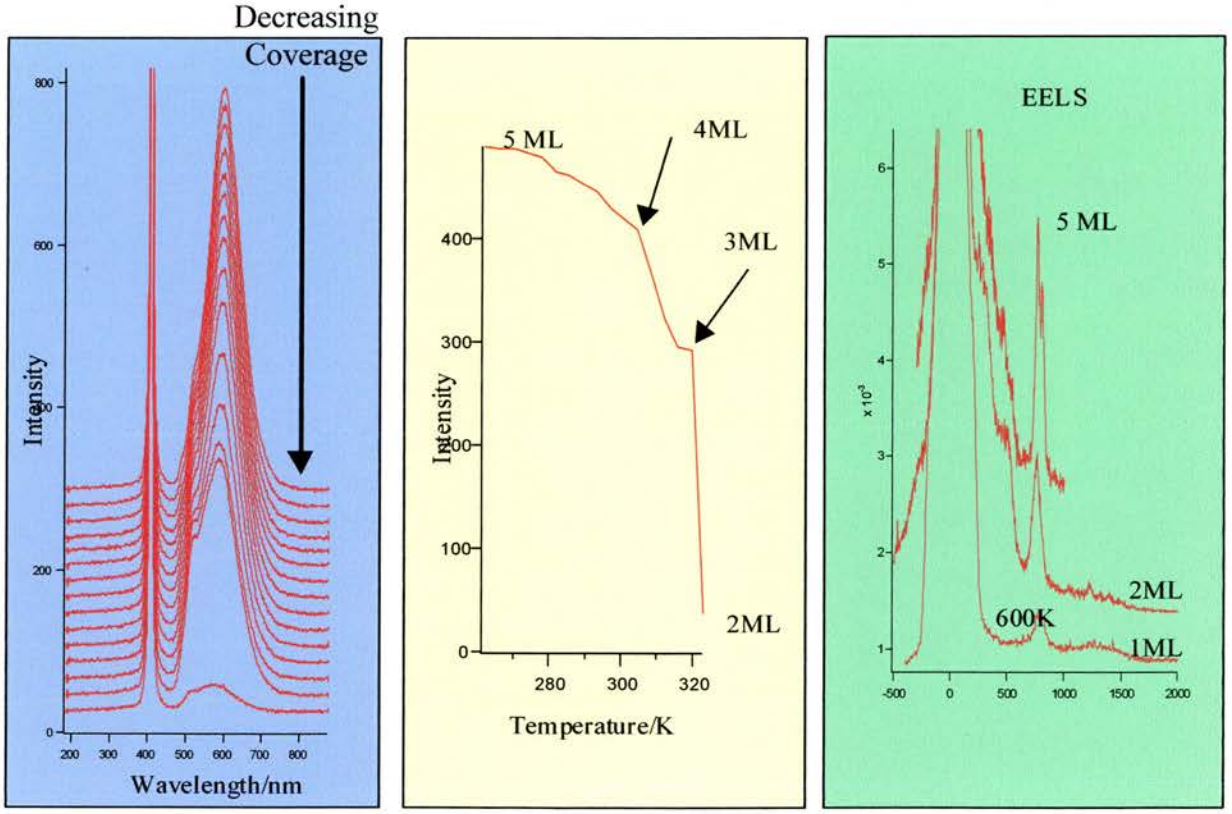

Fig. 85 Photoluminescence as a function of desorption. Intensity decreases with decreasing layer thickness. Between 3 and 2 monolayers photoluminescence is lost due to quenching from the substrate.

As expected, the desorption is a reverse of the deposition. The EELS spectra (Fig. 85 Right) confirm that the photoluminescence decreases steadily with coverage until between two and three monolayers. By two monolayers, the signal has disappeared completely. This may be explicable by the mechanism through which the structure grows. Photoluminescence from the initial monolayer (β-phase) is quenched so no emission is produced. As the second layer begins to grow, there is insufficient of the γ-phase for photoluminescence until some critical coverage is reached, close to the formation of the second layer. As the third layer grows, the structure is consolidated and photoluminescence increases. This is coupled with increasing separation from the copper substrate that inhibits the quenching effect of the substrate.

The temperature dependence of photoluminescence was monitored by growing a thick layer of perylene at 130K. As this did not have the necessary annealing stage, it was likely that the α-phase multilayer structured thin film was present as opposed to the more highly ordered γ-phase. At 130K, the luminescence signal (Fig. 86) was a slightly different shape than before (Fig. 85) with the principal peak at 590nm. The temperature could be ramped to 240K and cooled to 130K repeatedly with no change to the peak shape or position. Within this range, as temperature increased, the intensity of emitted light decreased. Above 240K, the peak shape changed irreversibly to that observed previously for the γ-phase (Fig. 85). As temperature increased, the intensity of luminescence increased up until 310K which is the multilayer desorption temperature above which emission is lost. This temperature dependent intensity change is the opposite of what was expected. If the film is not desorbed, but cooled back down to 130K, the luminescence intensity increases further and the peak shape does not change although the shoulder at 530nm becomes more obvious.

By comparing the intensity of emission of the first phase at 240K (~120 units) and the second phase, once annealing is complete, at 240K (~1450 units) it can clearly be seen that the intensity of the second phase is far greater (by roughly a factor of 10). This helps explain the observation of the increasing intensity during annealing of the film. If the film was held at 240K for a long period, the second phase would form and the photoluminescence intensity would be seen to rise. Once full transformation from the first phase to the second was complete, the intensity would stabilise. Cooling would then increase intensity and heating would reduce it as expected. What is observed in the experiment is an increase in intensity due to the structural changes, which is greater than the decrease in intensity due to the increased temperature.

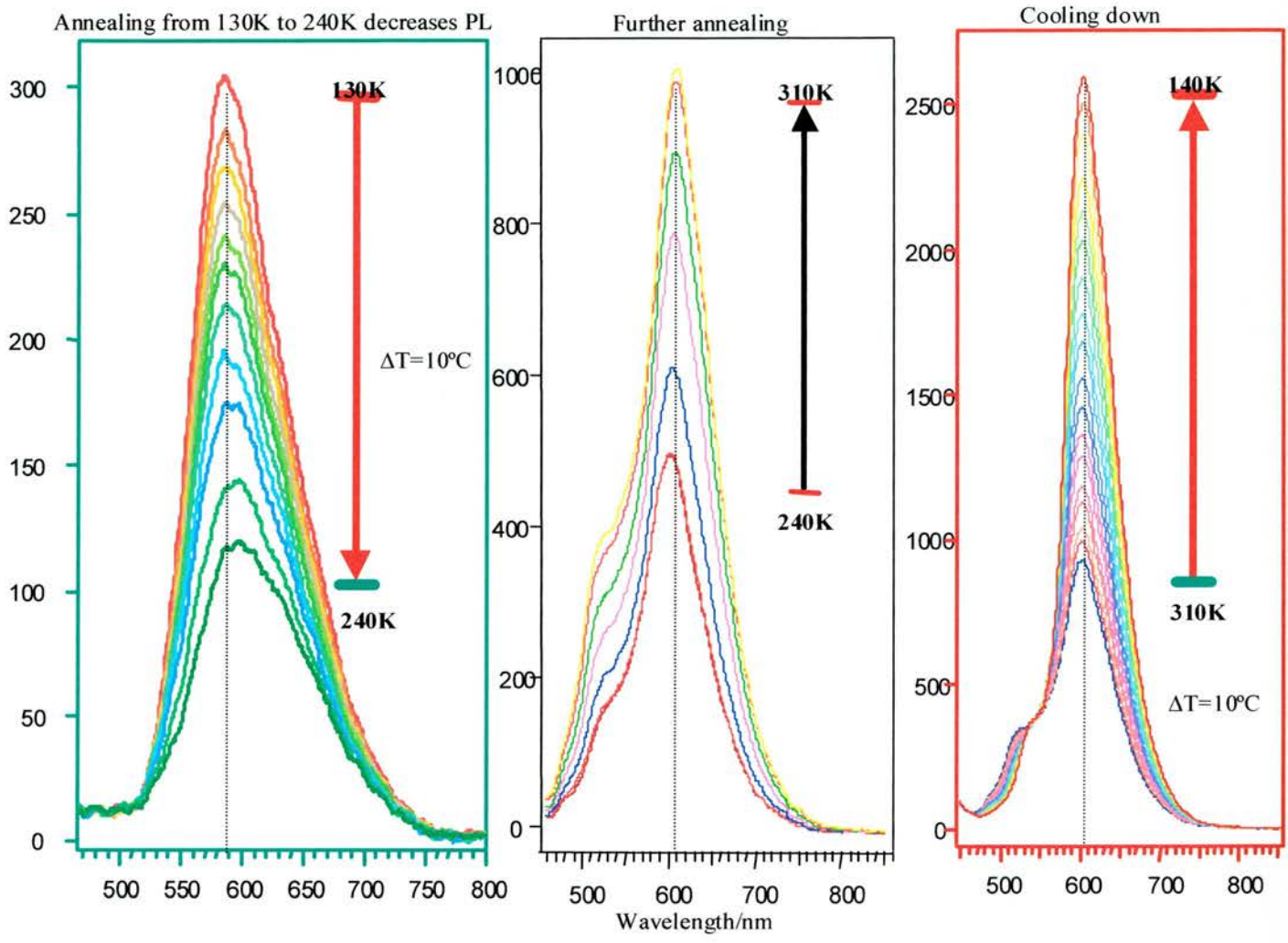

Fig. 86 Phase transition observed in perylene thin film after annealing. Between 130K and 240K intensity decreases. At 240K a phase change occurs to a more photo luminescent state. Once this phase is fully formed, intensity increases as the sample is cooled. Above 310K photoluminescence is lost due to multilayer desorption.

By comparison of the structures resolved using STM grown under specific temperature conditions with the temperature dependence of the photoluminescence, a close enough match is seen to assign the specific photoluminescence spectra to structures. The lowest temperature structure observed in the STM is the α-phase and is likely to produce emission at 590nm. At around 240K the change in energy of the emission and the peak shape

indicate that a structural change has occurred which is likely to be a change to the γ-phase which is known to form from annealing of the α-phase. Once the structure has fully changed, the luminescence signal from the γ-phase is retained even if the film is cooled below the temperature at which it formed. Once the γ-phase is grown, it is extremely stable and the α-phase cannot be recovered.

Tetracene

Infra-Red Spectroscopy

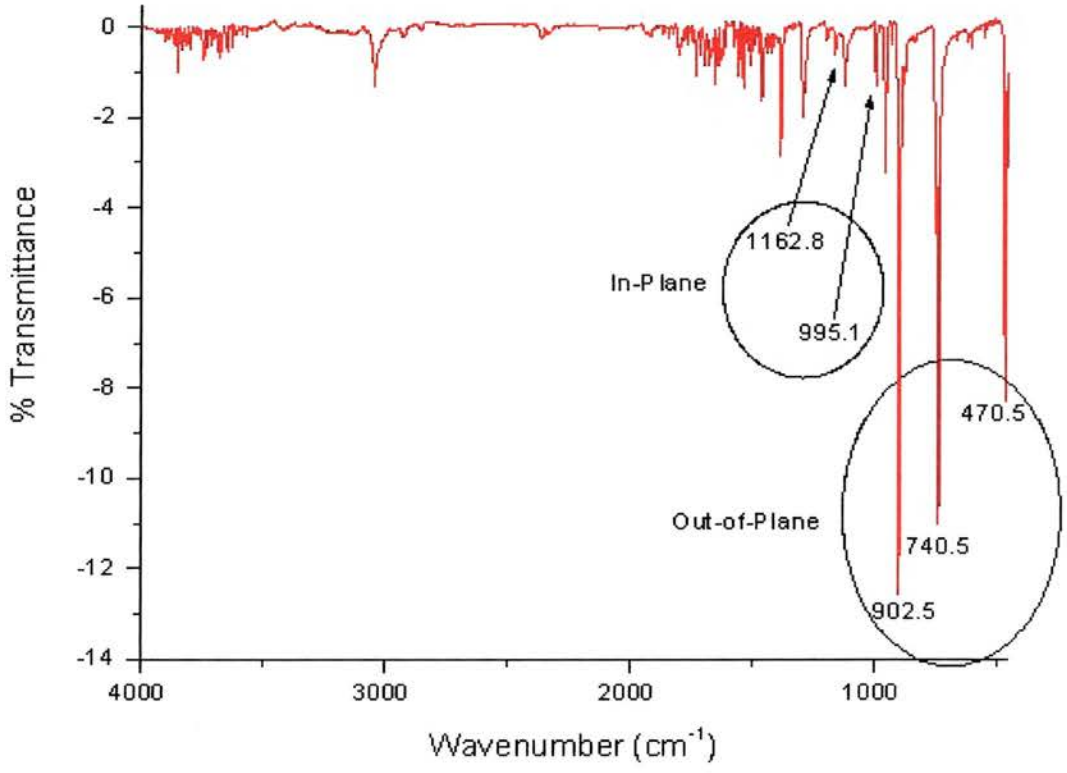

Fig. 87 Transmission IR of 5% tetracene in KBr. In-plane and out-of-plane modes are highlighted as their presence in RAIRS will indicate the plane in which the molecules lie on the surface.

As with the previous molecules studied for this project, IR was used to establish the known characteristics of the molecule in its bulk form before being introduced to the surface. An infra-red (IR) spectra was collected from a pellet of tetracene ground with KBr to a fine powder pressed at ~3 tons for 2minutes. The spectra (Fig. 87), provides information on all permitted vibrations which were assigned from the literature[151,152]. The vibrational

spectrum of the tetracene free molecule was calculated using Gaussian98® and provided an extremely close match with the experimental results, with errors in agreement less than 10%. Typically, Gaussian98 calculations overestimate vibrational frequencies by 2-6%.

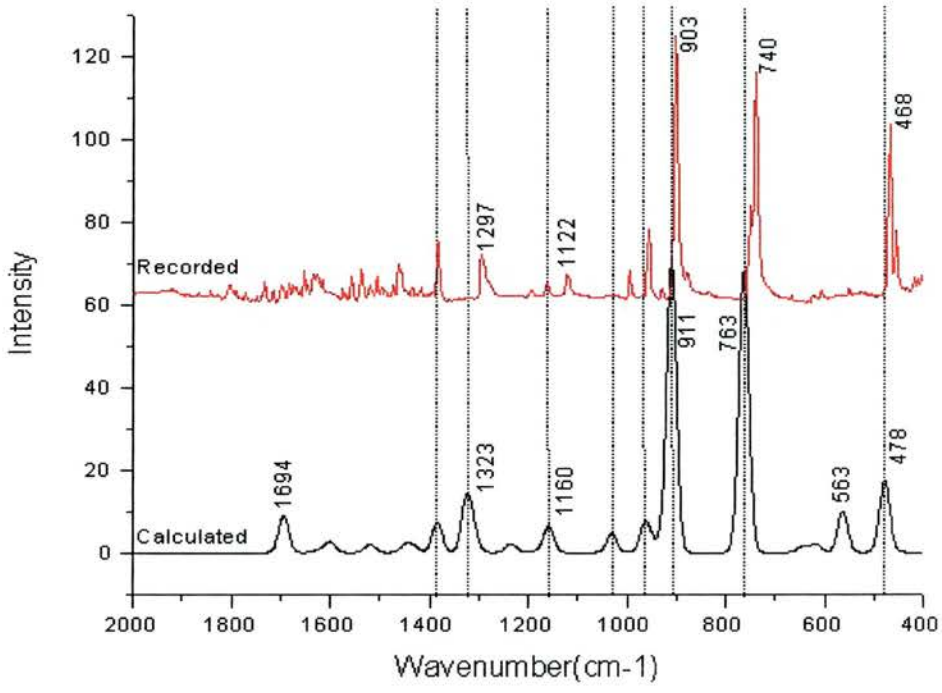

Fig. 88 Calculated v recorded vibrational spectra for an isolated tetracene molecule. The close match of the recorded and calculated spectra allow accurate identification of in –plane and out-of-plane modes.

The close match of the measured and calculated spectra for the free molecule (Fig. 88) indicates that there is nothing in the bulk crystal structure that hinders or promotes any of the vibrational frequencies. Specifically, the molecule in the bulk crystal clearly retains its planar structure. The two peaks at around 910 and 740cm^{-1} which correspond to out-of-plane C-H bending modes will be expected in RAIRS if the molecules are flat lying. The appearance of the less intense in-plane modes, particularly those above 1000cm^{-1} would indicate the molecules are upright.

RAIRS

Tetracene was deposited onto Cu(110) in UHV for RAIRS with the copper substrate held at room temperature (Fig. 89).

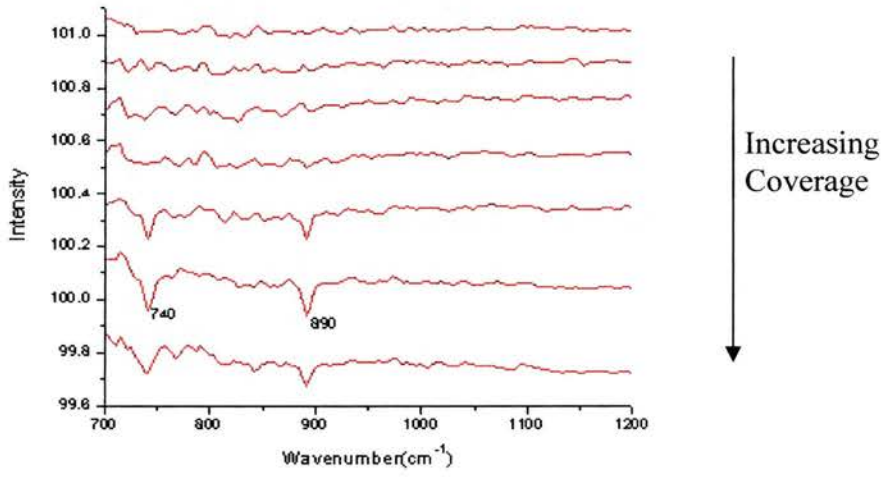

Fig. 89 RAIRS of tetracene on Cu(110) grown at room temperature. Peaks at 740 and 890cm^{-1} are out-of-plane bending modes. In-plane modes are absent.

The spectrum clearly shows the growth of only two peaks in the lower region of the spectra at 740 and 890 cm^{-1}. From the transmission spectra of the bulk sample and the Gaussian98® calculations, these vibrations can be confidently attributed to the C-H out-of-plane modes. As there are no in-plane modes present, it can be deduced that the molecules are flat lying on the surface. The fact that the peak intensities saturate very quickly leads to the conclusion that the initial monolayer is thermally stable at room temperature but subsequent layers are not so multilayer film growth is not possible. This implies that tetracene has the weakest molecule to molecule interactions of the three molecules investigated.

The experiment was repeated with cooling to the substrate. The thermocouple reading recorded a sample temperature of around 10°C instead of 30°C for the non-cooled sample. Due to the design of the manipulator and sample mounting, the actual sample temperature is likely to be slightly (5-10°C) lower than the recorded temperature.

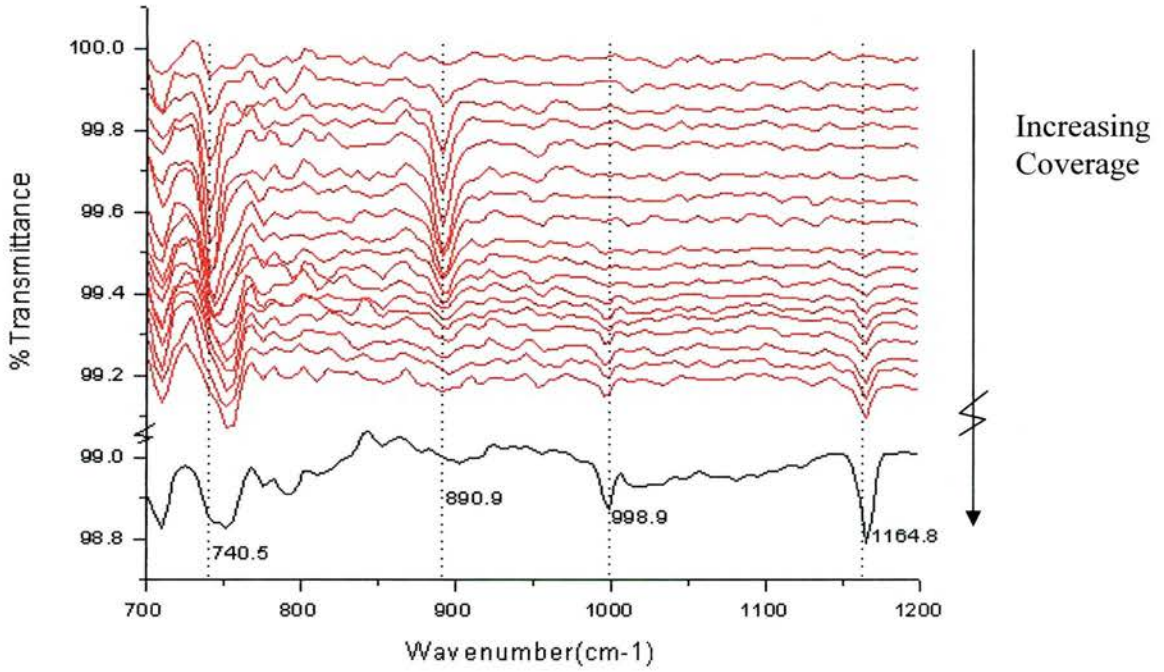

Fig. 90 RAIRS of tetracene on Cu(110) cooled to 10°C. Peak at 740cm^{-1} shifts to 752cm^{-1} as coverage increases. As coverage increases further, out-of-plane modes disappear and in-plane modes appear.

Significant differences could be seen in the evaluation of the spectrum of tetracene deposited on the cooled sample (Fig. 90) compared to that deposited and recorded at room temperature (Fig. 89). The initial growth stages are exactly the same with only two peaks seen at 740 and 890cm^{-1} (both C-H out-of-plane bending). As coverage is increased further, the out-of-plane mode at 890cm^{-1} disappears while the peak at 740cm^{-1} shifts to 752cm^{-1}. At the point where the out-of plane modes disappear, the in-plane modes appear.

All in-plane modes become visible but for clarity, only 998.9cm^{-1}: C-C stretching and 1164.8cm^{-1}: C-H in-plane stretching are shown in Fig. 90. As all the out-of-plane modes are not lost it can be deduced that the molecules are not switching to standing up. The first layer probably remains flat and has peak positions shifted and the intensities altered by the interactions with the subsequent layers. The new layers growing on top have the upright character. The RAIRS spectra clearly indicate a phase transition between the monolayer and subsequent layers. When heated, the exact reverse of the growth is seen, with the overlayers disappearing before the 890cm^{-1} peak reappears until it too is desorbed.

STM

It had been observed in the RAIRS experiments that only the first monolayer could be formed at room temperature and subsequent layers can only be grown at low temperature. This made the study of multilayers extremely difficult. Heating the monolayer structure and monitoring with LEED showed subtle changes in the monolayer structure that were investigated using STM.

A monolayer was deposited at room temperature and annealed to 70°C. A distinctive LEED pattern was recorded and STM images were collected after cooling to room temperature. From RAIRS it is known that the surface forms a complete monolayer with no additional layers present. The sample was cooled to room temperature and analysed by STM. The sample was then annealed to the higher temperature of 180°C and imaged again after cooling. The two sets of results (70°C and 180°C annealing) will be discussed side by side for ease of comparison (Fig. 91).

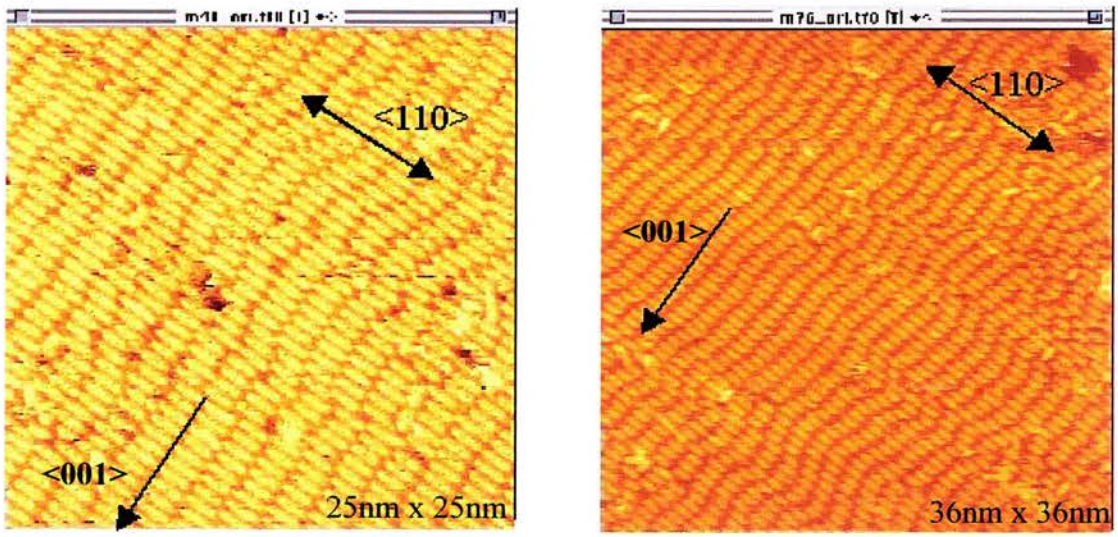

Fig. 91 STM of tetracene on Cu(110) deposited at room temperature and annealed to 70°C (left) Tunnelling Conditions: -0.169V, 1.682nA, 3.70% Loop gain, and 180°C (right) Tunnelling Conditions: -0.005V, 0.137nA, 0.87% Loop gain

It can clearly be seen that the molecules in both images line up with their long axis parallel to the <110> direction. This indicates an interaction between the substrate and molecule that reflects the linear shape of the molecule and the linearity of the close packed copper rows. Another indication that the molecules are aligned precisely along the <110> axis is that in all the areas scanned there is only the one orientation seen. If it were rotated away from a high symmetry direction then a domain of the mirror image would also be present. Analysis of the <001> direction (perpendicular to the <110> and shown as black arrows in Fig. 91) shows the first difference between the two images. In the left image of Fig. 91, the columns of molecules along the <001> direction appear to be aligned perfectly where there are no defects in the columns. In the right image of Fig. 91, first impressions suggest a higher level of order as there are less visible defects and the columns along <001> appear to be generally longer before they change direction. However, if the perpendicular <001> axis is overlaid then it becomes apparent that these columns are not parallel to <001>, but offset by ~10 degrees.

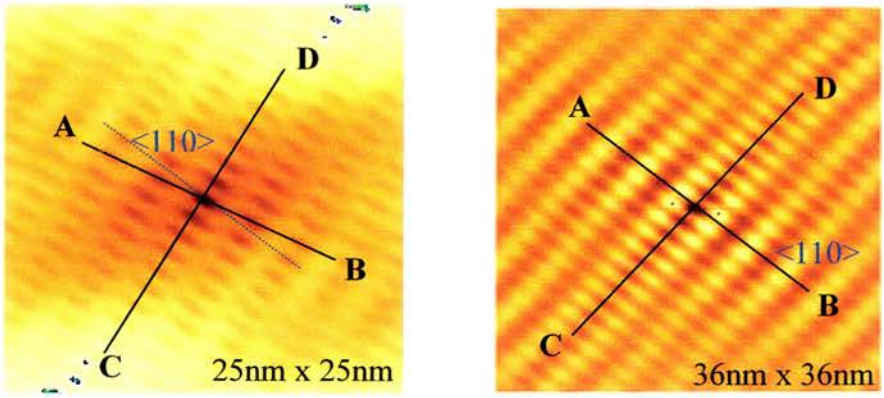

Fig. 92 Auto-correlation function images generated from STM images in Fig. 91 (70°C left, 180°C right).

The auto-correlation images (Fig. 92) instantly show that the two A-B cross-sections are different, yet in the STM images they both appear to be the same. Close investigation shows that although the molecules themselves are indeed aligned along the <110> direction, in the first structure, the majority of columns along <001> are offset by half a molecular spacing from each adjacent column. Drawing a line profile through these offset molecules exactly matches that of the A-B cross-section in the auto-correlation images (Fig. 92). The molecules in the 180°C structure are usually parallel so the auto-correlation shows them to be ordered along with the <110> direction.

Analysing the line profiles of the A-B and C-D cross sections also shows an interesting difference that starts to point towards the driving force of the different structures (Fig. 93).

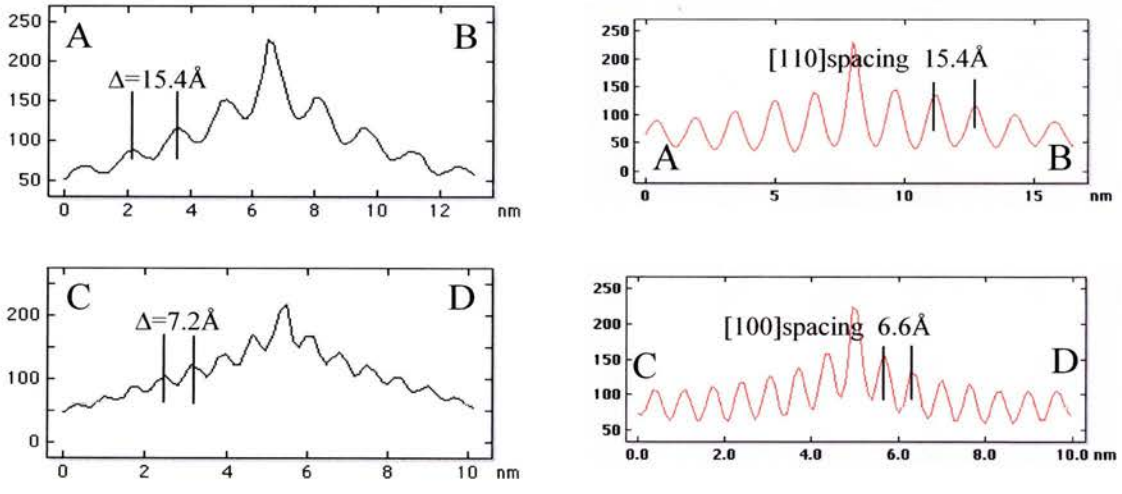

Fig. 93 Line profiles of cross-sections AB and CD of auto-correlation function images shown in Fig. 92 - 70°C sample: left, 180°C sample: right

As auto-correlation provides periodic information, the measurements taken from it are far more accurate for determination of unit cell dimensions than those taken directly from the STM images are. The two A-B cross-sections are approximately equal and correspond to a

commensurate spacing of six copper atoms, which is the minimum number of whole atoms per molecule. The molecule is 13.63Å long, which is greater than five copper spacings along the <110> direction (12.8Å). The difference between the measurements of the images is observed along the C-D direction. The 70°C sample's molecules are spaced 7.2Å apart, which equates to the width of two full copper rows. After annealing to 180°C the molecules are spaced only 6.6Å apart, which is narrower than the molecular width of 6.99Å. If the molecules are interdigitated i.e. offset sideways slightly so the hydrogen atoms are not head on, but fit into the gaps between each other as shown in Fig. 94, the closest the molecular centres can come is 6.6Å which fits the recorded distance perfectly.

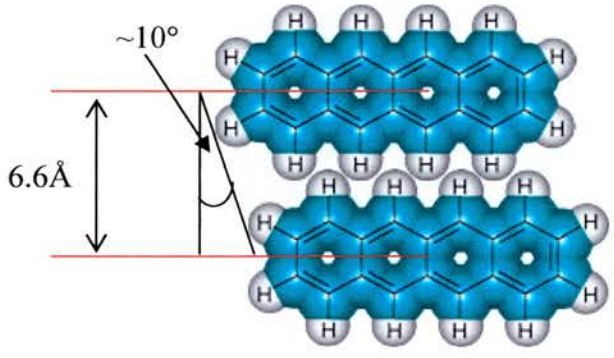

Fig. 94 Interdigitation of tetracene molecules. To allow tetracene molecules to pack at a distance of 6.6Å, the molecules must be offset to allow the hydrogen atoms to sit between one another.

This interdigitation also explains why the alignment of the columns molecules in the annealed sample is not exactly perpendicular to the <110> rows. Each molecule be offset to either the left or the right, and is too close to allow stacking in the <100> direction. The inter-hydrogen distance along the side of tetracene is 2.46Å which, given the 6.6Å

molecular spacing in the <001> direction suggests an offset angle of around 10°. This matches the offset angle recorded from the STM images.

LEED

The diffraction patterns of the two samples also show these subtle differences. The recorded LEED patterns were not too clear (Fig. 96) but generally are consistent with the diffraction patterns generated from the STM images (Fig. 95), which used as the basis of the following discussion as they showed more detail.

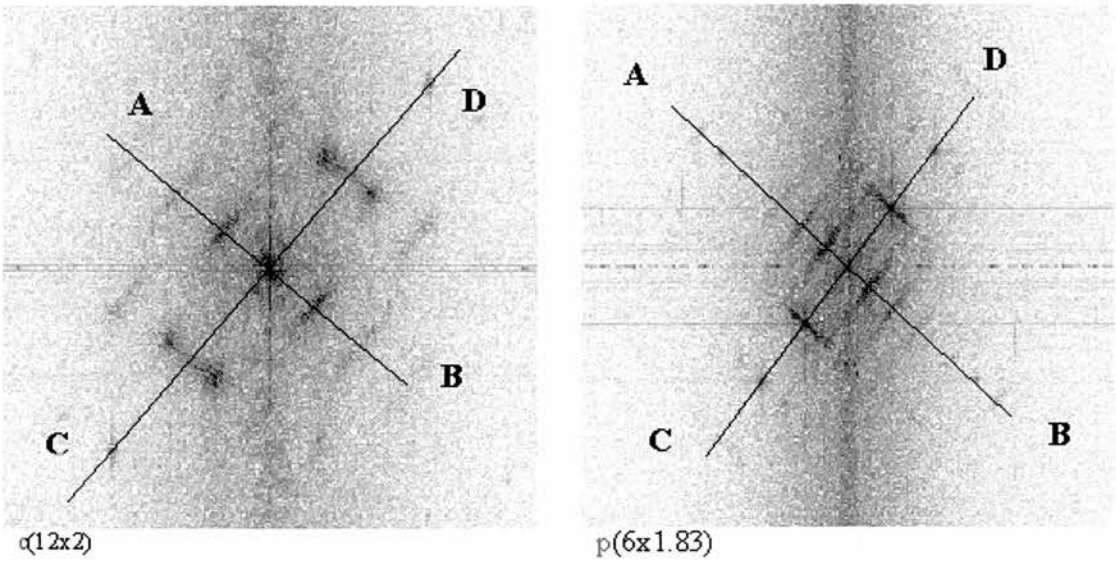

Fig. 95 Diffraction patterns based on the STM images in Fig. 91 and line profile positions (AB & CD) for tetracene on Cu(110) annealed to 70°C (left) and 180°C (right).

Fig. 96 Recorded LEED patterns for tetracene on Cu(110) annealed to 70°C (left) and 180°C (right). Recorded LEED patterns match the diffraction patterns produced by fourier tranformation of STM images

The first image (Fig. 95 left) shows a centred 12 x 2 structure and the second (Fig. 97 right) shows a primitive 6 x 1.83 structure. The compression has already been noted from the STM images, this too should be present in the diffraction patterns.

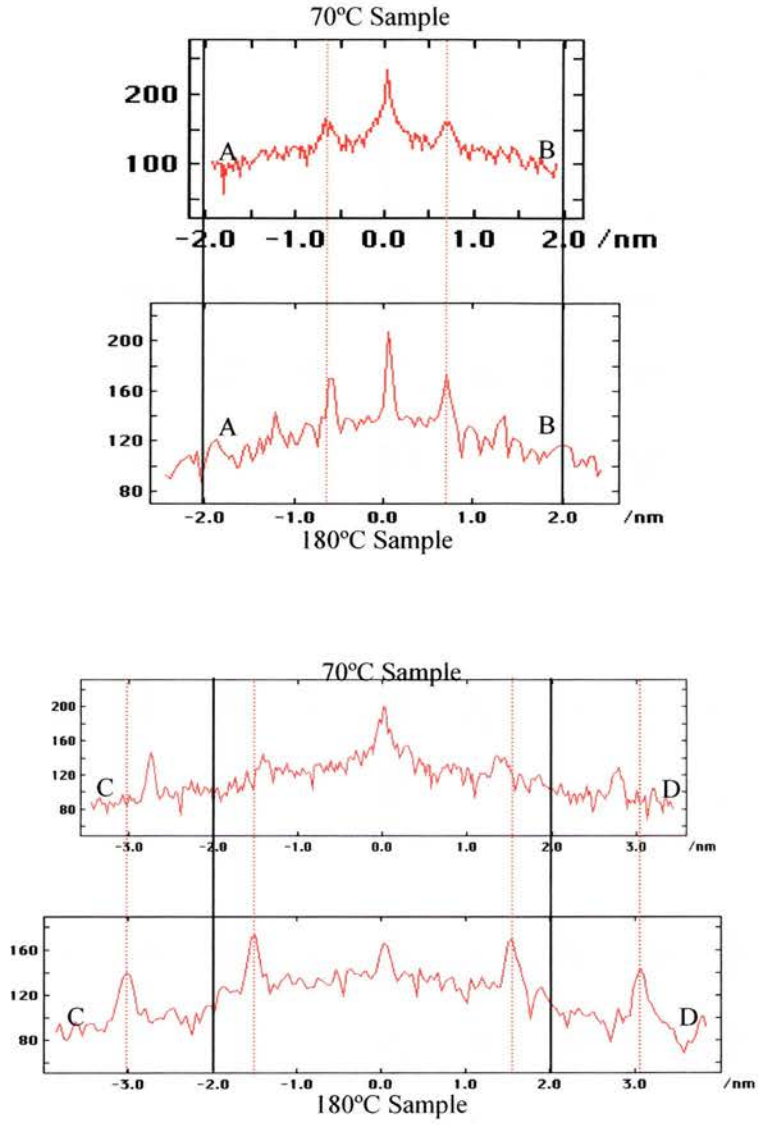

Fig. 97 Line profiles AB and CD from diffraction patterns in Fig. 95. Black lines align scale at 2nm. Red dashed lines show alignment and misalignment of intensity peaks. Increased spacing of 180°C sample peaks indicate a contraction of the unit cell in real space.

As expected, the peaks of the AB line profiles align perfectly, agreeing that the molecular spacing is equivalent along the <110> direction in both structures although the 70°C annealed results in a centred structure. In the CD line profiles, the intensity peaks of the

180°C sample are further apart than the peaks of the 70°C sample. An increase in distance in reciprocal space represents a compression in real space (i.e. molecules are closer together) which agrees with previous results. The compression is approximately 10% which makes the two diffraction patterns c(12 x 2) and p(6 x 1.83)

From this, models for the two structures can be suggested:

The 70°C sample is the simplest as it shows a clear commensurate relationship between the molecule and the substrate. The distance between molecular centres along the <110> direction is 15.4Å, which is equivalent to six copper atoms, but slightly larger than the minimum inter-molecular distance of 13.6Å. However, a commensurate structure with a spacing of five copper atoms along <110> would correspond to 12.8Å, which is smaller than the Van der Waals length of Tetracene. The molecular spacing along the <001> direction is 7.2Å, which equals two copper rows spacing. The diffraction pattern data indicates a centred structure and inspection of the STM images shows that many of the columns are offset by half a molecule from those that are adjacent. Combining all this we can produce the model shown in Fig. 98.

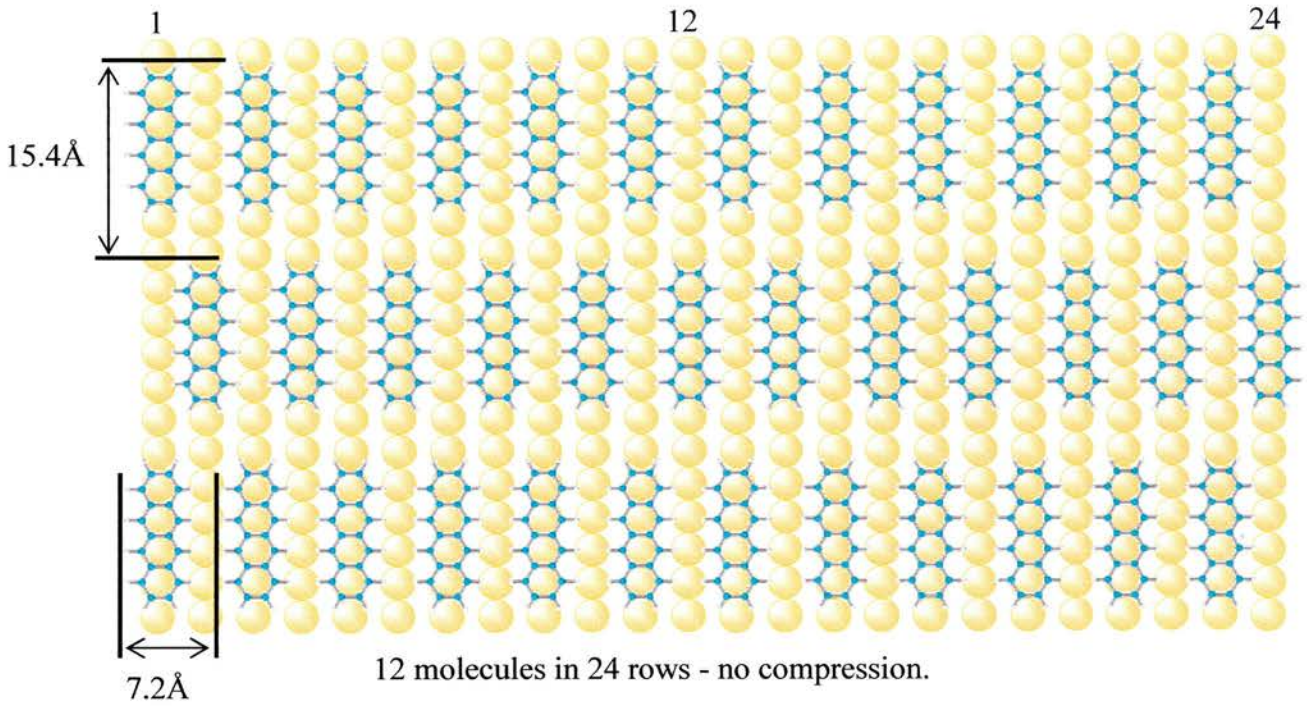

Fig. 98 Model of tetracene on Cu(110) after annealing to 70°C. Molecules are 6 copper atoms apart along the rows and offset by one row from column to column.

The model (Fig. 98) contains all the information collected and provides a good agreement between the STM data and includes the 12 x 2 periodicity from the diffraction data. Molecules are flat in agreement with RAIRS and STM images.

The model for the 180°C sample is more complicated because of the compression due to interdigitation of the molecules. The molecular spacing along the <110> direction is the same as before at 15.4Å between molecular centres. The distance between molecular centres along the <001> direction is now only 6.6Å, so for the molecules to lie flat - as indicated by RAIRS and STM- they must be interdigitated. If the molecules were offset to one side and then the other, overall, the columns would be perpendicular to the <110> direction. As this is not the case and the columns are straight but angled one way or the

other from the <001> direction, it is likely that the molecules are offset in one direction in long sequences rather than randomly.

The diffraction pattern shows a primitive structure and the STM images indicate that the columns tend to be exactly aligned. Combining this data, the following model is suggested:

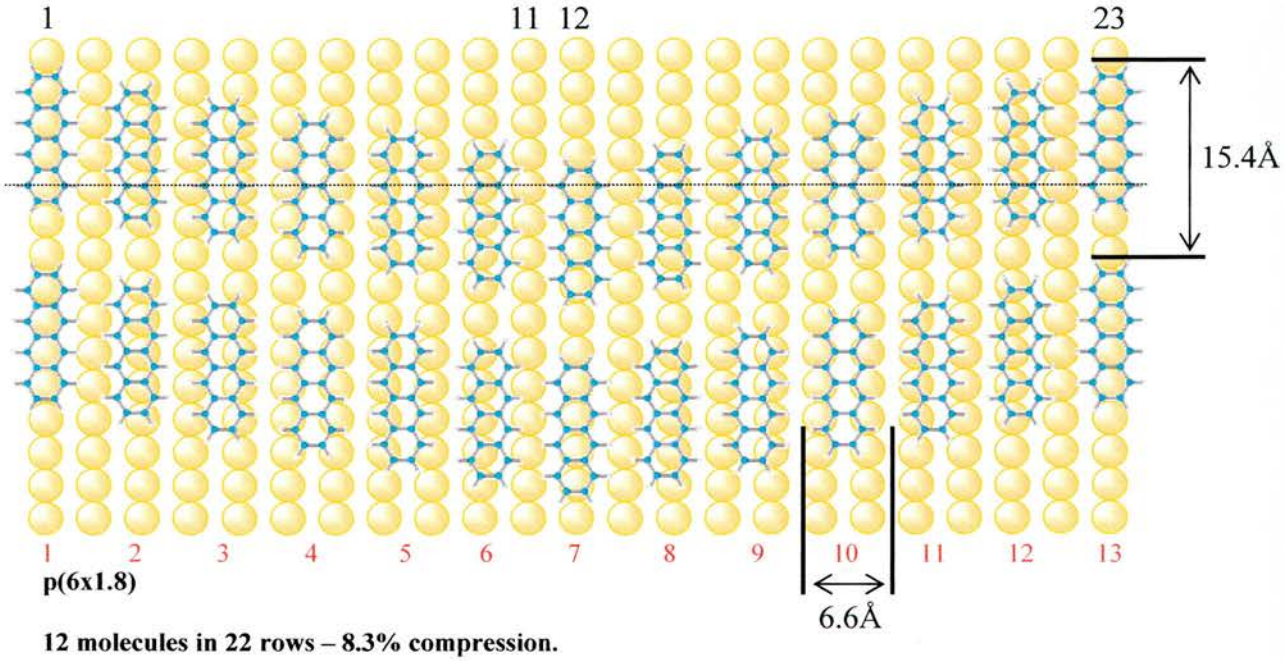

Fig. 99 Model of tetracene on Cu(110) after annealing to 180°C. Molecules are interdigitated and offset by the minimum amount with respect to adjacent molecules. To offset and return by the full length of the molecule provides a 12 molecule repeat unit.

The model, when completed illustrates a structural feature that was not immediately obvious from the data collected. From the auto-correlation image, closer inspection shows a wave pattern within the image. Comparing this to the C-D line profile (Fig. 100), a second wave can be seen superimposed on the initial wave of the molecular spacing. This has a wavelength equivalent to twelve of the smaller waves.

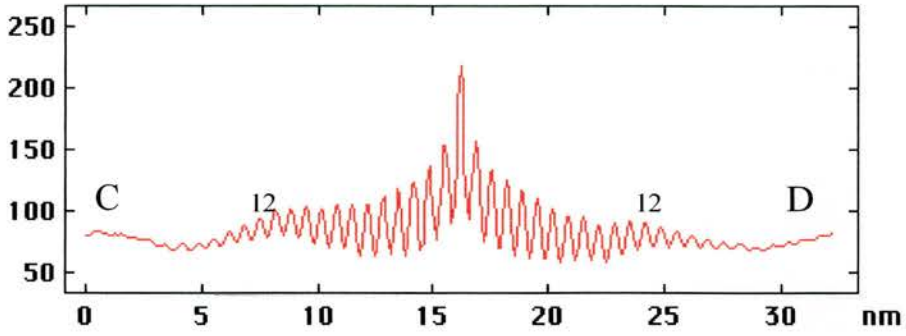

Fig. 100 Line profile of 180°C sample showing 12 repeat unit wave

While twelve seems apparently random, it can be explained easily by the offset of two adjacent rows of molecules. Assuming the model shown in Fig. 99 is correct, each subsequent molecule in the column is offset to the same side by the minimum amount until the last side hydrogen atom of the seventh molecule is aligned with the first. Each subsequent molecule offsets in the opposite direction until the thirteenth molecule has returned to an equivalent position of the first. This gives twelve molecules in twenty-two copper rows - an approximate 8.3% compression over the 70°C sample - which agrees with the p(6 x 1.83) unit cell. To explain why the wave is present and the molecules do not continue in the same direction indefinitely, we need to look at the incorrect model (Fig. 101).

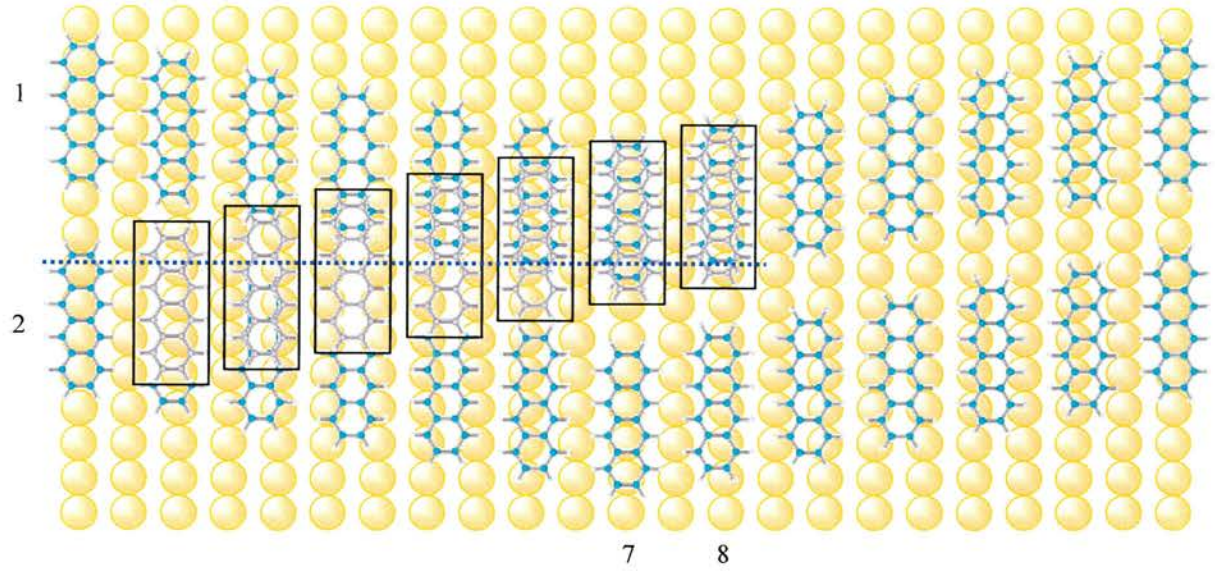

Fig. 101 Incorrect model for 180°C sample.

Constructing an incorrect model for the structure shows what drives the correct structure. From columns 1 and 2 in Fig. 101, each subsequent molecule in the column can offset up or down. The molecules in boxes from column two show the positions that the molecules would have if they offset upwards. The critical positions that define the structure occur in the seventh and eighth molecules in the column. By the seventh position, there is still no overlap of the two theoretical converging rows so in the absence of adjacent molecules, the structure is driven by the interdigitation of the previous molecule in the column. By the eighth position, the molecule of the theoretical row (outlined) and the real model row occupy a similar position on the surface. The real model site will be energetically optimised, the theoretical position will not. If a molecule were to in the eighth position of the theoretical row, it would shift to the more energetically stable eighth position of the real model. This combination of interactions between the molecule and the surface plus the interdigitation of the close packed molecules drives the structure towards the twelve-molecule wavelength structure. In the STM, images the columns rarely show exactly twelve molecules as the repeat unit but as the wave appears in the auto-correlation images, it is the average wavelength.

High Temperature Deposition

Due to the interesting structural differences observed in the annealed samples, it was investigated whether these structures could be reproduced in the initial growth stage of the film. During annealing in the initial experiment, LEED patterns were observed to improve at around 80°C and then not change until they disappeared at over 190°C. As two structures had been observed, one above and one below 80°C, it was decided to hold the substrate at around 100°C while tetracene was deposited. The LEED patterns collected from this experiment were not of high resolution, suggesting that a lesser degree of order was present in the new film. The spacing of the spots in the <110> direction indicate that the molecular spacing is similar to that of the previous two structures with the molecules aligned along this direction and packed closely over the minimum number but commensurate integral of copper atoms. The decreased order perpendicular to this indicates that there may no longer be columns of molecules in the <001> direction.

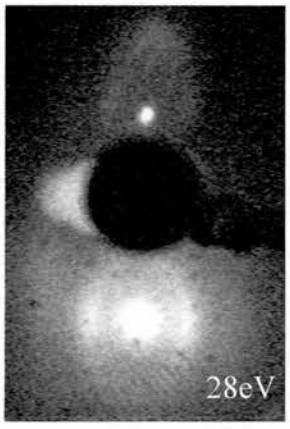

Fig. 102 LEED of tetracene deposited onto Cu(110) at 100°C. Semi-halo indicating an ordered inter row spacing <001> direction but disordered along the <110> direction.

The STM images proved this to be true as shown in fig. 103. Under conditions that would have produced a full monolayer, only a partial monolayer was present. The increased temperature must promote spontaneous desorption of the molecules. The images now only show molecules aligned along the <110> direction with patches of absent molecules where the underlying copper rows can be seen. In places, the molecules appear to be slightly off alignment with the underlying copper, but this can be accounted for as before by the molecules being off-set from each other by half their width. There were no longer any coherent column structures left in the <001> direction. Auto-correlation images show only the <110> alignment with no other periodicity present. Increasing coverage under the same deposition conditions as the original substrate was prepared, produces the same structure.

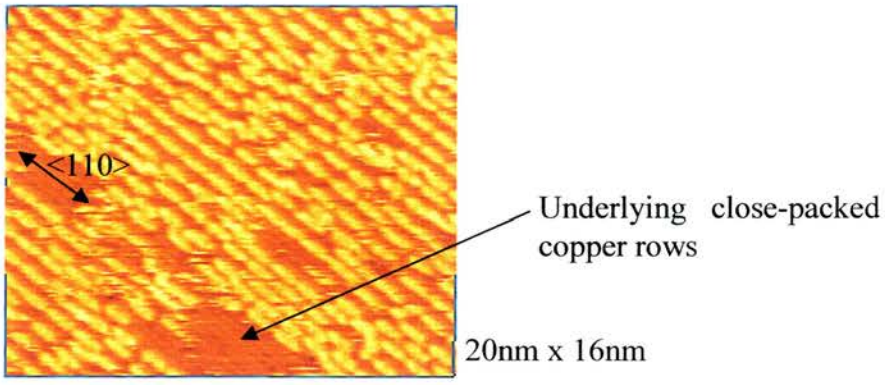

Fig. 103 High temperature deposition of tetracene on Cu(110). Tunnelling conditions: -0.183V, 1.034nA, Loop gain 1.403%. Tetracene molecules align along rows but do not form columns.

Perylene and Tetracene on Oxygen Covered Copper

During the course of the project, it became apparent that the molecules had interesting interactions with oxygen. Oxygen was introduced to the clean copper surface by direct deposition from a leak valve. Oxygen forms the well-known 2 x 1 structure with a characteristic LEED pattern it easy to monitor the evolution of the structure. The structure of the oxygen on copper is described in the earlier chapter discussing substrates (p59), a typical example is shown in Fig.104.

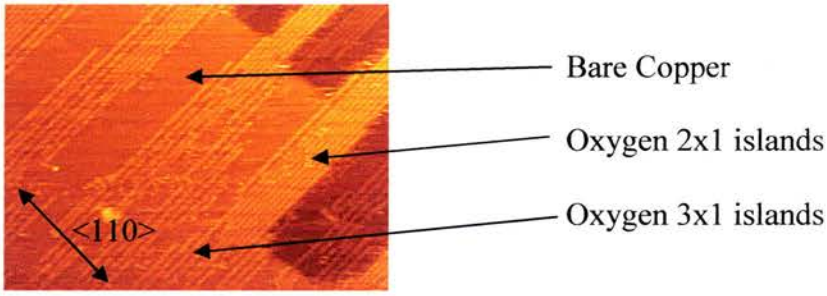

Fig. 104 Oxygen 2x1 islands on Cu(110) - 40 x 30nm

Perylene on Oxygen Covered Cu(110)

A clean Cu(110) substrate was prepared by exposure to oxygen. Coverage of O(2x1) islands occupied approximately 50% of the total surface area. The STM image shown in Fig. 105 shows two different structures. One clearly shows perylene molecules sitting upon the rows characteristic of the oxygen 2x1 structure. Due to the dimensions of the perylene molecules, it is not possible to determine whether they are aligned parallel or perpendicular to the oxygen rows. The patches in between the oxygen islands were originally assumed to be free of molecules but subsequent studies suggest they are covered with molecules that

are not tightly packed and therefore mobile under the influence of the STM tip. Height profiles across the islands show that the apparently clear areas are at least as high as the molecules on the oxygen. The visible molecules appear to be generally stable and do not move. A few molecules are seen to appear and disappear from image to image. The molecular spacing perpendicular to the <110> direction is 10.8Å, which equals three oxygen unit cells. Across the rows, the spacing equal six copper or three oxygen unit cells. This ties in with the p(6x1) LEED pattern observed.

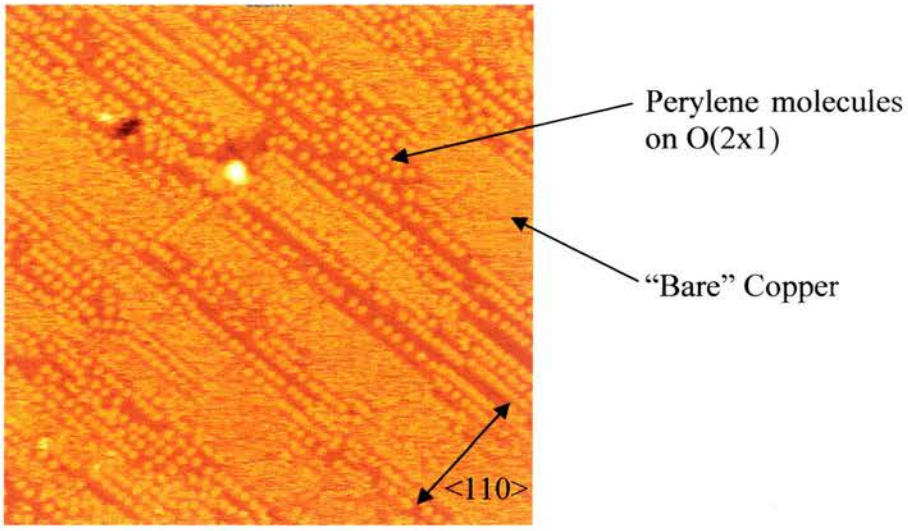

Fig. 105 Perylene on oxygen on copper

Subsequent studies involved the careful analysis of the oxygenated surface prior to exposure to perylene. These studies clearly showed perylene molecules on the patches in between the copper islands (Fig. 106). The islands of oxygen 2x1 can be seen in between the patches of molecules, indicating the molecules preference for bonding to the clean copper over the oxygen 2x1 structure. Some straight rows of molecules can be seen which are likely to sit over the oxygen 3x1 structure. The molecules are actually trying to stick to the copper but the linearity of the oxygen structure templates the perylene growth.

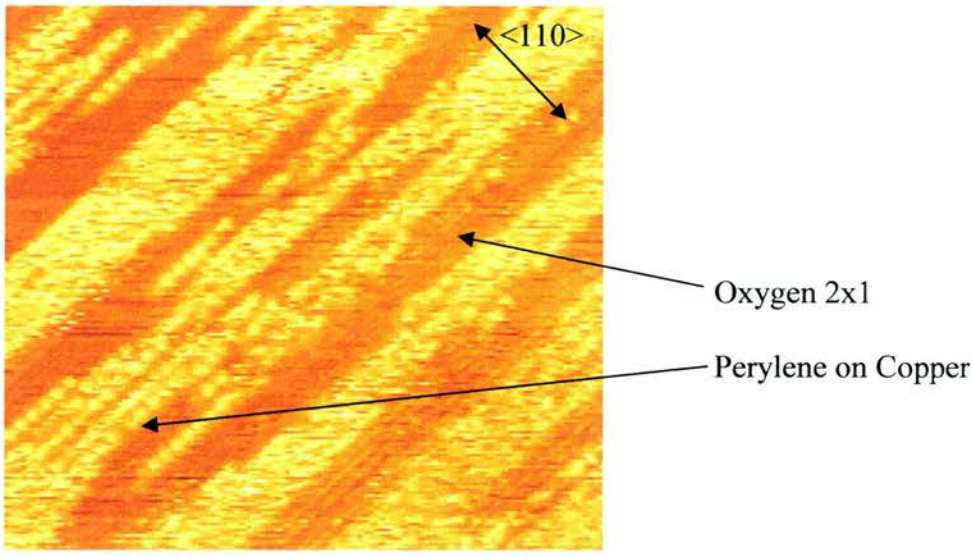

Fig. 106 Perylene on oxygen precovered copper - 40 x 40 nm

Although the resolution is relatively poor, molecules can be imaged while they are trapped by the 3x1 oxygen structure, they cannot be easily imaged on the bare copper. Further evidence that these patches are filled with perylene comes from scanning the image areas over a number of scans (Fig. 107). Over three or four images of the same area, small clusters appear and grow in size. The number of these clusters increases with time.

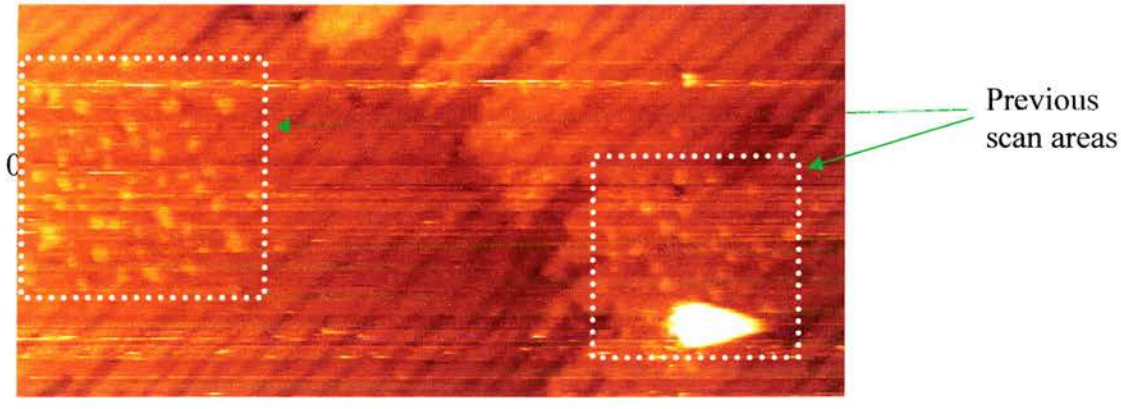

Fig. 107 Clusters of perylene in previous scan areas - 100 x 300 nm. Islands of perylene form under the influence of scanning that prevent good resolution images.

If the STM frame is zoomed out to cover a larger area, the previous scan area can be clearly identified. These clusters form with disappearance of the molecules from other areas, which suggests they are formed from highly mobile molecules that cannot be imaged, i.e. perylene molecules on the bare copper area.

Tetracene on Oxygen Covered Cu(110)

The oxygen precovered copper surface was prepared as before to produce ~50% coverage of the oxygen 2x1 structure. Tetracene was deposited onto the surface and imaged in the STM. As was observed with perylene, the 2x1 features of the surface can clearly be seen between the patches of tetracene (Fig. 108) which preferentially occupy the clean Cu(110) surface.

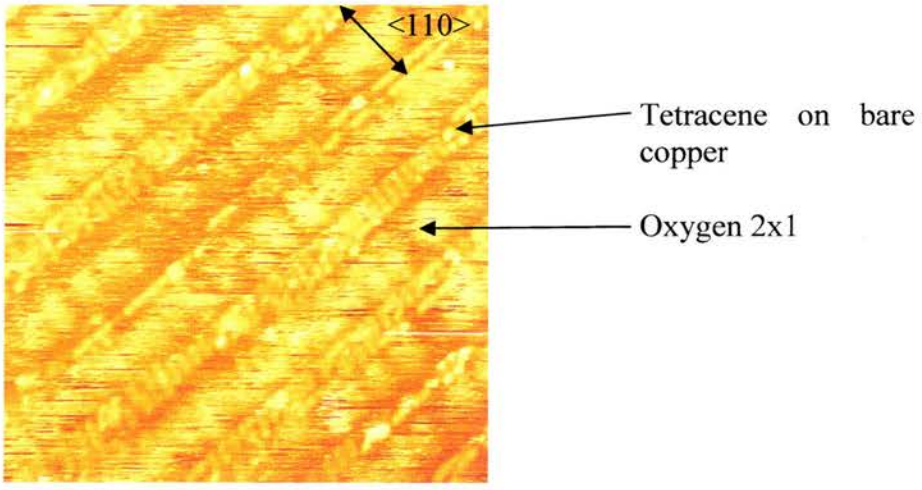

Fig. 108 Tetracene on oxygen precovered copper - 35 x 35nm Molecules fill gaps between oxygen islands

The tetracene molecules can be seen to preferentially orientate themselves parallel to the <110> direction as they do on the oxygen free surface. If there is not sufficient space for the molecules to lie parallel to this direction then they rotate by 90° and lie perpendicular to the <110> direction. It appears in Fig. 108 that there are no molecules on the oxygen 2x1 surface. In the case of perylene, once the bare copper is filled, molecules are also seen on the 2x1 surface. This indicates that tetracene interacts more weakly with the O(2x1) surface than perylene does.

Conclusions and Comparisons

Thin films of organic polyaromatic molecules 3,4,9,10-perylenetetracarboxylicdianhydride (PTCDA), perylene and tetracene have been investigated on copper single crystals. Investigations involved both qualitative and quantitative analyses using a number of bulk and surface sensitive techniques, the majority in ultra-high vacuum.

XPS results of PTCDA on Cu(211) indicated that the molecules lost their anhydride oxygen atoms to form strong bonds with the surface. Of the thermal desorption temperatures of the monolayers of the three molecules, PTCDA is around 100°C higher than that of tetracene and perylene, which are bonded through weaker interactions.

On Cu(110), all three molecules lie flat to form the initial monolayer. The packing of the molecules in all cases is extremely dependent on the substrate temperature during deposition and can be altered by annealing after growth. In all cases, annealing a deposited layer led to a higher density of molecules and increased structural order. For PTCDA and perylene, growth at raised substrate temperature led to the same structures as annealing a disordered film. For tetracene, a new structure was seen that had less order and less dense packing than the annealed layer.

The multilayer structures all proved to be significantly different. The initial monolayer of PTCDA is the same as the 102 plane of the bulk crystal structure. It is unsurprising that further layers follow this structure and the molecules remain flat. For perylene and tetracene, the initial monolayers are both flat. In the bulk crystal structures, there are no planes that can have solely planar molecules, so the multilayer structures must be novel. The tetracene multilayer structure was not resolved as it was not stable at room temperature, however, RAIRS indicated that all the multilayer molecules were upright. Inversely, the molecules of the perylene multilayer were all flat. RAIRS suggests an

inclination toward amorphism as layer thickness increases but no evidence of this was seen in STM of a ~20ML film.

The properties of the perylene multilayer were investigated using photoluminescence spectroscopy. Photon emission from the film stimulated by a 410nm laser was recorded at a wavelength of 608nm. Monomers of perylene are known to emit photons at 450nm and the excimer of the bulk α-phase crystal emits photons at 550nm. This implies that the π-orbital stacking and overlap of the thin film γ-phase forms an excimer of even lower energy allowing the emission at 608nm.

References

[1] Alivisatos A.P, Barbara P.F, Castleman A.W, Chang J, Dixon D.A, Klein M.L, McLendon G.L, Miller J.S, Ratner M.A, Sossky P.J, Stupp S.I, Thompson M.E, *Advanced Materials*, 10(16)(1998) 1297-1336.

[2] Bao Z, *Advanced Materials*, 12(3)(2000) 227-230.

[3] Böhler A, Urbach P, Ammermann D, Kowalsky W, *Materials Science and Engineering B*, 51(1998) 58-65.

[4] Dimitrakopoulos C.D, Malenfant P.R.L, *Advanced Materials*, 14(2)(2002) 99-117.

[5] Law K-Y, *Chemical Reviews*, 93(1993) 449-486.

[6] Shaw J.M, Seidler P.F, *IBM Journal of Research and Development*, 45(1)(2001) 3-9.

[7] Gross M, *Chemistry in Britain*, 37(7)(2001).

[8] Dittmer J.J, Lazzaroni R, Leclère Ph, Moretti P, Granström M, Petritsch K, Marseglia E.A, Friend R.H, Brédas J.L, Rost H, Holmes A.B, *Solar Energy Materials & Solar Cells,* 61(2000) 53-61.

[9] Gross M, *Chemistry in Britain,* 37(11)(2001) 22-23.

[10] Schmidt-Mende L, Fechtenkotter A, Mullen K, Moons E, Friend R.H, MacKenzie J.D, *Science,* 293(2001) 1119-1122.

[11] Rompf C, Hilmer B, Kowalsky W, *Japanese Journal of Applied Physics*, 33(1-1B)(1994) 832-835.

[12] McKeown N.B, *Phthalocyanine Materials: Synthesis, Structure and Function*, 1st, Chemistry of Solid State Materials 6 (Cambridge University Press, 1998).

[13] S Heutz, Imperial College London

[14] Bao Z, *Advanced Materials*, 12(3)(2000) 227-230.

[15] Dimitrakopoulos C.D, Malenfant P.R.L, *Advanced Materials*, 14(2)(2002) 99-117.

[16] Rajagopal A, Wu C.I, Kahn A, *Journal of Appled Physics*, 83(5)(1998) 2649-2655.

[17] Böhler A, Urbach P, Ammermann D, Kowalsky W, *Materials Science and Engineering*, B51(1998)58-65

[18] Fisbane, Physics for scientists and Engineers, Prentice Hall

[19] Forrest S.R, Kaplan M.L, Schmidt P.H, Feldmann W.L, Yanowski E, *Applied Physics Letters*, 41(1982) 90-93.

[20] Heutz S, Ferguson A.J, Rumbles G, Jones T.S, *Organic Electronics*, 3(2002) 119-127.

[21] Nanai N, Yudasaka M, Ohki Y, Yoshimura S, *Thin Solid Films*, 265(1995) 1-2.

[22] Schuerlein T, Schmidt A, Lee P.A, Bebesny K.W, Armstrong N.R, *Japanese Journal of Applied Physics*, 34(1995) 3837-3845.

[23] Stöhr M, Gabriel M, Möller R, *Surface Science*, 507-510(2002) 330-334.

[24] Schuerlein T.J, Armstrong N.R, *Journal of Vacuum Science & Technology A - Vacuum Surfaces and Films*, 12(4)(1994) 1992-1997.

[25] Wang D, Wan L-J, Xu Q-M, Wang C, Bai C-L, *Surface Science*, 478(1-2)(2001) L320-L326.

[26] Rang Z, Haraldsson A, Kim D.M, Ruden P.P, Nathan M.I, Chesterfield R.J, Frisbie C.D, *Applied Physics Letters*, 79(17)(2001) 2731-2733.

[27] Torii H, Ueno Y, Sakamoto A, Tasumi M, *Journal of Physical Chemistry A*, 103(1999) 5557-5566.

[28] Lukas S, Witte G, Wöll, *Physical Review Letters*, 88(2)(2002).

[29] Surface Explorer, http://www.fhi-berlin.mpg.de/~rammer/surfexp_prod/SXinput.html

[30] Tautz F.S, Sloboshanin S, Schaefer J.A, Scholz R, Shklover V, Sokolowski M, Umbach E, *Physical Review B*, 61(24)(2000) 16933-16947.

[31] Shklover V, Tautz F.S, Scholz R, Sloboshanin S, Sokolowski M, Schaefer J.A, Umbach E, *Surface Science*, 454(2000) 60-66.

[32] Staub R, Toerker M, Fritz T, Schmitz-Hübsch T, Sellam F, Leo K, *Surface Science*, 445(2-3)(2000) 368-379.

[33] Hill I.G, Kahn A, Cornil J, dos Santos D.A, Brédas J.L, *Chemical Physics Letters*, 317(2000) 444-450.

[34] Hoshino A, Isoda S, Kurata H, Kobayashi T, *Journal of Appled Physics*, 76(7)(1994) 4113-4120.

[35] Bondi A, *Journal of Physical Chemistry*, 68(1)(1968) 441.

[36] Nanai N, Yudasaka M, Ohki Y, Yoshimura S, *Thin Solid Films*, 265(1995) 1-2.

[37] Scholz R, Kobitski A.Yu, Kampen T.U, Schrieber M, Zahn D.R.T, *Physical Review B*, 61(20)(2000) 13659-13669.

[38] Cox J.J, Jones T.S, *Surface Science*, 457(2000) 311-318.

[39] Kaiser R, Freidrich M, Schmitz-Hübsch T, Sellam F, Kampen T.U., Leo K, Zahn D.R.T, *Fresenius Journal of Analytical Chemistry*, 363(1999) 189-192.

[40] Kampen T.U, Tenne D.A, Park S, Salvan G, Scholz R, Zahn D.R.T, *Solid State Physics A*, 215(1999) 1-4.

[41] Park S, Querner T, Kampen T.U, Braun W, Zahn D.R.T, *Applied Surface Science*, 166(1-4)(2000) 376-379.

[42] Burrows P.E, Zhang Y, Haskal E.I, Forrest S.R, *Applied Physics Letters*, 61(20)(1992) 2417-2419.

[43] Hoshino A, Isoda S, Kurata H, Kobayashi T, *Journal of Appled Physics*, 76(7)(1994) 4113-4120.

[44] Kendrick C, Kahn A, Forrest S.R, *Applied Surface Science*, 104/105(1996) 586-594.

[45] Schmitz-Hübsch T, Sellam F, Staub R, Törker M, Fritz T, Kübel Ch, Müllen K, Leo K, *Surface Science*, 445(2000) 358-367.

[46] Seo D-K, Ren J, Whangbo M-H, *Surface Science*, 370(1997) 252-258.

[47] Chizhov I, Kahn A, Scoles G, *Journal of Crystal Growth*, 208(2000) 449-458.

[48] Fenter P, Schreiber F, Zhou L, Eisenberger P, Forrest S.R, *Physical Review B*, 56(6)(1997) 3046-3053.

[49] Schmitz-Hübsch T, Fritz T, Sellam F, Staub R, Leo K, *Physical Review B*, 55(12)(1997) 7972-7976.

[50] Staub R, Toerker M, Fritz T, Schmitz-Hübsch T, Sellam F, Leo K, *Surface Science*, 445(2-3)(2000) 368-379.

[51] Shklover V, Tautz F.S, Scholz R, Sloboshanin S, Sokolowski M, Schaefer J.A, Umbach E, *Surface Science*, 454(2000) 60-66.

[52] Taborski J, Väterlein P, Dietz H, Zimmerman U, Umbach E, *Journal of Electron Spectroscopy and Related Phenomena*, 75(1995) 129-147.

[53] Seidel C, Awater C, Liu X.D, Ellerbrake R, Fuchs H, *Surface Science*, 371(1997) 123-130.

[54] Seidel C, Schafer A, Fuchs H, *Surface Science*, 459(3)(2000) 310-322.

[55] Tautz F.S, Sloboshanin S, Schaefer J.A, Scholz R, Shklover V, Sokolowski M, Umbach E, *Physical Review B*, 61(24)(2000) 16933-16947.

[56] Tautz F.S, Sloboshanin S, Shklover V, Scholz R, Sokolowski M, Schaefer J.A, Umbach E, *Applied Surface Science*, 166(1-4)(2000) 363-369.

[57] Tautz F.S, Eremtchenko M, Schaefer J.A, Sokolowski M, Shklover V, Glocker K, Umbach E.

[58] Gabriel M, Stöhr M, Möller R, *Applied Physics A - Materials Science and Processing*, 74(2001) 303-305.

[59] Schuerlein T, Schmidt A, Lee P.A, Bebesny K.W, Armstrong N.R, *Japanese Journal of Applied Physics*, 34(1995) 3837-3845.

[60] Schmidt A, Schuerlein T.J, Collins G.E, Armstrong N.R, *Journal of Physical Chemistry*, 99(30)(1995) 11770-11779.

[61] Schuerlein T.J, Armstrong N.R, *Journal of Vacuum Science & Technology A - Vacuum Surfaces and Films*, 12(4)(1994) 1992-1997.

[62] Umbach E, *Progress in Surface Science*, 35(1991) 113-127.

[63] Heutz S, Cloots R, Jones T.S, *Applied Physics Letters*, 77(24)(2000) 3938-3940.

[64] Schuerlein T.J, Armstrong N.R, *Journal of Vacuum Science & Technology A - Vacuum Surfaces and Films*, 12(4)(1994) 1992-1997.

[65] Chkoda L, Schneider M, Shklover V, Kilian L, Sokolowski M, Heske C, Umbach E, *Chemical Physics Letters,* 371(2003) 548-553

[66] Chen Q, Rada T, Bitzer T, Richardson N.V, *Chemistry of Materials*, -(-)(In Press) -.

[67] Ogawa T, Kuwamoto K, Isoda S, Kobayashi T, Karl N, *Acta Crystallographica*, B55(1999) 123-130.

[68] Forrest S.R, *Chemical Reviews*, 97(1997) 1793-1896.

[69] Möbus M, Karl N, Kobayashi T, *Journal of Crystal Growth*, 116(1992) 495-504.

[70] Heutz S, Ferguson A.J, Rumbles G, Jones T.S, *Organic Electronics*, 3(2002) 119-127.

[71] Schmidt A, Schuerlein T.J, Collins G.E, Armstrong N.R, *Journal of Physical Chemistry*, 99(30)(1995) 11770-11779.

[72] Schlaf R, Schroeder P.G, Nelson M.W, Parkinson B.A, *Journal of Applied Physics,* 86(3)(1999) 1499-1509.

[73] Haq S, Bainbridge R.C, Frederick B.G, Richardson N.V, *Journal of Physical Chemistry B*, 102(44)(1998) 8807-8815.

[74] Schewe P.F, Stein B, "Perylene," *The AIP Bulletin of Physics News*, http://www/aip.org/physnews/update/514-3.html: 29th November 2000.

[75] Wang D, Wan L-J, Xu Q-M, Wang C, Bai C-L, *Surface Science*, 478(1-2)(2001) L320-L326.

[76] Fryer J.R, Ewins C, *Philosophical Magazine A,* 66(6)(1992) 889-898

[77] Kasai H, Kamatani H, Yoshikawa Y, Okada S, Oikawa H, Watanabe A, Itoh O, Nakanishi H, *Chemistry Letters* (11)(1997) 1181.

[78] Camerman A, Trotter J, *Proceedings of the Royal Society*, 279(1963) 129-146.

[79] Iuliucci R.J, Phung Cu.G, Facelli J.C, Grant D.M, *Journal of the American Chemical Society*, 118(1996) 4880-4888.

[80] Zimmermann U, Schnitzler G, Wustenhagen V, Karl N, Dudde R, Koch E.E, Umbach E, *Molecular Crystals and Liquid Crystals,* 339(2000) 231-259.

[81] Tanaka J, *Bulletin of the Chemical Society of Japan*, 36(10)(1963) 1237-1249.

[82] Taborski J, Väterlein P, Dietz H, Zimmerman U, Umbach E, *Journal of Electron Spectroscopy and Related Phenomena*, 75(1995) 129-147.

[83] Wang D, Wan L-J, Xu Q-M, Wang C, Bai C-L, *Surface Science*, 478(1-2)(2001) L320-L326.

[84] Littke W, Haber M, Güntherodt H-J, *Journal of Crystal growth,* 122(1992) 80-92.

[85] Overney R.M, Howald L, Frommer J, Meyer E, Güntherodt H-J, *Journal of Chemical Physics,* 94(12)(1999) 8441-8443.

[86] Yannoulis P, Frank K-H, Koch E.E, *Surface Science,* 2431-3(1991) 58-64.

[87] Yokoi K, *Molecular Physics,* 85(3)(1995) 449-462.

[88] Yoshikawa H, Sasaki K, Masuhara V, *Journal of Physical Chemistry,* 104(2000) 3429-3437.

[89] Lukas S, Witte G, Wöll, *Physical Review Letters*, 88(2)(2002).

[90] Shaw J.M, Seidler P.F, *IBM Journal of Research and Development*, 45(1)(2001) 3-9.

[91] Robertson J.M, Sinclair V.C, Trotter J, *Acta Crystallographica*, 14(1961) 697-704.

[92] Campbell R.B, Robertson J.M, Trotter J, *Acta Crystallographica*, 14(1961) 705-711.

[93] Campbell R.B, Robertson J.M, *Acta Crystallographica,* 15(1962) 289

[94] Chambers A, Fitch R.K, Halliday B.S, Basic Vacuum Technology, 2nd (Bristol: Institute of Physics, 1998).

[95] Briggs D, Seah M.P, Practical Surface Analysis, 2nd (Wiley, 1990).

[96] Nix R, "An Introduction to Surface Chemistry," English, http://www.chem.qmw.ac.uk/surfaces/scc/: Queen Mary's College, London, 10th January 1999.

[97] Vickerman J.C, Surface Analysis: The Principal Techniques, 1st (Wiley, 1998).

[98] Vickerman J.C, Surface Analysis: The Principal Techniques, Wiley, 1997

[99] Nicolet Literature Supplied with Magna 860 spectrometer.

[100] Willard H.H, Merrit L.L, Dean J.A, Settle F.A, Instrumental Methods of Analysis, 7th (California: Wadsworth Publishing company, 1988).

[101] Colangeli L, Mennella V, Baratta G.A, Bussoletti E, Strazzulla G, *The Astrophysical Journal*, 396(1992) 369-377.

[102] Szczepanski J, Vala M, *The Astrophysical Journal* (414)(1993) 646-655.

[103] Greener R.G, *Journal of Chemical Physics*, 44(1)(1966) 310-315.

[104] Williams D.H, Fleming I, Spectroscopic Methods in Organic Chemistry, 5th (McGraw - Hill, 1995).

[105] Binnig G, Rohrer H, *Reviews of Modern Physics*, 71(2)(1999)S324-S330

[106] Stroscio J.A, Kaiser W.J, Scanning Tunneling Microscopy, 1st (Academic Press Inc., 1993).

[107] Omicron, Tip Etching Kit User Manual, Omicron 1998

[108] Rada-Crespo T, PhD thesis, Adsorption and Growth Of Organic Molecular Films on Silicon Surfaces, October 2002

[109] www.hidenanalytical.com/info

[110] Willard H.H, Merrit L.L, Dean J.A, Settle F.A, Instrumental Methods of Analysis, 7th (California: Wadsworth Publishing company, 1988).

[111] Schuerlein T, Schmidt A, Lee P.A, Bebesny K.W, Armstrong N.R, *Japanese Journal of Applied Physics*, 34(1995) 3837-3845.

[112] Curie D, *Luminescence in Crystals* (London: Butler and Tanner Ltd, 1963).

[113] Chua F.M, Kuk Y, Silverman P.J, *Physical Review Letters,* 63(4)(1989) 386-389

[114] Kuk Y, Chua F.M, Silverman P.J, Meyer J.A, *Physical Review B*, 41(18)(1990) 12393-12402.

[115] Carley A.F, Davies P.R, Jones R.V, Harikumar K.R, Roberts M.W, *Chemical Communications*, (2000) 185-186.

[116] Bowker M, Private disscussion.

[117] Bowker M, Rowbotham E, Leibsle F.M, Haq S, *Surface Science*, 349(1996) 97-110

[118] Dorenbos G, Breeman M, Boerma D.O, *Physical Review B*, 47(3)(1993) 1580-1588.

[119] Coulman D, Wintterlin J, Barth J.V, Ertl G, *Surface Science*, 240(1990) 151-162.

[120] Feidenhans'l R, Grey F, Nielsen M, Besenbacher F, Jensen F, Laegsgaard E, Stensgaard I, Jacobsen K.W, Nørskov J.K, Johnson R.L, *Physical Review Letters*, 65(16)(1990) 2027-2034.

[121] de Paula J.C, Spectroscopy and Photochemistry: Molecular Orbital Calculations http://www.haverford.edu/chem/302/mo2001.pdf

[122] Hyperchem Instructional Literature

[123] Ochterski J.W. Vibrational Analysis in Gaussian http://www.gaussian.com/g_whitepap/vib.htm

[124] Schmidt A, Schuerlein T.J, Collins G.E, Armstrong N.R, *Journal of Physical Chemistry*, 99(30)(1995) 11770-11779.

[125] Haq S, Bainbridge R.C, Frederick B.G, Richardson N.V, *Journal of Physical Chemistry B*, 102(44)(1998) 8807-8815.

[126] Thermo VG Scientific, "XPS, AES, UPS," www.lasurface.com:11th Oct 2002.

[127] Chizhov I, Kahn A, Scoles G, *Journal of Crystal Growth*, 208(2000) 449-458.

[128] Colangeli L, Mennella V, Baratta G.A, Bussoletti E, Strazzulla G, *The Astrophysical Journal*, 396(1992) 369-377.

[129] Szczepanski J, Vala M, *The Astrophysical Journal* (414)(1993) 646-655.

[130] Shklover V, Tautz F.S, Scholz R, Sloboshanin S, Sokolowski M, Schaefer J.A, Umbach E, *Surface Science* 454-456(2000) 60-66

[131] Tautz F.S, Sloboshanin S, Schaefer J.A, Scholz R, Sklover V, Sokolowski M, Umbach E *Physical Review B* 61(24)(2000) 16933-16947

[132] Davidson G, Group Theory for Chemists, Macmillan, 1991

[133] Vincent A, Molecular Symmetry and Group Theory, Wiley, 2001

[134] Tautz F.S, Sloboshanin S, Schaefer J.A, *Physical Review B*, 61(24)(2000) 16933-16947

[135] Gabriel M, Stöhr M, Möller R, *Ecoss20-Poster* (2001).

[136] Gabriel M, Stöhr M, Möller R, *Applied Physics A - Materials Science and Processing*, 74(2001) 303-305.

[137] Stöhr M, Gabriel M, Möller R, *Surface Science*, 507-510(2002) 330-334.

[138] Colangeli L, Mennella V, Baratta G.A, Bussoletti E, Strazzulla G, *The Astrophysical Journal*, 396(1992) 369-377.

[139] Szczepanski J, Vala M, *The Astrophysical Journal* (414)(1993) 646-655.

[140] Ong K.K, Jensen J.O, Hameda H.F, *Journal of Molecular Structure (Theochem)*, 459(1999) 131-144

[141] Chen Q, University of St. Andrews, *Unpublished work.*

[142] Chen Q, Rada T, McDowall A, Richardson N, *Chemistry of Materials*, 14(2002)743-749

[143] Turnbull G, University of St. Andrews, Department of Physics, *Unpublished work.*

[144] Vitukhnovsky A.G, Sluch M.I, Warren J.G, Petty M.C, *Chemical Physics Letters,* 173(5-6)(1990) 425-429.

[145] Kasai H, Oikawa H, Okada S, Nakanishi H, *Bulletin of the Chemical Society of Japan*, 71(1998) 2597-2601.

[146] Kasai H, Kamatani H, Yoshikawa Y, Okada S, Oikawa H, Watanabe A, Itoh O, Nakanishi H, *Chemistry Letters* (11)(1997) 1181.

[147] Mahrt J, Willig F, Storck W, Weiss D, Kietzmann R, Schwarzburg K, Tufts B, Trosken B, *Journal of Physical Chemistry,* 98(1994) 1888-1894

[148] Matsui A, Mizumo K, Iemura M, *Journal of the Physical Society of Japan,* 51(6)(1982) 1871-1877.

[149] Nishimura H, Matsui A, Iemura M, *Journal of the Physical Society of Japan,* 51(5)(1982) 1341-1342.

[150] Nishimura H, Yakaomka T, Mizuno K, Iemura M, *Journal of the Physical Society of Japan,* 53(11)(1984) 3999-4008.

[151] Colangeli L, Mennella V, Baratta G.A, Bussoletti E, Strazzulla G, *The Astrophysical Journal*, 396(1992) 369-377.

[152] Szczepanski J, Vala M, *The Astrophysical Journal* (414)(1993) 646-655.

Additional References (no specific ref. mark or duplicate information)

- Atkins P.W, Physical Chemistry, 5th ed, Oxford University Press, 1997.
- Callister W.D, Materials Science and Engineering: An Introduction, 4th ed, Wiley, 1997.
- Barbarella G et al, *Advanced Materials,* 11(16)(1999) 1375-1379.
- Cox J.J, Structure of Organic Molecular Thin Films Vapour Deposited on III-V Semiconductor Surfaces, PhD Thesis, 1999.
- Donaldson D.M, Robertson J.M, White J.G, *Proceedings of the Royal Society,* 220(1953) 311-321.
- Fink R, Gador D, Stahl U, Zou Y, Umbach E, *Physical Review B,* 60(4)(1999) 2818-2826.
- Gador D, Buchberger C, Fink R, Umbach E, *Journal of Electron Spectroscopy and related Phenomena,* 96(1998) 11-17.
- Hirose Y, Forest S.R, Kahn A, *Physical Review B,* 52(19)(1995) 14040-14047.
- Hirose Y, Kahn A, Aristov V, Soukiassia P, Bulovic V, Forrest S.R, *Physical Review B,* 54(19)(1996) 13748-13758
- Kowalsky W et al, *Physical Chemistry Chemical Physics,* 1(1999) 1719-1725.
- LovingerA.J et al, *Journal of Applied Physics,* 55(2)(1984) 476-482.

- Penn D.R, *Journal of electron Spectroscopy and Related Phenomena,* 9(1)(1976) 29-40.
- Scofield J.H, *Journal of Electron Spectroscopy and Related Phenomena,* 8(1976) 129-137.
- Seah M.P, Dench W.A, *Surface and Interface Analysis,* 1(1)(1979) 2-11.
- Umbach E, Glocker K, Sokolowski M, *Surface Science,* 404(1-3)(1998) 20-31.